Списък на публикациите, участващи в конкурса като еквивалентен брой статии за хабилитационен труд

2006

- **Rangelov MA**, Vayssilov, GN, Petkov, DD. Quantum chemical model study of the acyl migration in 2 '(3 ')-formylnucleosides. INTERNATIONAL JOURNAL OF QUANTUM CHEMISTRY, 106, 6, JOHN WILEY & SONS INC, 2006, DOI:10.1002/qua.20892, 1346-1356. ISI IF:1.432

2010

- **Rangelov, Miroslav A.**, Petrova, Galina P., Yomtova, Vihra M., Vayssilov, Georgi N.. Hierarchical approach to conformational search and selection of computational method in modeling the mechanism of ester ammonolysis. JOURNAL OF MOLECULAR GRAPHICS & MODELLING, 29, 2, ELSEVIER SCIENCE INC, 2010, DOI:10.1016/j.jmgm.2010.07.006, 246-255. ISI IF:1.722

- **Rangelov M.**, Petrova GP, Yomtova VM, Vayssilov GN. Catalytic Role of Vicinal OH in Ester Aminolysis: Proton Shuttle versus Hydrogen Bond Stabilization. J. Org. Chem., 75, 20, 2010, DOI:10.1021/jo100886p, 6782-6792. ISI IF:4.002

2011

- **Rangelov M.**, Petrova G., Yomtova V., Vayssilov G.. Determination of the optimal position of adjacent proton-donor centers for the activation or inhibition of peptide bond formation – A computational model study. Journal of Molecular Graphics and Modelling, 30, Elsevier, 2011, DOI:https://doi.org/10.1016/j.jmgm.2011.05.004, 10-14. ISI IF:2.391

2018

- Todorov, P., **Rangelov, M.**, Peneva, P., Todorova, N., Tchekalarova, J.. Anticonvulsant evaluation and docking analysis of VV-Hemorphin-5 analogues. Drug Development Research, Wiley, 2019, DOI:10.1002/ddr.21514, ISI IF:2.646

WILEY InterScience® DISCOVER SOMETHING GREAT

Quantum Chemical Model Study of the Acyl Migration in 2′(3′)-Formylnucleosides

MIROSLAV A. RANGELOV,[1] GEORGI N. VAYSSILOV,[2] DIMITER D. PETKOV[1]

[1]*Laboratory of BioCatalysis, Institute of Organic Chemistry, Bulgarian Academy of Sciences, Sofia 1113, Bulgaria*

[2]*Faculty of Chemistry, University of Sofia St. Kliment Ohridski, 1 James Bourchier Ave., Sofia 1126, Bulgaria*

Received 22 November 2004; accepted 9 May 2005
Published online 12 December 2005 in Wiley InterScience (www.interscience.wiley.com).
DOI 10.1002/qua.20892

ABSTRACT: This work reports a density functional study of the mechanism of acyl migration between vicinal OH groups in monoformylated *cis*-tetrahydrofuran-3,4-diol as a model system for the acyl migration in amino-acylated tRNA. In addition, migration toward the ionized hydroxyl group was modeled, which simulates the process in the presence of basic reagents. The polarized continuum model (PCM) for four solvents evaluated the solvent effect on the reaction energetics. The computational results suggest that the stepwise mechanism via an orthoester intermediate is preferred by 45–48 kJ/mol over the concerted mechanism where migration of the formyl group, and the proton from the vicinal OH group occurs simultaneously via a four-atom transition state. The conformational constrains of the THF ring could increase the energy of the transition states by ~24 and 37 kJ/mol for the stepwise and concerted reaction paths, respectively. The calculated lowest activation energy of the reaction both in vacuum and in solvents is rather high, at 188 and 172–182 kJ/mol, respectively. These results suggest that in real systems, the process is most likely catalyzed by preliminary deprotonation of the vicinal OH group. In this case, the formyl group migration proceeds spontaneously, and the intermediate formed is 15–30 kJ/mol more stable than the initial anion of the monoformylated diol. © 2005 Wiley Periodicals, Inc. Int J Quantum Chem 106: 1346–1356, 2006

Key words: diols; vicinal hydroxyl; DFT; acyl migration; tRNA

Correspondence to: G. N. Vayssilov; e-mail: gnv@chem.uni-sofia.bg

Contract grant sponsor: National Science Foundation (Bulgaria).

© 2005 Wiley Periodicals, Inc.

Introduction

The acyl group migration in monoacylated diols or acylated carbohydrates is an important reaction both in living cells and in synthetic organic chemistry. While this reaction is undesirable for most chemical synthetic reactions due to reduction of selectivity, it is necessary for the living cell, where such chemical transformations are responsible for an acyl group shift in a wide variety of species, as lipids, acylated sugars, and nucleosides. One of the most interesting acyl migration reactions is that between vicinal hydroxyl groups in the amino-acylated tRNA, which is the substrate in peptide bond synthesis in the ribosome. It is well known that in the cell such amino-acylated tRNA exists in two isomeric forms, 2′-acylated and 3′-acylated, with an equilibrium between them, but the ribosome can process only 3′-amino-acylated tRNA.

The acyl migration reaction is very fast in situ as well as in living cells, where there are a wide variety of enzymes that can increase the overall reaction rates. One example for the rapidity of acyl migration reactions in situ is the well-known fact that diacylglycerols can isomerize slowly on standing in inert solvents or in the solid state, even at low temperatures, and form an equilibrium mixture that contains about 67% of the 1,3-isomer. However, the fastest acyl migration rates occur when vicinal hydroxyls are fixed in the *cis* position by steric hindrance or by participation in a cycle, as in the case of amino-acylated tRNA mentioned above where acyl group migration is between *cis* vicinal hydroxyls in the 2′ and 3′ position.

The monomolecularity of this type of reactions is deduced from the results of several groups that have studied the stability and acyl migration of many *O*-acyl glucuronides [1–4]. In all these cases, acyl migration occurs when the hydroxyl groups on the glucose ring are roughly in the same plane. When the ribose hydroxyls are also in the same plane of the furanose ring, acyl migration would be expected. As has been shown by kinetic investigations [5, 6], the acyl migration reaction in 2′/3′-O-amino-acyladenosine is very rapid, exceeding the rate of hydrolysis by four orders of magnitude.

Acyl migration between the adjacent hydroxyl groups in partially acylated carbohydrates (usually acetylated or benzoylated) under acidic or basic conditions, via an *ortho* ester intermediate, has also been well documented [7–10]. It has been shown that under these conditions the acyl migration is highly accelerated, suggesting acid/base catalysis of the reaction.

The purpose of the present computational study is to shed some light on the mechanism of acyl migration between vicinal OH groups, thus contributing to understanding the process in partially acylated nucleosides, carbohydrates, and synthetic organic chemistry. In addition to the migration toward an intact vicinal OH group, we modeled the migration toward an ionized hydroxyl group that simulates the process in the presence of basic reagents or species. To keep the results applicable to organic synthesis conditions, we also studied the effect of three different solvents on the reaction energetics using the polarized continuum model (PCM) [11].

Model System and Method

One of the smallest but still reasonable model systems for acyl migration in amino-acylated tRNA is monoformylated *cis*-tetrahydrofuran-3,4-diol. This compound is very suitable, because as with amino-acyl tRNA, it has a vicinal *cis*-hydroxyl group near the acylated hydroxyl and similar conformational minima due to the same ring skeleton. In model studies, we consider only the *cis* isomer because of the similarity to the ribofuranose ring and the experimental data suggesting acyl group migration only in the *cis* configuration of the vicinal hydroxyl groups [2–5]. For the description of THF ring conformations, we use the *east* and *west* notation [12, 13]. According to this notation [12, 13], the conformer is denoted as *east* or *west* when the O heteroatom of the THF ring Of is oriented *opposite* or at the *same* side, of the THF ring with respect to the substituting OH and OCHO groups. To differentiate between the various structures of the transition states and intermediates, we used an additional notation for the conformers describing the relative position/orientation of the carbonyl Oc atom of the migrating formyl group and in some cases the position of the carbonyl C atom or migrating proton (see Appendix for details).

Molecular orbital calculations were carried out with the Gaussian 98 [14] program suite. Analytical gradient optimization methods were used to locate the minima, corresponding to reactants, intermediates, and products, as well as saddle points corresponding to transition states. Calculations were performed at the B3LYP [15] level with the 6-31+G [16a–e] basis set. [The check for the influence of the

TABLE I

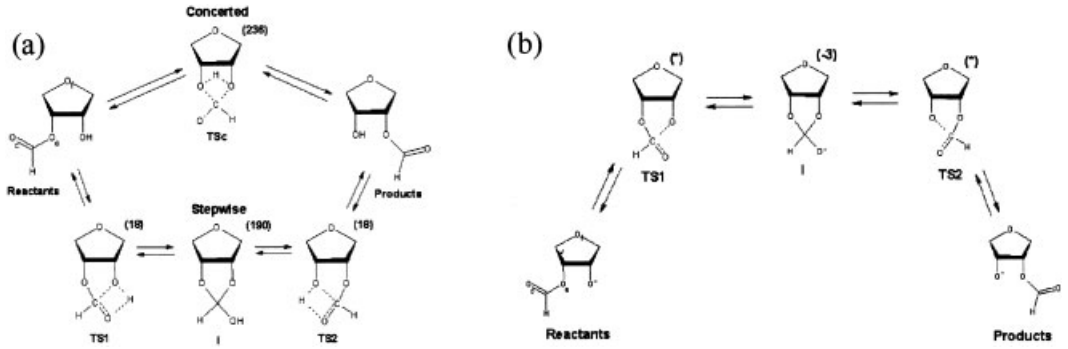
Energy of the species (kJ/mol) for formyl group migration in THF-3, 4-diol with respect to the energy of the most stable initial structure, and imaginary frequencies of the transition states, *Freq*, in cm^{-1}.

Structure	Vacuum	Chloroform	Acetonitrile	Methanol	Water	*Freq*
Initial/final conformations						
AN	0	0	0	0	0	
MCl	20	18	19	23	23	
PCl	1	0	−11	−11	0	
TSc						
W–Ct–Oc	236	229	227	218	217	1472
W–Ct–Ot	249	237	232	226	225	1519
W–Cc–Ot	253	247	245	246	244	1492
W–Cc–Oc	272	263	261	253	251	1493
E–Ct–Oc	245	240	238	236	235	1451
E–Ct–Ot	256	246	242	238	237	1498
E–Cc–Ot	273	264	260	260	259	1547
E–Cc–Oc	265	266	266	260	262	1518
TS1/TS2						
W–Ot	190	182	180	173	172	1775
W–Oc	194	187	185	179	178	1809
E–Ot	188	183	183	185	184	1727
E–Oc	212	203	201	199	198	1847
Intermediates						
W–Ot–Han	13	4	1	−6	−7	
W–Oc–Han	6	−1	−2	−5	−6	
W–Ot–Hpc	18	7	4	−7	−8	
W–Ot–Hmc	18	7	4	−7	−8	
W–Oc–Hpc	25	16	14	5	3	
E–Ot–Han	22	13	10	1	0	
E–Oc–Han	26	16	14	5	4	
E–Ot–Hpc	26	17	16	7	5	
E–Oc–Hmc	26	18	16	10	9	
E–Ot–Hmc	26	17	16	7	5	
E–Oc–Hpc	26	18	16	10	9	

size of basis set on the obtained energies was performed for one transition state of the concerted mechanism, E–Cc–Ot, with 6-31+G** and 6-31++G** basis sets showed a decrease of activation energy by only 3 and 4 kJ/mol, respectively.] All transition states were identified by finding only one negative eigenvalue of the analytic force constant matrix (Table I) and by geometric analysis of its eigenvector components, as well as by IRC path following. No symmetry constraints have been applied. The solvent effects were evaluated by PCM [11], as included in the Gaussian 98 program. Single-point PCM calculations at the B3LYP/6-31+G level were performed to refine the energy changes of all stationary points along the modeled rate-determining reaction paths. We used standard dielectric constants implemented in Gaussian 98 for the solvents used. The energies of all structures are calculated with respect to the energy of the most stable conformation of the reactant molecule. The activation barriers of the TS1 and TSc transition states are calculated with respect to the reactant, while the activation barriers of TS2 are calculated with respect to the intermediate, which is geometrically closest to TS2.

Results and Discussion

There are two possible mechanisms for acyl migration in our model system: stepwise, a two-step mechanism via *ortho* ester intermediate [lower part



SCHEME 1. Formyl group transfer mechanisms in neutral monoformylated THF-3,4-diol (a) and in its monoanion (b). The energies (in kJ/mol) of the intermediate species with respect to reactant are added in parentheses. Asterisk (*) denotes that such transition states are not observed.

of Scheme 1(a)]; and concerted, a one-step mechanism [upper part of Scheme 1(a)]. The stepwise mechanism includes the formation of an orthoester intermediate, **I**, where the vicinal hydroxyl oxygen is attached to the carbon atom of the C═Oc bond of the ester. The transition state for formation of this intermediate is **TS1**, and those for transformation of the intermediate to product—**TS2**. In the concerted mechanism, the reaction occurs in one step via transition state **TSc**. Unlike the migration toward intact vicinal OH group, where the formyl group and the proton from the OH group migrate in opposite directions, in the case of the monoanion the formyl group only migrates and only one mechanism could be considered [Scheme 1(b)]. Since the intermediate species were found to be local minima but not transition states, this mechanism is considered Stepwise.

INITIAL CONFORMATIONS

Both the initial and final structures along the reaction path are monoformylated *cis*-tetrahydrofuran-3,4-diol, and the conformers of final structures are enantiomers of the corresponding initial ones. For this reason, we will discuss only the conformers of the initial structure. We found three stable conformations for it (Fig. 1) that differ by rotation of the formyl group with respect to the THF ring around the Oe—C3 bond between the ester oxygen atom and the carbonyl carbon atom C3 from the THF ring bound to it. For this reason, the structures are denoted according to the orientation of the formyl group with respect to the C2—C3 bond of the THF skeleton, AN, PCl, and MCl for antiperiplanar, plus clinal (+clinal), and minus clinal (−clinal), respectively (see Appendix). The conformers of the initial compound cannot be classified suitably by the *east/west* notation, since the Of heteroatom is in the same plane as the other three C atoms of the ring, while the remaining C atom, C2 or C5, is out of plane.

All three conformers have hydrogen bonds with the vicinal hydroxyl group as proton donor. In one of the most favorable conformation PCI (Fig. 1), the hydrogen bond is formed with the carbonyl Oc atom of the formyl group as proton acceptor, but the H–Oc distance is relatively long, 2.3 Å. Because of the appropriate active group orientation for both reaction paths and its lowest energy, we use this conformation as the starting point in calculating the energy of different species along the reaction paths. In the second conformation, AN, the ester Oe atom of the formyl group plays the role of proton acceptor of the hydrogen bond (2.2 Å). This conformation has essentially the same stability as the previous conformation, but the orientation of the formyl group in it is not appropriate for further reaction. The third conformation MCI has a shorter hydrogen bond (1.9 Å), with the Oc atom of the formyl group as proton acceptor. However, this conformation is 20 kJ/mol higher than the other two structures, as the formyl group in this conformer is positioned below the THF ring, thus causing steric hindrance.

CONCERTED MECHANISM

The concerted mechanism involves nucleophilic attack of the oxygen atom from the vicinal hydroxyl group (Ov) to the formyl carbon atom and simultaneous proton transfer from the vicinal hydroxyl

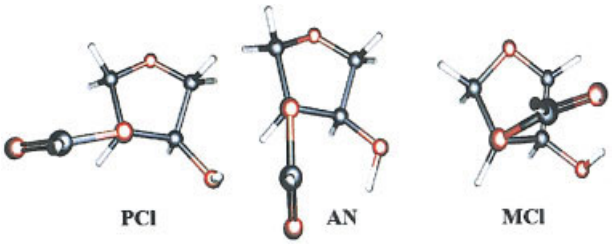


FIGURE 1. Geometry of initial conformations.

group directly to the ester oxygen, Oe. This is accompanied by cleavage of the ester C—Oe bond and formation of the products in one step via one transition state **TSc** along the path. We found eight conformations for this transition state (Fig. 2), all of which feature a symmetry plane that passes along the THF oxygen heteroatom, Of, the transferred proton and the formyl group. All feature rather high activation energy, >230 kJ/mol in vacuum. The main reason for this high barrier is that the transfer of the formyl group and the proton occur simultaneously and, due to different requirements for the optimal O—O distance for each of these transfers, the four-atom ring formed is strongly constrained.

The geometries obtained for the transition state **TSc** (Fig. 2) correspond to only two, *east* and *west*, of the four conformational minima of the furanose ring [12, 13]. This is probably due to the larger distance between vicinal oxygen atoms in the *south* and *north* conformations that leads to a long path for the formyl group in the migration process that is energetically unfavorable. The activation energies obtained for the *west* conformation of the transition state are on average 8 kJ/mol lower than the energies of the *east* conformation, since they fit the optimal distance better between vicinal oxygen atoms in the transition state, 2.19–2.23 Å (Table II). Typically, in the *west* conformation, the C2—H and C5—H bonds on the side of the Of heteroatom are in an equatorial orientation, while those on the opposite side of the ring are in an axial-like orientation; i.e., the orientation of both hydrogen atoms at the C3 and C4 carbon atoms of the THF ring should be close to equatorial. This brings the two vicinal oxygen atoms in the TSc closer when the structure is in the *west* as compared with the *east* conformation.

In addition to the conformation of the THF ring, some other geometrical factors influence the stability of the TSc. As shown in Table I, the most stable ones are the TSc structures E/W–Ct–Oc/Ot in which the transferred formyl group is in the *trans* position with respect to the THF ring and the repulsion with it is reduced. Among these structures is the most stable one, W–Ct–Oc, with an energy barrier of 236 kJ/mol. W–Cc–Ot is the only structure with a Cc configuration that is relatively stable due to the formation of a weak hydrogen bond (2.1 Å) between the hydrogen atom of the formyl group and the furanose ring oxygen atom. The least stable

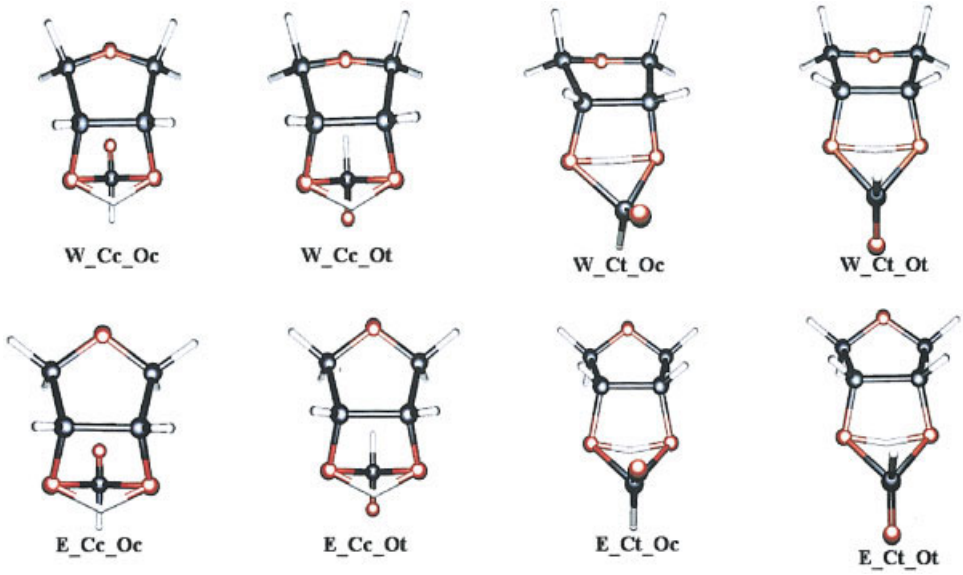


FIGURE 2. Geometry of transition states in concerted reaction path.

TABLE II
Some geometrical parameters of the optimized structures.

Structure	O—O[a]	H—H[b]	H—H[c]	H—H[d]
Initial/final conformations				
AN	2.79	2.36	3.96	2.85
MCl	3.09	2.32	3.08	3.87
PCl	2.69	2.43	3.89	3.07
TSc				
W–Ct–Oc	2.19	2.50	2.50	4.01
W–Ct–Ot	2.21	2.52	2.52	4.01
W–Cc–Ot	2.23	2.48	2.71	4.01
W–Cc–Oc	2.22	2.46	3.03	3.90
E–Ct–Oc	2.21	2.46	4.00	2.72
E–Ct–Ot	2.22	2.48	4.00	2.70
E–Cc–Ot	2.22	2.43	3.94	2.95
E–Cc–Oc	2.21	2.43	3.96	2.86
TS1/TS2				
W–Ot	2.44	2.44	2.85	3.96
W–Oc	2.43	2.46	2.77	3.98
E–Ot	2.46	2.46	3.93	2.95
E–Oc	2.38	2.46	3.94	2.92
Intermediates				
W–Ot–Ha	2.26	2.48	2.64	4.01
W–Oc–Ha	2.25	2.49	2.56	4.04
W–Ot–Hpc	2.25	2.45	2.68	4.00
W–Ot–Hmc	2.25	2.45	2.68	4.00
W–Oc–Hpc	2.26	2.47	2.76	3.98
W–Oc–Hmc	2.26	2.47	2.76	3.98
E–Ot–Ha	2.27	2.44	4.00	2.70
E–Oc–Ha	2.26	2.41	3.99	2.71
E–Ot–Hpc	2.26	2.42	3.99	2.73
E–Oc–Hmc	2.26	2.44	3.99	2.71
E–Ot–Hmc	2.26	2.42	3.99	2.73
E–Oc–Hpc	2.26	2.44	3.99	2.71

[a] Distance between vicinal oxygens.
[b] Distance between hydrogen atoms at C3 and C4 atoms of the THF ring.
[c] Distance between hydrogen atoms at C2 and C5 atoms of the THF ring positioned over THF ring (in *trans* position with respect to the vicinal O atoms).
[d] Distance between hydrogen atoms at C2 and C5 atoms of the THF ring positioned below THF ring (in *cis* position with respect to the vicinal O atoms).

structures are W–Cc–Oc and E–Cc–Ot due to the repulsion between the carbonyl Oc atom and the Of heteroatom, in the former case, and of the H atom from the transferred formyl group and the axial H atoms at C2 and C5 carbon atoms of the THF ring, in the latter case.

The highest-energy path in the concerted mechanism (via W–Cc–Oc) has a barrier of 273 kJ/mol due to steric hindrance between the THF oxygen and the carbonyl oxygen atom. The lowest energy path (via W–Ct–Oc) has no such hindrances and has an energy of 236 kJ/mol, which is still 48 kJ/mol higher than in the stepwise mechanism.

STEPWISE MECHANISM

As shown in Scheme 1(a), the stepwise mechanism includes the formation of an intermediate, **I**, in which the former carbonyl carbon atom is tetrahedral with OH, H, and two vicinal oxygen atoms from tetrahydrofuran-3,4-diol as substituents. The transition state for formation of this intermediate, **TS1**, includes nucleophilic attack of the lone pair of the vicinal oxygen at the carbonyl carbon atom and simultaneous transfer of the proton from the vicinal hydroxyl group to the carbonyl oxygen atom, Oc. The second transition state in the stepwise mechanism, **TS2**, includes proton transfer from the OcH group of the intermediate **I** to the Oe oxygen atom. Simultaneously, cleavage of the former ester C—Oe bond and restoration of the double carbonyl bond C═Oc takes place. In our model system, the reaction path is symmetric, so the transition states **TS1** and **TS2** are enantiomers, i.e., structurally and energetically equivalent. For this reason, we modeled and discuss only **TS1** below.

Unlike transition states in the concerted mechanism **TSc**, where there are two possible orientations of the formyl group with respect to the plane between the vicinal hydroxyls and the corresponding C atoms from the THF ring, *cis* and *trans* to the THF ring, in both transition states and the intermediate of the concerted mechanism, **TS1** and **I**, the C atom of the formyl group is located very close to the reference plane. In this way, the strong hindrance between the furanose ring and the formyl group transferred is avoided and in general the activation barrier of the reaction via the stepwise mechanism is lower (188 kJ/mol), although this value is still rather high for a reaction that is supposed to occur spontaneously.

In three of the four obtained structures of **TS1**, the proton from the vicinal OH group is essentially transferred to the carbonyl Oc atoms, while the new bond between the formyl carbon atom and the vicinal Ov atom is not formed. These three structures have similar energy barriers, 188–194 kJ/mol, where the lowest energy structure is E–Ot (Fig. 3). In the fourth structure of the transition state, E–Oc,

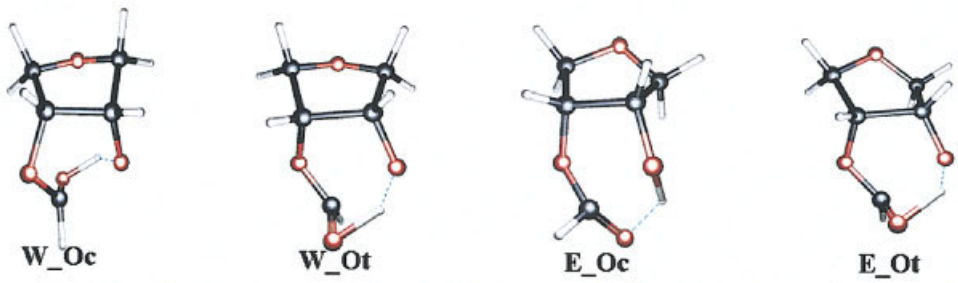


FIGURE 3. Geometry of first transition states in stepwise reaction path.

the proton is still not transferred, while the C—Ov bond is close to formation, with a C–Ov distance of 1.75 Å. This structure was found to be 24 kJ/mol less stable than E–Ot structure (Table I).

We found various structures of the intermediate **I**. Like the case of the concerted mechanism transition states, the intermediates in the stepwise mechanism are also in *east* or *west* conformations because of the newly formed five-member ring between vicinal oxygens in the *ortho* ester intermediate. In analogy with the discussion on **TSc**, the intermediates with *west* conformation are by ~8 kJ/mol more stable than those in the *east* conformation due to more suitable orientation of the hydrogen atoms at C3 and C4 atoms of THF ring; in the *west* conformations this H—H distance is 0.04 Å longer than in *east* ones. In addition to the conformation of the THF ring, the energy of the intermediate is also influenced by the location and orientation of the OH group. In the most stable structure of the intermediate, W–Oc–Ha (Fig. 4) with 6 kJ/mol energy higher than reactant, this OH group participates in a hydrogen bond with the furanose oxygen atom Of, that reduces the energy of the intermediate by 8–12 kJ/mol as compared with other similar structures without hydrogen bonds.

To obtain the energy profiles for the stepwise mechanism, we assume that the intermediate for every reaction path is geometrically closest to the transition states of the path. Surprisingly, for all mechanisms these intermediates are with lowest energy too. This is probably due to favorable interactions between the orthoester hydroxyl group and two *gauche* positioned oxygens. In the case of W–Oc–Ha, the energy is lower than other rotational conformations by 19 kJ/mol because of the hydrogen bond formed between the orthoester hydroxyl and the furanose oxygen (2.1 Å). The energetic dif-

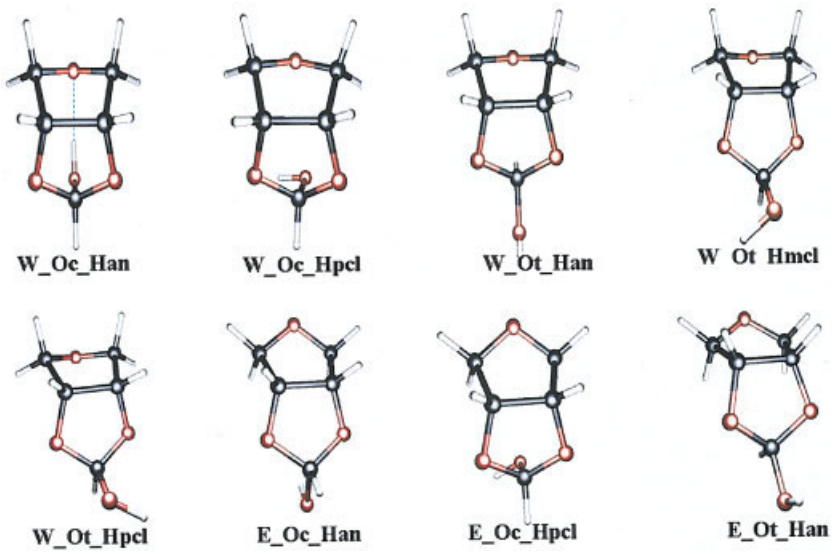


FIGURE 4. Geometry of some intermediates in stepwise reaction path.

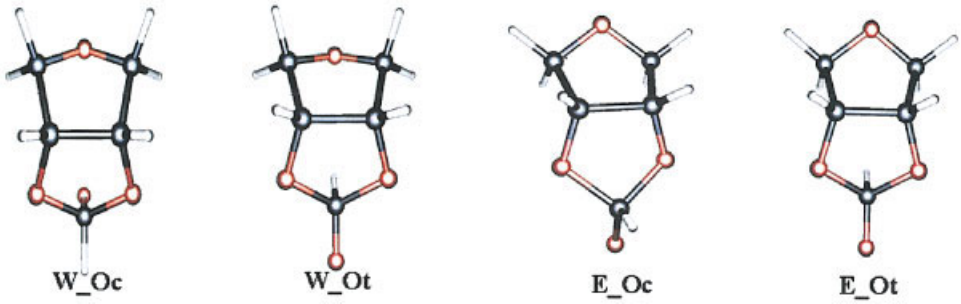


FIGURE 5. Geometry of intermediates in monoanione stepwise reaction path.

ferences in the rotational conformations of the intermediates of the other reaction paths are rather small, <5 kJ/mol.

The lowest energy path in the stepwise mechanism (via E–Ot) has a barrier of 188 kJ/mol mainly due to the lack of steric hindrance in the structures of the transition states. The highest energy path in that mechanism (via E–Oc) has a barrier of 212 kJ/mol.

MONOANION MECHANISM

Because the calculated energy barrier for formyl group migration in formylated *cis*-tetrahydrofuran-3,4-diol was found to be rather high in both the stepwise and the concerted mechanisms, we also considered the reaction with an ionized vicinal hydroxyl group. This situation is relevant to the reaction that takes place in the presence of strong bases.

In this case, only one initial conformation of the reactant with a hydrogen bond (2.3 Å) between the formyl group hydrogen and vicinal oxygen as proton acceptor was found.

As reported in the literature, in reaction paths that include an alkoxide attack on a carbonyl carbon atom, transition states are missing [17–19]. After an extensive search for possible transition states, we did not find any reliable structure corresponding to a transition state. For this reason, we discuss the obtained intermediates. As in the case of transition states of the concerted mechanism in the nonionized reactant, the intermediates for the ionic reactant are symmetrical and ribose rings are in the *east* or *west* conformation (Fig. 5). Because of strong intramolecular repulsion between Of and Oc oxygen atoms, the structure W–Oc has 9–11 kJ/mol higher energy than the other structures, which are with essentially the same stability as the reactant in vacuum (Table III).

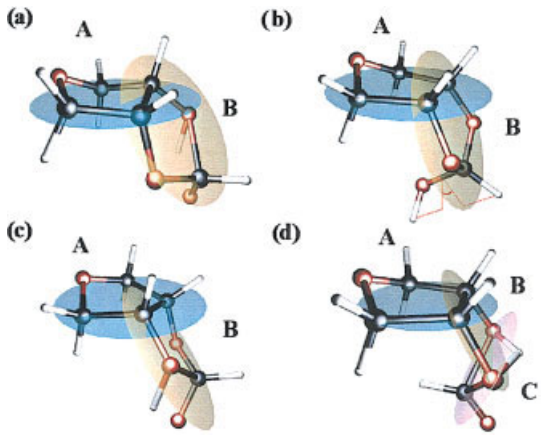


FIGURE 6. Visualization of planes used in the notation: (a) TS1; (b) I; (c) TS2; (d) TSc.

SOLVENT EFFECT

To refine the solvent effect on the reaction energetics, we performed single-point calculations on optimized structures using the PCM method for four different solvents—water, methanol, acetonitrile and chloroform—to cover different parts of the dielectric constant scale.

The results (Table I) suggest that the presence of a solvent lowers all barriers of both concerted and stepwise reaction paths for formyl group transfer in formylated tetrahydrofuran-3,4-diol. [We also checked the energy of a sample transition state, E–Cc–Ot, in acetonitrile obtained after complete geometry optimization with PCM. This optimization results in reduction of the activation barrier by 7 kJ/mol (~3%) with respect to the barrier obtained with single-point PCM calculation using the geometry of the transition state optimized in vacuum.] This effect could be attributed to the generation of a

TABLE III

Energy of the intermediate species (kJ/mol) for formyl migration in THF-3, 4-diol monoanion with respect to the energy of the most stable initial conformer.

Structure	Vacuum	Chloroform	Acetonitrile	Methanol	Water
Intermediates					
W–Oc	8	−9	−13	4	2
W–Ot	−1	−25	−30	−15	−16
E–Oc	−3	−22	−25	−5	−6
E–Ot	−2	−22	−24	−5	−6

mirror charge in the solvent in the case of transition states because of their larger localized charges in the reaction center. This gives rise to stabilization of the transition-state species with respect to the reactants and, respectively, to reduction of the reaction barriers. Furthermore, the energy barriers decrease with increasing the dielectric constant of the solvent in the order: vacuum > chloroform > acetonitrile > methanol > water. The relative stability of different structures of the intermediates and transition states is, however, not influenced by the presence of the solvent. The stepwise reaction path remains the most favorable, by 45–47 kJ/mol, as found from the calculations in vacuum. Despite the reduction, the lowest reaction barrier is still rather high, at 172 kJ/mol.

In the case of the monoanion intermediates (Table II), the solvent stabilizes the intermediates formed, most of which are more stable than the reactant itself. In chloroform and acetonitrile, the intermediates are 24–30 kJ/mol more stable, and one should expect that in these solvents the reactant would not be present in the solution. In water and methanol, the stabilization of the intermediates is lower, and one of the structures, W–Ot (Fig. 5), is 10 kJ/mol more stable than the rest, probably due to the formation of a weak hydrogen bond.

We also estimated the deprotonation energy of formylated tetrahydrofuran-3,4-diol solvated in acetonitrile by the reaction energy of the following process:

$$\{C_4H_6O(OOCCH_3)OH\}_{solv} + \{CH_3CN\}_{solv} \rightarrow \{C_4H_6O(OOCCH_3)O^-\}_{solv} + \{CH_3CNH^+\}_{solv}.$$

In this study, we considered explicitly the acetonitrile molecule that accepts the proton released from the reactant, while the rest of the solvent is modeled by PCM. The obtained deprotonation energy is 277 kJ/mol, as acetonitrile is a weak base. We also checked the deprotonation in presence of ammonia or $N(CH_3)_3$ in the acetonitrile solution and the energy decreases to 137 and 93 kJ/mol, respectively, considerably lower than the calculated reaction barriers for acyl migration in a nonionized substrate. In the presence of stronger bases, this energy should be significantly reduced.

Conclusion

Two alternative paths (stepwise and concerted) for formyl group migration between vicinal hydroxyl groups in tetrahydrofuran-3,4-diol were considered. According to our theoretical investigations, the stepwise mechanism for the formyl group migration between vicinal hydroxyl groups is preferred by 45–48 kJ/mol in vacuum or in solution. Owing to the high conformational constraints in the THF ring, the steric hindrances can increase the energy of the transition states by ~24 kJ/mol in the stepwise reaction path and ~37 kJ/mol in the concerted reaction path. The calculated activation energy of the reaction in vacuum, 188 kJ/mol, is rather high. After taking into account the influence of the solvent, this energy is reduced, but only by 16 kJ/mol. These considerations suggest that in the real systems the process is most likely catalyzed, e.g., by preliminary deprotonation of the vicinal OH group. Indeed, the calculations suggest that acyl group migration proceeds spontaneously when the vicinal OH group is deprotonated. Moreover, in all solvents considered, the intermediate formed is 15–30 kJ/mol more stable than the initial/final anion of the monoformylated THF-3,4-diol; i.e., such ionized orthoester species could be observed experimentally in the presence of a strong enough base.

References

1. Corcoran, O.; Mortensen, R. W.; Hansen, S. H.; Troke, J.; Nicholson, J. K. Chem Res Toxicol 2001, 14, 1363.
2. Hasegawa, H.; Akira, K.; Shinohara, Y.; Kasuya, Y.; Hashimoto, T. Biol Pharm Bull 2001, 24, 852.
3. Mortensen, R. W.; Corcoran, O.; Cornett, C.; Sidelmann, U. G.; Lindon, J. C.; Nicholson, J. K.; Hansen, S. H. Drug Metab Dispos 2001, 29, 375.
4. Jemnitz, K.; Levai, F.; Monostory, K.; Szatmari, I.; Vereczkey, L. Eur J Drug Metab Pharmacokinet 2000, 25, 153.
5. Wolfenden, R.; Rammler, D. H.; Lipmann, F. Biochemistry 1964, 3, 329.
6. Reese, C. B.; Trentham, D. R. Tetrahedron Lett 1965, 29, 2467.
7. Haines, A. H. Adv Carbohydr Chem Biochem 1976, 33, 11.
8. Horrobin, T.; Tran, C. H.; Crout, D. J Chem Soc Perkin Trans 1 1998, 1069.
9. Khan, S.; Teitz, D. S.; Jemal, M. Anal Chem 1998, 70, 1622.
10. Chung, S.-K.; Chang, Y.-T. J Chem Soc Chem Commun 1995, 13.
11. (a) Miertus, S.; Scrocco, E.; Tomasi, J. Chem Phys 1981, 55, 117; (b) Miertus, S.; Tomasi, J. Chem Phys 1982, 65, 239; (c) Cossi, M.; Barone, V.; Cammi, R.; Tomasi, J. Chem Phys Lett 1996, 255, 327; (d) Barone, V.; Cossi, M.; Tomasi, J. J Comp Chem 1998, 19, 404; (e) Barone, V.; Cossi, M. J Phys Chem A 1998, 102, 1995; (f) Mennucci, B.; Tomasi, J. Chem Phys 1997, 106, 5151.
12. Kilpatrick, J. E.; Pitzer, K. S.; Spitzer, R. J Am Chem Soc 1947, 69, 2483.
13. Plavec, J.; Tong, W.; Chattopadhyaya, J. J Am Chem Soc 1993, 115, 9734.
14. Frisch, M. J.; Trucks, G. W.; Schlegel, H. B.; Scuseria, G. E.; Robb, M. A.; Cheeseman, J. R.; Zakrzewski, V. G.; Montgomery, J. A.; Stratmann, R. E.; Burant, J. C.; Dapprich, S.; Millam, J. M.; Daniels, A. D.; Kudin, K. N.; Strain, M. C.; Farkas, O.; Tomasi, J.; Barone, V.; Cossi, M.; Cammi, R.; Mennucci, B.; Pomelli, C.; Adamo, C.; Clifford, S.; Ochterski, J.; Petersson, G. A.; Ayala, P. Y.; Cui, Q.; Morokuma, K.; Malick, D. K.; Rabuck, A. D.; Raghavachari, K.; Foresman, J. B.; Cioslowski, J.; Ortiz, J. V.; Stefanov, B. B.; Liu, G.; Liashenko, A.; Piskorz, P.; Komaromi, I.; Gomperts, R.; Martin, R. L.; Fox, D. J.; Keith, T.; Al-Laham, M. A.; Peng, C. Y.; Nanayakkara, A.; Gonzalez, C.; Challacombe, M.; Gill, P. M. W.; Johnson, B. G.; Chen, W.; Wong, M. W.; Andres, J. L.; Head-Gordon, M.; Replogle, E. S.; Pople, J. A. Gaussian: Pittsburgh, PA, 1998.
15. Becke, A. D. J Chem Phys 1993, 98, 5648.
16. (a) Ditchfield, R.; Hehre, W. J.; Pople, J. A. J Chem Phys 1971, 54, 724; (b) Hehre, W. J.; Ditchfield, R.; Pople, J. A. J Chem Phys 1972, 56, 2257; (c) Hariharan, P. C.; Pople, J. A. Mol Phys 1974, 27, 209; (d) Gordon, M. S. Chem Phys Lett 1980, 76, 163; (e) Hariharan, P. C.; Pople, J. A. Theor Chim Acta 1973, 28, 213.
17. Madura, J.; Jorgensen, W. J Am Chem Soc 1986, 108, 2517.
18. (a) Weiner, S.; Singh, C.; Kollman, P. J Am Chem Soc 1985, 107, 2219; (b) Bakowies, D.; Kollman, P. J Am Chem Soc 1999, 121, 5712.
19. Rangelov, M. A.; Vayssilov, G. N.; Yomtova, V. M.; Petkov, D. D. Org Biomol Chem 2005, 3, 737.

Appendix

NOTATION OF THE DIFFERENT CONFORMERS OF THE TRANSITION STATES AND INTERMEDIATES

To differentiate structures of the transition states and intermediates, we used the following notation describing the location of the O atom outside the plane of the THF ring, the carbonyl Oc atom of the migrating formyl group, and in some cases the position of the carbonyl C atom or migrating proton.

TRANSITION STATE TS1

X–Oy

- **X:** (E) east or (W) west, depending on the position of the O atom in THF ring with respect to the vicinal hydroxyl groups; see plane A in Figure 6(a).
- **y:** (**c**) *cis* or (**t**) *trans,* depending on the relative positions of THF ring and carbonyl oxygen atom of the migrating formyl group with respect to the plane of the carbonyl carbon, vicinal O atom, and the C from THF connected to it; see plane B in Figure 6(a).

INTERMEDIATE I

X–Oy–HZ

- **X:** (E) east or (W) west, depending on the position of the O atom in (THF) ring with respect to the vicinal hydroxyls; see plane A in Figure 6(b).
- **y:** (**c**) *cis* or (**t**) *trans,* depending on the position of the THF ring and carbonyl oxygen atom toward the RMS plane between carbonyl carbon, vicinal hydroxyls, and carbons from THF connected to vicinal hydroxyls; see plane B in Figure 6(b).
- **z:** **AN, PCl,** or **MCl** for antiperiplanar, +clinal, or −clinal conformations of the O—H bond with respect to the C—H bond at the tetrahedral C atom; see the torsional angle shown in red in Figure 6(b).

TRANSITION STATE TS1

X–Oy

- **X:** (E) east or (W) west, depending on the position of the O atom in (THF) ring with respect to the vicinal hydroxyls; see plane A in Figure 6(c).
- **y**: (**c**) *cis* or (**t**) *trans,* depending on the relative positions of THF ring and carbonyl oxygen atom with respect to the plane of the carbonyl carbon, vicinal O atom, and the C from THF connected to it; see plane B in Figure 6(c).

TRANSITION STATE TSC

X–Cy–Oz

- **x:** (E) east or (W) west, depending on the position of the O atom in (THF) ring with respect to the vicinal hydroxyls; see plane A in Figure 6(d).
- **y:** (**c**) *cis* or (**t**) *trans,* depending on the position of the THF ring and carbonyl carbon atom toward the RMS plane between vicinal hydroxyls and carbons from THF connected to vicinal hydroxyls; see plane B in Figure 6(d).
- **z:** (**c**) *cis* or (**t**) *trans,* depending on the position of the carbonyl oxygen and furanose ring toward the plane between vicinal hydroxyls and carbonyl carbon; see plane C in Figure 6(d).

INITIAL/FINAL CONFORMATION

AN, PCl, or **MCl** for antiperiplanar, +clinal, or −clinal conformations of the formyl group with respect to the C2—C3 bond of THF ring.

For a description of ionized intermediates, the first two signs of nonionized intermediates description will be used.

Journal of Molecular Graphics and Modelling 29 (2010) 246–255

Contents lists available at ScienceDirect

Journal of Molecular Graphics and Modelling

journal homepage: www.elsevier.com/locate/JMGM

Hierarchical approach to conformational search and selection of computational method in modeling the mechanism of ester ammonolysis

Miroslav A. Rangelov[a,*], Galina P. Petrova[b], Vihra M. Yomtova[a], Georgi N. Vayssilov[b,*]

[a] Laboratory of BioCatalysis, Institute of Organic Chemistry, Bulgarian Academy of Sciences, Sofia 1113, Bulgaria
[b] Faculty of Chemistry, University of Sofia "St. Kliment Ohridski"; 1, James Bourchier Ave., Sofia 1126, Bulgaria

ARTICLE INFO

Article history:
Received 24 April 2010
Received in revised form 17 July 2010
Accepted 20 July 2010
Available online 30 July 2010

Keywords:
Reaction mechanisms
Computational chemistry
Conformational search
Transition states

ABSTRACT

We describe automated procedures for the first stages of a systematic computational investigation of reaction mechanisms. They include (i) selection of computational method and basis set based on statistical analysis of structural and energy data relating to experimental values, (ii) determination of all distinct conformations of transition states with large conformational freedom, and (iii) generation of unknown geometry of the transition states, based on pre-defined connectivity of the atoms involved in the reaction. For the conformational search we employed an efficient procedure for exploration of various possible conformations of the transition states and elimination of the equivalent structures in several steps using molecular-mechanical and quantum-mechanical methods. The procedure was applied to the determination of the structures of transition states and intermediates in the ammonolysis of monoformylated 1,2-ethanediol, which were subsequently used for identification of the lowest energy reaction paths. For the same reaction system we also used the approach for generation of the initial structures of transition states with unknown geometry. The reported procedures are implemented in the MolRan program suite.

© 2010 Elsevier Inc. All rights reserved.

1. Introduction

The computational modeling of reaction mechanisms and energetics has become an important step in the investigation of different processes, occurring in biological systems [1–4], catalytic systems [5–8], organic synthesis [9–11], etc. The selection of the computational method [12] and construction of the initial structures of the reactants, transition states, intermediates and products are often carried out after comparison with previous knowledge and chemical intuition. This approach becomes, however, inappropriate when the rigorous study of the reaction mechanism requires calculation of a large number of structures of the stationary points because of the size or flexibility of the modeled system. Here, we propose automated procedures for these first stages of a systematic computational investigation of reaction mechanisms that provide both computational efficiency and reliability.

The initial step in a computational modeling is the selection of the computational method and basis set that are appropriate for the explored chemical system. In order to determine which method is reliable and at the same time computationally efficient, we performed an exhaustive test of different computational method/basis set combinations and statistical analysis of the obtained structural and energetic data, which were compared with experimental values (Section 3).

Each rigorous theoretical investigation requires systematic inspection of all possible transition state structures and intermediates, belonging to different reaction paths, and identification of the structures corresponding to the lowest barriers in order to define the most energetically favorable reaction route. This search is particularly complicated in systems with large conformational freedom where it is important to check various possible conformations of the transition states and intermediates, in order to select among them a set of distinct structures with low energy, to be computed at the final stage by a chemically adequate (but more time consuming) computational method. Hereby, we describe a smooth and automated procedure for conformational search of transition state structures. The procedure is applied to the ammonolysis of 1-O-formyl 1,2-ethanediol (Section 4.1) and it helped us to find all lowest energy structures of the stationary points along different reaction paths. In addition, in Section 4.2 we report an approach to the automatic construction of the initial structures of transition states with desired atomic connectivity but unknown geometry using the same model reaction. We selected this reaction since it is a suitable model for elucidation of the mechanism of biosynthesis of peptide bonds in the ribosome, in connection with recent theoretical [13–17] and experimental [18–20] investigations.

* Corresponding authors.
E-mail addresses: mran@orgchm.bas.bg (M.A. Rangelov), gnv@chem.uni-sofia.bg (G.N. Vayssilov).

1093-3263/$ – see front matter © 2010 Elsevier Inc. All rights reserved.
doi:10.1016/j.jmgm.2010.07.006

All described procedures are implemented and performed with the program MolRan [21] (see Section 2.1 for more details).

2. Computational details

2.1. Method

All quantum-chemical calculations described in the current work were performed with the program package Gaussian03 [22]. The search of appropriate level of theory for modeling the studied processes included different methods—HF, MP2 [23,24], B3LYP [25–29], MP4(SDQ) [30,31], and CCD [32]. The basis sets were varied from 3-21G [33] to 6-311G [34] as polarization and diffuse functions were also considered.

Preliminary optimization of the structures was performed at molecular-mechanical level with a modified version of MM force field [35,36] as the calculations were carried out with the MM optimizer module within MolRan program [21] by applying a combined conjugate-gradient quasi-Newton minimization algorithm [37,38]. Since in many processes the structures with inter- or intramolecular hydrogen bonds are of special interest, the program allows the addition of a small exponential term in the MM field in order to account for the contribution of hydrogen bonds to the energy of the system in a more precise way [39]. This term depends on the distances between the atoms in the proton-donor group and between the proton and the potential proton-acceptor, which are calculated at each step of the relaxation procedure.

The conformational search of the transition states is performed with the help of different modules implemented in the MolRan program suite [21].

2.2. MolRan program

MolRan [21] is a graphical tool for visualization and generation of molecular geometry and analysis of the chemical properties and electronic structure information obtained by means of quantum-chemical calculations with specialized computational software, e.g., Gaussian03 [22]. Various pre-defined z-matrix, Cartesian and fractional file formats (e.g., xyz, pdb, cif) are supported as in addition a fully customized file reader can extract and present structural data from text files, i.e., output files generated by computing software. Various graphical representation tools are implemented which allow the user to visualize the Hessian, gradients and other vectors, Newman projections along selected atoms, MD trajectories, RMS (root mean square) structures, etc.

The program also includes a set of tools for generating, loading, and displaying meshes generated on the base of different data, e.g., Van der Waals spheres, solvent accessible surfaces, meshes from loaded orbital coefficients and primitives producing AO or MO surface. In the last case the mesh could be also loaded from Gaussian03 cube file. The implemented tool allows mathematical modification of the generated/visualized meshes.

A system of tools is available for constructing job files for conformational analysis (see Section 4) and for analysis of the results obtained. The implemented file constructor can generate multiple job file with linear and nonlinear structures varied by selected structural parameters (interatomic distances, valence angles or dihedral angles) as the chosen variables can be altered synchronously or independently.

3. Selection of computational method and basis set

One of the important decisions in each quantum-chemical study is the selection of the method and basis set appropriate for simulation of the chosen system. In order to choose the theory level for our modeling, we considered a simple model system—formic acid and its dimer, which allows comparison of the theoretically obtained results with the available experimental data for the structure in the gas phase of both species [40,41]. The Gibbs free energy of the reaction of ammonolysis of formic acid in the gas phase was also estimated and compared to the experimental data [42]. In addition to the availability of experimental and theoretical [43–45] data for this process, another reason for choosing this model for testing different combinations of methods and basis sets is that the interaction between formic acid and ammonia is the minimal model for the aminolysis reaction, related to peptide bond formation.

The calculations consisted of geometry optimization of the structures at each combination of method and basis set (Section 3.1), followed by computation of the matrix of the analytical force constants and determination of the thermochemical characteristics of the system (Section 3.2). The calculations were performed at 60 different levels representing a combination of method and basis set as the applied quantum-chemical methods were HF, MP2, B3LYP, MP4(SDQ), and CCD. All obtained data were statistically scrutinized by means of cluster and canonical analyses. The hierarchal complete-linkage approach was applied for the cluster analysis as the data were standardized and Euclidean distance was used as similarity measure.

3.1. Structural parameters

The dendrogram obtained from the analysis of the errors in the geometry characteristics of formic acid and its dimer is presented in Fig. 1a. The bold line in the dendrogram (Fig. 1a; at distance 3.5) corresponds to the distance defined by the experimental error. As can be seen, the experimental data are connected with two clusters, {**4**} and {**5**} (see Fig. 1a), containing mainly data at B3LYP, MP2, and MP4 levels with basis sets with polarization functions as the main difference between the two clusters is the presence (cluster {**5**}) or absence (cluster {**4**}) of diffuse functions. The data included in the other three clusters differ more significantly from the experimental data. Cluster {**2**} consists mainly of methods which take into account the electron correlation, combined with basis sets without polarization functions or with basis sets including polarization functions but with a few primitives (3–21). The other two clusters contain the HF method with or without polarization function in the basis sets (clusters {**1**} and {**3**}, respectively). Thus, if we consider the computational time necessary for modeling the system at the different levels of theory, as well as the necessity of polarization function at least for the heavy atoms, the optimal method for the correct description of the geometry of the modeled structures and eventually formed hydrogen bonds should be B3LYP with basis set at least 6-31G*.

In order to quantify the influence of the different factors (i.e., method, basis set, presence or absence of polarization and diffuse functions), we also performed a canonical analysis. The canonical correlations of the elements of the computational procedure compared to their error relating to the experimental results are provided in Table 1. The negative values of the correlation coefficients result from the fact that the error is correlated. As can be seen, the factor with strongest influence on the accuracy in the simulation of the single bonds length is the presence of polarization functions at the heavy atoms. This factor is also important in the case of the double bonds, however for the correct simulation of the double bonds the computational method is more important. For the accurate description of the hydrogen bonds, the presence of polarization functions for the H atoms forming the bond is essential, while the inclusion of diffuse functions for these H atoms plays a modest role, even smaller with respect to the diffuse functions for the heavy atoms. The overall size of the basis set is important for the correct simulation of the valence angles in the modeled structures.

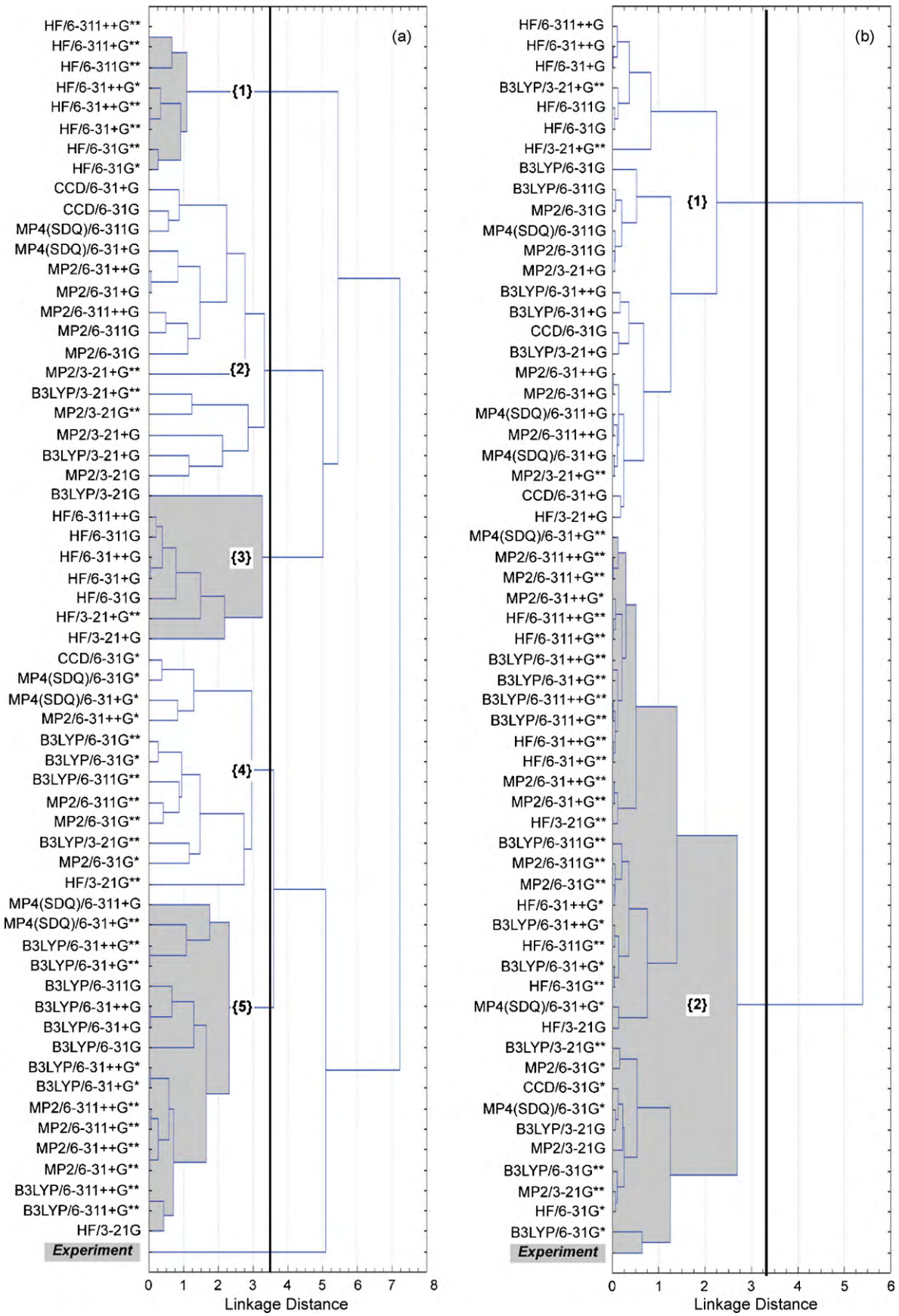


Fig. 1. Dendrogram obtained by cluster analysis of the computational data at the different tested levels of theory: (a) the clustering of the available data is performed on the base of the errors in the description of the geometry of formic acid and its dimer; (b) the clustering of the available data is performed on the base of the errors in the description of the thermochemistry of formic acid ammonolysis.

Table 1
Correlation coefficients between the computational procedure and the error relating to the experimental data. The numbers in bold show the characteristic of the computational procedure that affects the most strongly the selected structural parameter.

	Single bonds	Double bonds	Hydrogen bonds	Angles
Computational method	0.36	**−0.41**	−0.25	−0.08
Basis set	−0.25	−0.21	−0.13	**−0.35**
Diffuse functions (heavy atoms)	−0.06	−0.21	−0.21	−0.26
Diffuse functions (H atoms)	−0.20	−0.14	−0.14	−0.21
Polarization functions (heavy atoms)	**−0.61**	−0.37	−0.32	−0.13
Polarization functions (H atoms)	−0.36	−0.19	**−0.53**	−0.11

3.2. Thermochemistry

The dendrogram based on the errors in the description of the thermochemistry of formic acid ammonolysis is presented in Fig. 1b (the bold line at distance about 3.3 corresponds to the distance defined by the experimental error). As can be seen in the figure, the methods and basis sets could be divided into two groups as the main difference between the two groups is again the presence or absence of polarization functions in the basis set (cluster {**2**} and cluster {**1**}, respectively). Since cluster {**2**}, defined by the basis sets with polarization functions, include the experimental data, it is necessary to consider basis sets with polarization functions for the correct description of the thermochemistry of the modeled reaction. Thus, the method B3LYP with basis set at least 6-31G**, proposed on the base of the previous cluster analysis of the geometry data, should provide results comparable with the experimental data.

Due to the necessity to compare the energies between reactions with neutral molecules and anions requiring the presence of diffuse functions in the basis set, we chose to perform our computational study at B3LYP/6-31 + G* level of theory. The structures optimized at B3LYP/6-31 + G* and B3LYP/6-31 + + G** levels were analyzed for geometric similarities by means of the procedure described in Section 4 and, in consistence with the cluster analysis (Fig. 1), they were found to be similar since the RMS differences of the interatomic distances between equivalent atoms of the equivalent structures optimized at the two levels of theory were estimated at 0.025 Å.

In summary of this section, the density functional approach with the hybrid functional B3LYP was found the best compromise allowing accuracy of the calculated structural parameters and reaction energies for the modeled type of systems at reasonable computational time. One should note, however, that this may not be the case for other systems, for example for systems, in which the dispersion interactions plays a crucial role [46]. For such more "difficult" systems and problems one could employ new types of density functionals [12,47].

4. Search of transition state structures

The formation of the peptide bond is the key reaction step in protein synthesis which in living cells is catalyzed by the ribosome [48]. During protein synthesis, the amino group of the amino acid in the ribosome's A-site plays the role of the nucleophile, while the carbonyl belongs to the P-site amino acid, esterified to the 3′-ribose of tRNA. Thus, the reaction is actually an aminolysis of esters, which is often considered as a model reaction for the formation of peptide bonds during translation in both experimental and theoretical investigations [13–18,43]. Despite the numerous investigations of the reaction [18,49–51], its mechanism in the ribosome remains unresolved. For our model study we investigated the interaction between monoformylated ethanediol and ammonia. This selection of the reagents is not accidental but determined by the presence in the formylethanediol molecule of a vicinal hydroxyl next to the reaction center analogously to the ribose ring in tRNA. As shown in our theoretical investigations of the mechanism for this model reaction (Scheme 1a and b) [17,52], the latter one based on the transition state search reported here, the catalytic role of this vicinal hydroxyl group could be explained by the stabilization of the transition state structures via formation of intramolecular hydrogen bonds (tetragonal transition states in Scheme 1a) or by a direct participation of this vicinal hydroxyl in the proton transfer process (hexagonal transition states in Scheme 1b). Both possible reaction paths are presented in Scheme 1a and b, while the applied notation of the atoms is presented in Scheme 1c on the example of the tetrahedral intermediate I.

In the case of the reaction path through tetragonal transition states the geometry of the reaction ring is well known from previous theoretical data [43] and the search of transition states was oriented towards defining their most stable conformers by means of the conformational search algorithm described in Section 4.1. On the other hand, the geometry of the reaction ring for the proposed hexagonal transition states was unknown and the structural search consisted of generation of relevant initial structures based on pre-defined bonding between atoms from the reaction ring (see Section 4.2). In Section 4.3 we summarize the calculated results for the different modeled types of transition states and analyze the preference for the alternative reaction paths.

4.1. Conformational search algorithm for the tetragonal transition states

The optimized structures of the tetragonal transition states for the stepwise and concerted mechanisms are presented in Fig. 2 as the first structure in each line corresponds to a system without intramolecular hydrogen bond, while the second one represents the most stable conformer with hydrogen bond found by means of the proposed procedure. The applied search algorithm is schematically presented in Scheme 2 and consists of the following steps:

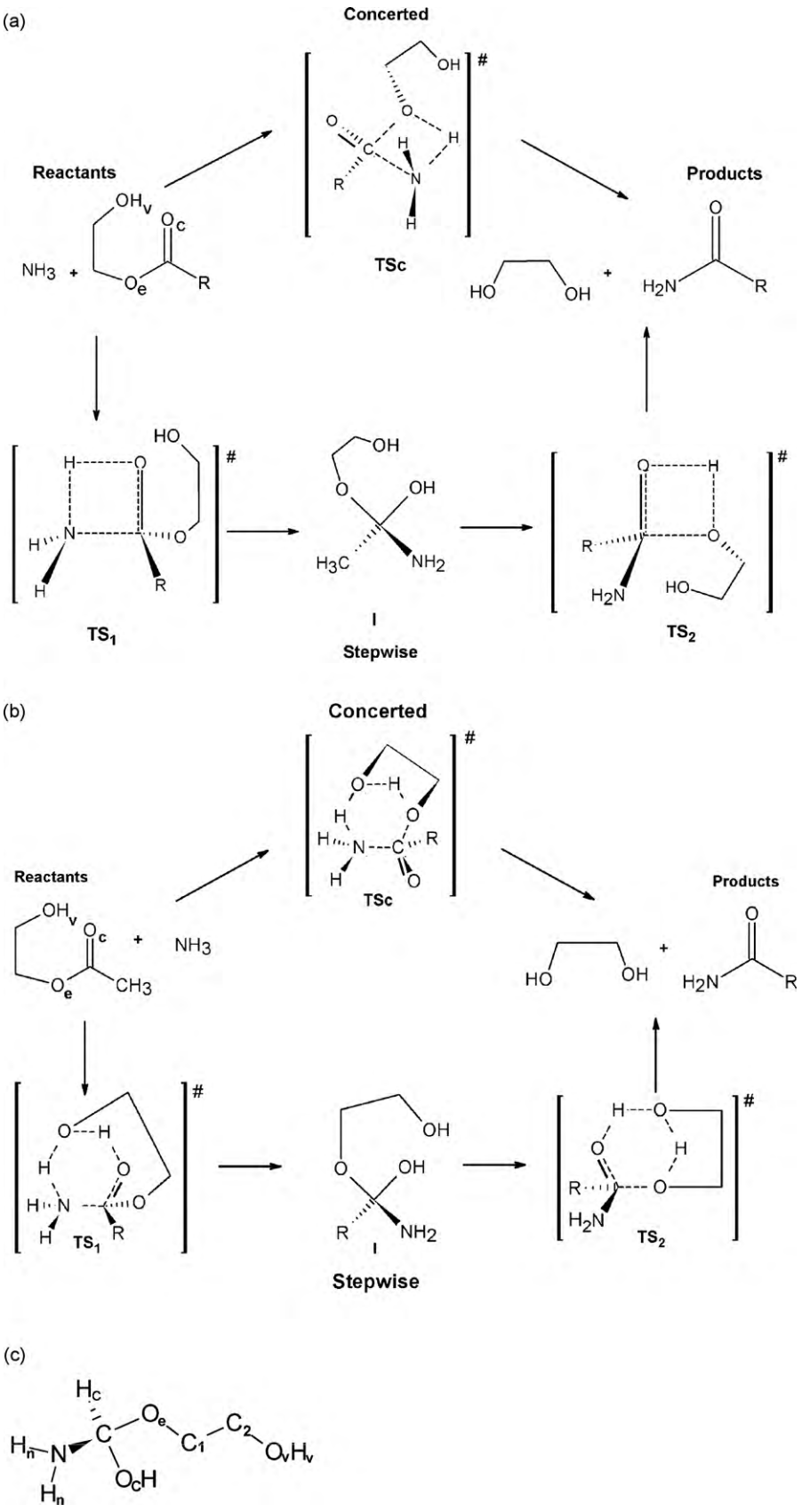
1. Generation of transition state initial structures.

In the example of ammonolysis of formylethanediol at this first stage all structures in completely periplanar conformation for the concerted and the stepwise mechanism were optimized at HF/6-31G level. The obtained structures of the tetragonal transition states and the intermediates correspond to those described in the literature for the ammonolysis of methylformiate [43,53–55].

2. Generation of series of modified structures.

These structures were based on the structures of transition states and intermediates obtained in the first step. The new sets of geometries were generated by stepwise variation of all dihedral angles not involved in the tetragonal reaction ring by 10°, i.e., 36 positions were initially considered, while the positions of the atoms participating in the reaction ring were kept fixed. The generation of the different structures is performed with the module for conformational search implemented in the program MolRan [21].

For the transition states and intermediates in the ammonolysis of formylethanediol for TSc and TS2 transition states the angles



Scheme 1. Mechanism of ammonolysis of 1-O-formyl 1,2-ethanediol (R≡H) via tetragonal (a) and hexagonal (b) transition states, and (c) notation of the atoms on the example of intermediate I. In panels (a) and (b) the upper reaction route corresponds to the concerted mechanism, while the lower one represents the stepwise mechanism.

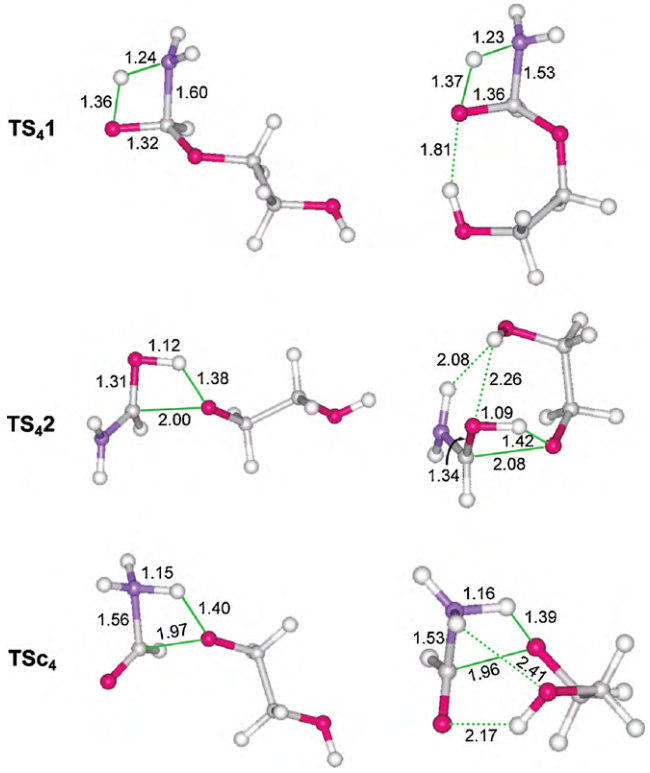
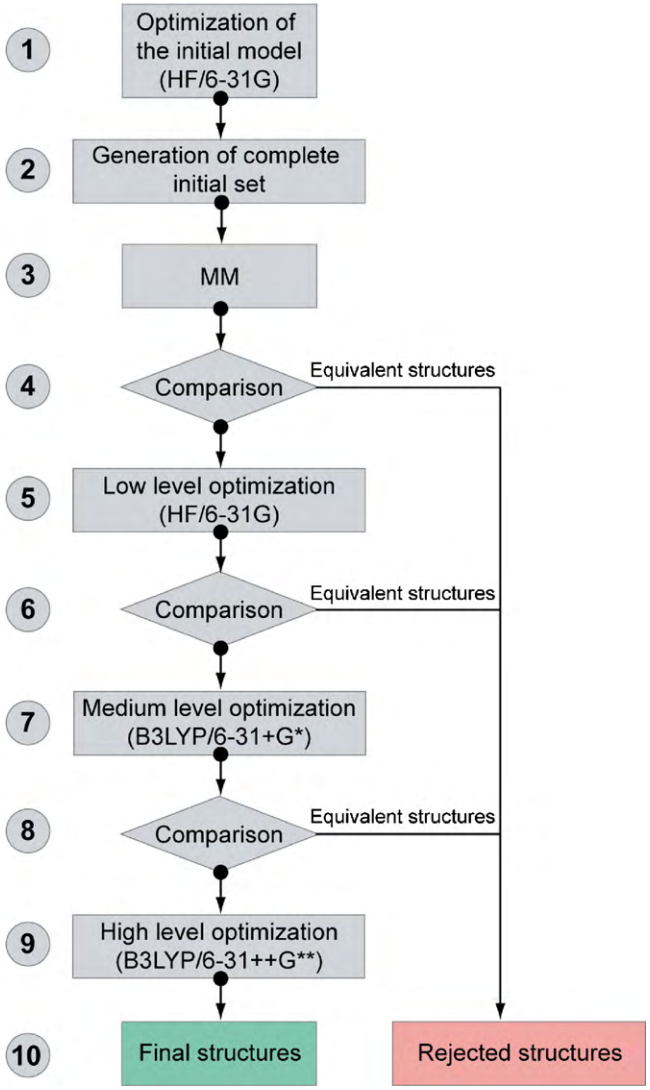


Fig. 2. Optimized structures of the tetragonal transition states of the stepwise ($TS_4$1 and $TS_4$2) and of the concerted (TSc_4) mechanism without (left-hand side) and with intramolecular (right-hand side) hydrogen bond. The bond lengths and some important interatomic distances are given in Å.



Scheme 2. Conformational search algorithm applied for defining the final set of structures in the case of formylethanediol model.

C–O_e–C1–C2, O_e–C1–C2–O_v and C1–C2–O_v–H_v were varied while for TS1 and intermediate I the dihedral angle N–C–O_e–C1 was also included (for the used notation see Scheme 1c). As could be seen from Scheme 1a, the chosen dihedral angles do not participate in the reaction ring. By means of this methodology we prepared ca. 46 000 initial structures for the transition states TSc and TS2 and ca. 160 000 for TS1 and intermediate I due to additional variation of the fourth angle N–C–O_e–C1 with the participation of the nitrogen atom from the attacking nucleophile.

3. Relaxation of the obtained structures at molecular-mechanical (MM) level.

This optimization is performed with the program MolRan [21] with conjugated gradient optimization procedure using analytical first derivatives. As described in Section 2, for this preliminary optimization we used modified version of MM force field supplemented by an exponential term for description of hydrogen bonds. During the geometry optimization of the structures at MM level the atoms from the cleaving/forming bonds are kept fixed with respect to each other.

4. Removal of equivalent structures.

After the MM relaxation of the structures, the equivalent ones were removed from the modeled series by calculating the root mean square deviation (RMSD) of the distances between equivalent atoms of each pair of structures. This procedure is performed as one of the structures is translated at the center of the coordinate system while the other structure of the pair is set over it by completing one translation and one rotation. The geometrical similarity of the structures is further estimated by numerical optimization of the geometry position of one molecule with respect to the other one by conjugated gradient quasi-Newton method. The gradients are calculated by means of Ridder polynomial extrapolation method and the RMSD distance between equivalent atoms from the two molecules in the pair serves as minimization function. The procedure applied for the elimination of the equivalent structures as described here is implemented in the program MolRan [21]. This step of the procedure allows reduction of the number of structures to be treated at higher computational level.

In tracing the reaction path of formylethanediol we also excluded the structures which do not contain any intramolecular hydrogen bonds except for the structures with O atoms of the ethanediol in *trans* position, which we used as referent structures.

5. Optimization at higher computational level.

The nonidentical structures of transition states and intermediates remaining from the previous step were optimized, respectively as saddle points and minima, at the next computational level (HF/6-31G) without any geometry restriction. All transition state structures were confirmed by calculating the matrixes of the analytical force constants and checking of the transition vector components. The optimized structures were again subjected to the elimination procedure described in step 4.

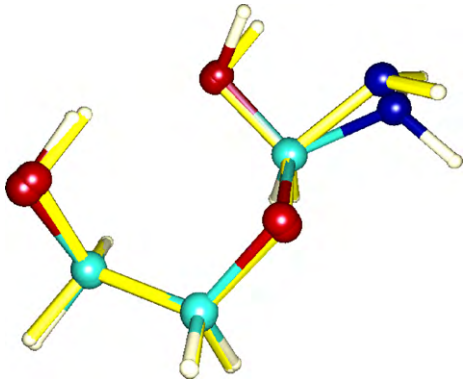


Fig. 3. Graphical result of the procedure for search of an intermediate structure which geometry is closest to a defined transition state structure. The transition state structure, which is varied relatively to the position and the transition vector, is presented with yellow bonds between the atoms.

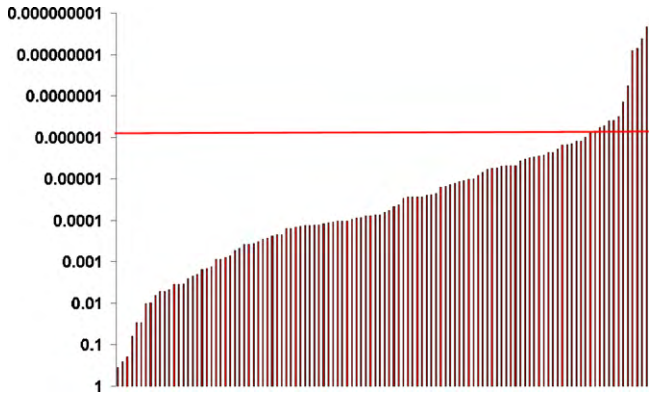


Fig. 4. Population of the conformers with intramolecular hydrogen bonds of the intermediate in the stepwise mechanism of formylethanediol ammonolysis relating to the most stable intermediate structure. The population of the referent structure of the intermediate without hydrogen bond is presented with a horizontal line.

The following steps (see Scheme 2, steps 6–10) include successive optimization of the obtained structures and further elimination of the equivalent ones at medium and higher level of theory. In the particular example the medium optimization level was B3LYP/6-31+G* level and the higher level for final optimization of the remaining structures was B3LYP/6-31++G** with additional polarization and diffuse functions at H atoms.

Due to the complexity of the transition vector of the modeled transition structures and the variation of the atoms, over which the main components of the vector are positioned along the reaction coordinate, the IRC search cannot reach the stable structures. For this reason, in order to find the intermediates, to which the different transition structures of TS1 will lead, and the intermediates, from which the transition structures of TS2 could be obtained, a technique similar to the procedure applied for elimination of the equivalent structures described above is used (see Fig. 3). In the current procedure each couple of intermediate and transition state structures are positioned over each other as the structure of the intermediate is translated into the centre of the coordination system and the position of the transition state structure is set via translation and rotation. The next step consists of variation of the structure of the transition state by enforcing over the atoms the transition vector of the structure multiplied by a variation coefficient. Analogously to the equivalent structures search, the optimization is performed by conjugated gradient quasi-Newton method and the RMSD distance between equivalent atoms from the two molecules in the pair serves as minimization function. The graphical result of the described procedure is presented in Fig. 3.

As a result of the performed conformational search we obtained 14, 9, and 6 stable structures for TS_41, TS_42 and TSc transition states, respectively, and more than 100 conformers of the intermediate structure, I. In Fig. 4 the population of the different conformers of I (assuming Boltzman distribution) with respect to the most stable structure is presented.

The common methods for transition state search focus on obtaining the local structures in the region in which the bonds are cleaved or formed. In various cases, however, the conformation of the rest of the molecule can affect strongly the energy of the obtained transition state, as it is shown here for ammonolysis of formylethanediol. Thus, our extensive conformational search approach complements the common TS search algorithms by accounting for the contribution of the mobility of the parts of the reactants that are not directly involved in the reaction center.

Frequently the transition state conformer with lowest energy does not correspond to the most stable conformers of the reactants or intermediates. Therefore, most of the methods for transition state search as linear synchronous transit (LST) cannot find transition state conformer with lowest energy starting from reactants or intermediates in their most stable conformers. Our approach systematically generates all possible conformers of the transition states and intermediates and compares all structures in the pool of the intermediates with the pool of the transition state structures. Thus, one can find the transition state structure with lowest energy and the intermediate conformer that corresponds to it.

4.2. Structure search for hexagonal transition states using the complex method

The search of the hexagonal transition states was based on completely different approach. Since these structures were not known in advance, we applied the *complex* algorithm. The *complex* algorithm was first proposed by Box [56] as extension of the simplex method for constrained optimization and in different modifications it is widely applied for identifying global extrema. The method is helpful for search of stable conformers of structures with predefined (intuitively guessed) topology but with unknown geometry and its main advantage is that it does not require any derivatives of the minimizing function and thus, is computationally very simple and efficient. Since the iterative procedure of this approach is described in details elsewhere [37,56], we are not going to discuss it here and will present only the basic idea of the method. With this approach one constructs a sequence (complex) of points in the phase space of geometry coordinates, which allows identification of the point corresponding to the global minimum eventually obeying imposed constrains. In the concrete application the procedure results in locating of the lowest energy transition state with desired connectivity by pre-definition of the forming and cleaving bonds in the hexagonal reaction ring (see Scheme 1b) and the covalent bonds in the reacting species. The minimizing function was defined from the modified MM field as implemented in the MolRan program suite [21] as the terms, taking into account the formation of hydrogen bonds, were excluded. The initial complex consisted of $2N/5$ (N is the number of all degrees of freedom in the system) random geometries as up to 1×10^{-4} of the volume of the complex (in the space of Cartesian coordinates) was optimized and the variation of the volume in the complex was 1×10^{-3}. The obtained structures were further optimized at the B3LYP/6-31G** level and the corresponding hexagonal transition states of the stepwise and concerted mechanisms are presented in Fig. 5. Due to the formation of a large reaction cycle with participation of the vicinal OH group in these transition states, their conformational freedom is strongly restricted and exhaustive conformational search (as described in Section 4.1) is not necessary.

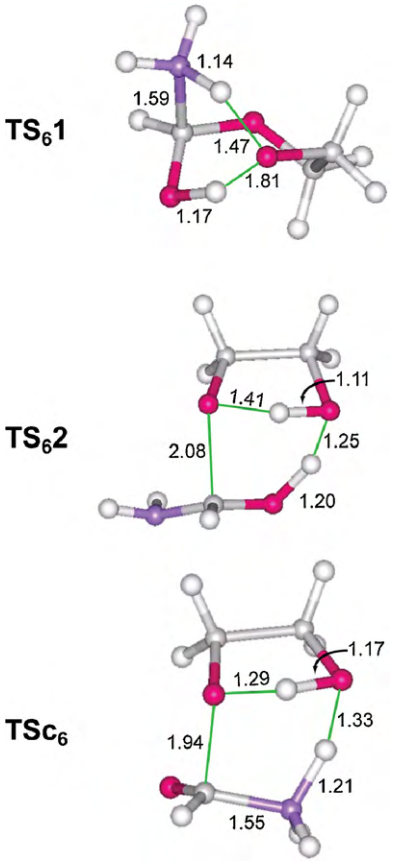


Fig. 5. Optimized structures of the hexagonal transition states of the stepwise ($TS_6$1 and $TS_6$2) and of the concerted (TSc_6) mechanism. The bond lengths and some important interatomic distances are given in Å.

Unlike other methods used for finding of transition states structures, this approach is capable to find lowest energy transition state structure with pre-defined topology without initial guess of the structure. This method is particularly useful when the reaction system undergoes large unpredictable changes from reactants to products, or when the elementary reaction step includes cleavage/formation of more than one bond where the applicability of most of the traditional approaches for transition state search is limited.

4.3. Comparison of different reaction paths

The detailed search of the tetragonal transitions state structures with various conformations (Section 4.1) and of the hexagonal transition states (Section 4.2) allowed us to identify the transition states with the lowest energy in the alternative stepwise and concerted reaction paths (see Scheme 1a and b). The calculated electronic energies with B3LYP functional and two types of basis sets, 6-31+G* and 6-31++G**, are reported in Table 2 (only the values obtained with the larger basis set are discussed in the following). In order to evaluate the influence of the vicinal OH group in formylethanediol on the reaction paths for ester ammonolysis as a reference we consider the reaction with the structure, in which the two O atoms of the ethanediol are in *trans* position and an intramolecular hydrogen bond cannot be formed. In this case the reaction can be accomplished only via tetragonal transition states, $TS_4$1, $TS_4$2, or TSc. The rate-determining step of the stepwise mechanism is the first transition state with ΔE = 52.7 kcal/mol, but the transition state of the concerted mechanism has slightly lower energy, 51.5 kcal/mol.

In the most stable conformers of the tetragonal transition states with intramolecular hydrogen bonds from the vicinal hydroxyl group the electronic energies of $TS_4$1, $TS_4$2, or TSc are reduced to 44.9, 41.2, and 43.8 kcal/mol. Thus, similarly to the reference process, the reaction occurs preferably via concerted mechanism with catalytic effect of the vicinal OH group (reduction of the activation energy barrier) estimated at 7.7 kcal/mol. The reason for this weak catalytic effect is the preservation of the tetragonal structure of transition states, as it is in the case of non-catalyzed process, since this structure imposes rather small angles for proton transfer in the transition states, around 125–130°, much smaller than the optimal angle of 180°.

The other mechanism of catalytic activation of the ester ammonolysis of formylethanediol—by participation of the vicinal OH in the proton transfer via hexagonal transition states, stabilizes considerably the first transition state of the stepwise mechanism, by 21.5 kcal/mol with respect to the referent value. The main reason for this effect is the replacement of single unfavorable proton transfer in $TS_4$1 by two favorable proton transfers via a six-atomic ring in $TS_6$1 that decreases the angular distortions for the proton transfers (the angles for proton transfers are larger, 149° and 155°). However, the energy of the other two transition states TSc_6 and $TS_6$2 is reduced by only 2.2 and 4.9 kcal/mol compared to the reference reaction since their structures are partially constrained from five-atomic ring for proton transfer (see Scheme 1b and Fig. 5). Comparing the activation energy barriers for the hexagonal transition states, 31.2 kcal/mol, 25.2 kcal/mol (with respect to the intermediate), and 49.3 kcal/mol for $TS_6$1, $TS_6$2 and TSc_6, one finds that the reaction occurs preferably by stepwise mechanism with its first step as rate-determining. Since this barrier, 31.2 kcal/mol, is significantly lower than the energy barriers for the tetragonal transition states with or without hydrogen bond from the vicinal hydroxyl, 43.8 and 51.5 kcal/mol, we can conclude that the process via hexagonal transition states is preferable.

The analysis of the activation energies of the lowest energy transition states of the different reaction pathways for ammonolysis of acylated diol suggests that the total catalytic effect of the vicinal OH group can be estimated at 21.5 kcal/mol when the reaction occurs via hexagonal transition states. As reported elsewhere [52], the analysis of the Gibbs free energy of activation of different transition states resulted in essentially the same conclusion.

Table 2
Electronic energy ΔE (in kcal/mol) of the intermediate, product, and transition state structures with lowest energy for each type of transition state for 1-O-formyl 1,2-ethanediol ammonolysis[a]. The energies are calculated with respect to the initial state.

Energy	Basis set	I	Product[b]	TSc	TS1	TS2
Reference (no H-bond)	6-31+G*	16.7	−2.6	53.5	54.7	48.3
Tetragonal TS		11.2	−2.6	45.0	46.4	44.1
Hexagonal TS		11.2	−2.6	50.9	32.5	42.3
Reference (no H-bond)	6-31++G**	16.6	−4.5	51.5	52.7	45.2
Tetragonal TS		9.9	−4.5	43.8	44.9	41.2
Hexagonal TS		9.9	−4.5	49.3	31.2	40.3

[a] The reaction mechanism is shown in Scheme 1 and the structures corresponding to the stationary points along the reaction paths are provided in Figs. 2 and 5.
[b] The reported energy values correspond to a complex formed by the species produced during the reaction.

In order to evaluate the influence of the polarization and diffuse functions in the basis set of hydrogen atoms, we can compare the calculated energies of different stationary points along the reaction paths obtained with 6-31 + G* and 6-31 + + G** basis sets (Table 2). With the larger basis set all energies are reduced compared to the initial state by up to 3.1 kcal/mol. The largest reduction is found for TS2 transition states by 2.0–3.1 kcal/mol, while the intermediates are stabilized by at most 1.4 kcal/mol. This difference likely reflects the importance of the proton transfer in the transition states, which is described better with diffuse and polarization functions added for hydrogen atoms.

The results reported here can be related to an experimental study of the intramolecular aminolysis reactions in presence and absence of a vicinal OH group [57]. In agreement with the computational results for acceleration of the reaction via the hexagonal transition states, the lactamization of ornithinyl adenosine is orders of magnitude faster as compared to the lactamization of the corresponding deoxy compound.

5. Conclusions

By modeling the structure of formic acid and its dimer and of the ammonolysis of formic acid at different levels of theory including about sixty combinations of 6 quantum-chemical methods and different basis sets and further statistical analysis of the obtained structural and energetic data, we defined B3LYP/6-31G** level as the least time consuming, yet still reliable method for correct description of the geometry of the modeled structures and the reaction energies.

The conformational search procedure described in the current paper and implemented in the MolRan program suite allows identification of all distinguishable conformers of the transition states and selection of the lowest energy structures thus, leading to prediction of the energy favorable reaction route. As demonstrated here, the procedure is appropriate for tuning the geometry of transition states with known structure of the reaction center and with large conformational freedom of the parts of the reacting molecules not involved in the reaction center. On the other hand, we have also showed the successful application of the complex method for generation of initial structures of unknown transition states based on pre-defined bonding (topology) between atoms participating in bond-breaking and forming.

Acknowledgement

The work was supported by Bulgarian National Fund for Scientific Research (contracts DOO2-133 and DOO2-210).

References

[1] M.R.A. Blomberg, P.E.M. Siegbahn, Quantum chemistry as a tool in bioenergetics, Biochim. Biophys. Acta 1797 (2010) 129–142.
[2] P. Banáš, P. Jurečka, N.G. Walter, J. Šponer, M. Otyepka, Theoretical studies of RNA catalysis: hybrid QM/MM methods and their comparison with MD and QM, Methods 49 (2009) 202–216.
[3] T. Dudev, C. Lim, Metal binding affinity and selectivity in metalloproteins: insights from computational studies, Ann. Rev. Biophys. 37 (2008) 97–116.
[4] J. Gao, S. Ma, D.T. Major, K. Nam, J. Pu, D.G. Truhlar, Mechanisms and free energies of enzymatic reactions, Chem. Rev. 106 (2006) 3188–3209.
[5] N. Rösch, V.A. Nasluzov, K.M. Neyman, G. Pacchioni, G.N. Vayssilov, Supported metal species and adsorption complexes on metal oxides and in zeolites: density functional cluster model studies, in: J. Leszczynski (Ed.), Computational Material Science. Theoretical and Computational Chemistry Series, vol. 15, Elsevier, Amsterdam, 2004, pp. 367–450.
[6] K. Morokuma, Theoretical studies of structure, function and reactivity of molecules—a personal account, Proc. Jpn. Acad. B 85 (2009) 167–182.
[7] L.V. Moskaleva, Z.-X. Chen, H.A. Aleksandrov, A.B. Mohammed, Q. Sun, N. Rösch, Ethylene conversion to ethylidyne over Pd(1 1 1): revisiting the mechanism with first-principles calculations, J. Phys. Chem. C 113 (2009) 2512–2520.
[8] D. Loffreda, F. Delbecq, F. Vigné, P. Sautet, Fast prediction of selectivity in heterogeneous catalysis from extended brønsted-evans-polanyi relations: a theoretical insight, Angew. Chem., Int. Ed. 48 (2009) 8978–8980.
[9] T. Mineva, E. Sicilia, N. Russo, Density-functional approach to hardness evaluation and its use in the study of the maximum hardness principle, J. Am. Chem. Soc. 120 (1998) 9053–9058.
[10] F.P. Rotzinger, Treatment of substitution and rearrangement mechanisms of transition metal complexes with quantum chemical methods, Chem. Rev. 105 (2005) 2003–2037.
[11] B. Galabov, V. Nikolova, J.J. Wilke, H.F. Schaefer, W.D. Allen, Origin of the S_N2 benzylic effect, J. Am. Chem. Soc. 130 (2008) 9887–9896.
[12] E. Proynov, J. Kong, Assessment of a new hybrid functional on thermochemistry, metal–ligand bonding and reaction barriers, in: G.N. Vayssolov, T. Mineva (Eds.), Theoretical Aspects of Catalysis, vol. 3, Heron Press, Sofia, 2009, pp. 1–9.
[13] M.A. Rangelov, G.N. Vayssilov, V.M. Yomtova, D.D. Petkov, Theoretical study of the *o*-OH participation in catechol ester ammonolysis, Org. Biomol. Chem. 3 (2005) 737–744.
[14] M.A. Rangelov, G.N. Vayssilov, D.D. Petkov, Quantum chemical model study of the acyl migration in 2′(3′)-formylnucleosides, Int. J. Quant. Chem. 106 (2006) 1346–1356.
[15] A. Gindulyte, A. Bashan, I. Agmon, L. Massa, A. Yonath, J. Karel, The transition state for formation of the peptide bond in the ribosome, Proc. Natl. Acad. Sci. U.S.A. 103 (2006) 13327–13332.
[16] G. Wallin, J. Åqvist, The transition state for peptide bond formation reveals the ribosome as a water trap, Proc. Natl. Acad. Sci. U.S.A. 107 (2010) 1888–1893.
[17] M.A. Rangelov, G.N. Vayssilov, V.M. Yomtova, D.D. Petkov, The syn-oriented 2-OH provides a favorable proton transfer geometry in 1,2-diol monoester aminolysis: implications for the ribosome mechanism, J. Am. Chem. Soc. 128 (2006) 4964–4965.
[18] M.V. Rodnina, M. Beringer, W. Wintermeyer, Mechanism of peptide bond formation on the ribosome, Quart. Rev. Biophys. 39 (2006) 203–225.
[19] M.M. Changalov, G.D. Ivanova, M.A. Rangelov, P. Acharia, S.N. Acharya, Minakawa, A. Foldesi, I.B. Stoineva, V.M. Yomtova, C.D. Roussev, A. Matsuda, J. Chattopadhyaya, D.D. Petkov, 2′/3′-O-peptidyl adenosine as a general base catalyst of its own external peptidyl transfer: implications for the ribosome catalytic mechanism, ChemBioChem 6 (2005) 992–996.
[20] M.H. Zhong, S.A. Strobel, Synthesis of isotopically labeled P-site substrates for the ribosomal peptidyl transferase reaction, J. Org. Chem. 73 (2008) 603–611.
[21] M.A. Rangelov, *MolRan*, Version 1.8, 2008. More information about the program can be obtained from the author via e-mail: mran@orgchm.bas.bg.
[22] M.J. Frisch, G.W. Trucks, H.B. Schlegel, G.E. Scuseria, M.A. Robb, J.R. Cheeseman, J.A. Montgomery Jr., T. Vreven, K.N. Kudin, J.C. Burant, J.M. Millam, S.S. Iyengar, J. Tomasi, V. Barone, B. Mennucci, M. Cossi, G. Scalmani, N. Rega, G.A. Petersson, H. Nakatsuji, M. Hada, M. Ehara, K. Toyota, R. Fukuda, J. Hasegawa, M. Ishida, T. Nakajima, Y. Honda, O. Kitao, H. Nakai, M. Klene, X. Li, J.E. Knox, H.P. Hratchian, J.B. Cross, V. Bakken, C. Adamo, J. Jaramillo, R. Gomperts, R.E. Stratmann, O. Yazyev, A.J. Austin, R. Cammi, C. Pomelli, J.W. Ochterski, P.Y. Ayala, K. Morokuma, G.A. Voth, P. Salvador, J.J. Dannenberg, V.G. Zakrzewski, S. Dapprich, A.D. Daniels, M.C. Strain, O. Farkas, D.K. Malick, A.D. Rabuck, K. Raghavachari, J.B. Foresman, J.V. Ortiz, Q. Cui, A.G. Baboul, S. Clifford, J. Cioslowski, B.B. Stefanov, G. Liu, A. Liashenko, P. Piskorz, I. Komaromi, R.L. Martin, D.J. Fox, T. Keith, M.A. Al-Laham, C.Y. Peng, A. Nanayakkara, M. Challacombe, P.M.W. Gill, B. Johnson, W. Chen, M.W. Wong, C. Gonzalez, J.A. Pople, Gaussian 03, Revision E.01, Gaussian, Inc., Wallingford, CT, 2004.
[23] J.A. Pople, J.S. Binkley, R. Seeger, Theoretical models incorporating electron correlation, Int. J. Quant. Chem. 10 (1976) 1–19.
[24] M.J. Frisch, M. Head-Gordon, J.A. Pople, A direct MP2 gradient method, Chem. Phys. Lett. 166 (1990) 275–280.
[25] R. Ditchfield, W.J. Hehre, J.A. Pople, Self-consistent molecular-orbital methods. IX. An extended gaussian-type basis for molecular-orbital studies of organic molecules, J. Chem. Phys. 54 (1971) 724–728.
[26] W.J. Hehre, R. Ditchfield, J.A. Pople, Self-consistent molecular orbital methods. XII. Further extensions of gaussian-type basis sets for use in molecular orbital studies of organic molecules, J. Chem. Phys. 56 (1972) 2257–2261.
[27] P.C. Hariharan, J.A. Pople, Accuracy of AH_n equilibrium geometries by single determinant molecular orbital theory, Mol. Phys. 27 (1974) 209–214.
[28] M.S. Gordon, The isomers of silacyclopropane, Chem. Phys. Lett. 76 (1980) 163–168.
[29] P.C. Hariharan, J.A. Pople, The influence of polarization functions on molecular orbital hydrogenation energies, Theor. Chim. Acta 28 (1973) 213–222.
[30] R. Krishnan, J.A. Pople, Approximate fourth-order perturbation theory of the electron correlation energy, Int. J. Quant. Chem. 14 (1978) 91–100.
[31] R. Krishnan, M.J. Frisch, J.A. Pople, Contribution of triple substitutions to the electron correlation energy in fourth order perturbation theory, J. Chem. Phys. 72 (1980) 4244–4245.
[32] J.A. Pople, R. Krishnan, H.B. Schlegel, J.S. Binkley, Electron correlation theories and their application to the study of simple reaction potential surfaces, Int. J. Quant. Chem. 14 (1978) 545–560.
[33] J.S. Binkley, J.A. Pople, W.J. Hehre, Self-consistent molecular orbital methods. 21. Small split-valence basis sets for first-row elements, J. Am. Chem. Soc. 102 (1980) 939–947.
[34] A.D. McLean, G.S. Chandler, Contracted Gaussian basis sets for molecular calculations. I. Second row atoms, $Z = 11–18$, J. Chem. Phys. 72 (1980) 5639–5648.
[35] N.L. Allinger, Conformational analysis. 130. MM2. A hydrocarbon force field utilizing V_1 and V_2 torsional terms, J. Am. Chem. Soc. 99 (1977) 8127–8134.

[36] A. Hocquet, M. Langgård, An evaluation of the MM + force field, J. Mol. Model. 4 (1998) 94–112.
[37] S.S. Rao, Engineering Optimization: Theory and Practice, Wiley–Interscience, 1996.
[38] S. Stoyanov, Optimization of Technological Processes, Tehnika, Sofia, Bulgaria, 1993 (in Bulgarian).
[39] J. Hermans, Hydrogen bonds in molecular mechanics force fields, Adv. Protein Chem. 72 (2005) 105–119.
[40] A. Almenningen, O. Bastiansen, T. Motifeldt, A reinvestigation of the structure of monomer and dimer formic acid by gas electron diffraction technique, Acta Chem. Scand. 23 (1969) 2848–2864.
[41] A.F. Wells, Structural Inorganic Chemistry, Oxford University Press, Oxford, UK, 1984.
[42] J.D. Cox, G. Pilcher, Thermochemistry of Organic and Organometallic Compounds, Academic Press, New York, 1970.
[43] T. Oie, G.H. Loew, S.K. Burt, J.S. Binkley, R.D. MacElroy, Quantum chemical studies of a model for peptide bond formation: formation of formamide and water from ammonia and formic acid, J. Am. Chem. Soc. 104 (1982) 6169–6174.
[44] J.H. Jensen, K.K. Baldridge, M.S. Gordon, Uncatalyzed peptide bond formation in the gas phase, J. Phys. Chem. 96 (1992) 8340–8351.
[45] S. Chalmet, W. Harb, M.F. Ruiz-Lopez, Computer simulation of amide bond formation in aqueous solution, J. Phys. Chem. A 105 (2001) 11574–11581.
[46] O. Takahashi, Y. Kohno, M. Nishio, Relevance of weak hydrogen bonds in the conformation of organic compounds and bioconjugates: evidence from recent experimental data and high-level *ab initio* MO calculations, Chem. Rev. (2010), doi:10.1021/cr100072x.
[47] Y. Zhao, D. Truhlar, The M06 suite of density functionals for main group thermochemistry, thermochemical kinetics, noncovalent interactions, excited states, and transition elements: two new functionals and systematic testing of four M06-class functionals and 12 other functionals, Theor. Chem. Acc. 120 (2008) 215–241.
[48] M. Simonović, T.A. Steitz, A structural view on the mechanism of the ribosome-catalyzed peptide bond formation, Biochim. Biophys. Acta 1789 (2009) 612–623.
[49] M.V. Rodnina, W. Wintermeyer, Peptide bond formation on the ribosome: structure and mechanism, Curr. Opin. Struct. Biol. 13 (2003) 334–340.
[50] M. Beringer, M.V. Rodnina, The ribosomal peptidyl transferase, Mol. Cell. 26 (2007) 311–321.
[51] I. Wekselman, C. Davidovich, I. Agmon, E. Zimmerman, H. Rozenberg, A. Bashan, R. Berisio, A. Yonath, Ribosome's mode of function: myths, facts and recent results, J. Pept. Sci. 15 (2009) 122–130.
[52] M.A. Rangelov, G.P. Petrova, V.M. Yomtova, G.N. Vayssilov, Catalytic Role of Vicinal OH in Ester Aminolysis - Proton Shuttle versus Hydrogen-Bonds Stabilization, submitted for publication.
[53] G.M. Blackburn, W.P. Jencks, The mechanism of the aminolysis of methyl formate, J. Am. Chem. Soc. 90 (1968) 2638–2645.
[54] K. Takashima, J.M. Riveros, Gas-phase pathways for ester hydrolysis, J. Am. Chem. Soc. 100 (1978) 6128–6132.
[55] S. Ilieva, B. Galabov, D.G. Musaev, K. Morokuma, H.F. Schaefer, Computational study of the aminolysis of esters. The reaction of methylformate with ammonia, J. Org. Chem. 68 (2003) 1496–1502.
[56] M.J. Box, A new method of constrained optimization and a comparison with other methods, Comput. J. 8 (1965) 42–52.
[57] S.G. Bayryamov, M.A. Rangelov, A.P. Mladjova, V. Yomtova, D.D. Petkov, Unambiguous evidence for efficient chemical catalysis of adenosine ester aminolysis by its 2′/3′-OH, J. Am. Chem. Soc. 129 (2007) 5790–5791.

JOC Article
pubs.acs.org/joc

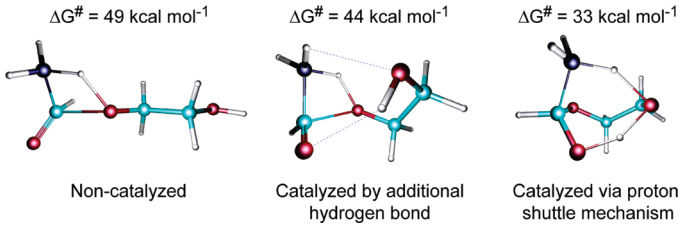
Catalytic Role of Vicinal OH in Ester Aminolysis: Proton Shuttle versus Hydrogen Bond Stabilization

Miroslav A. Rangelov,*[,†] Galina P. Petrova,[‡] Vihra M. Yomtova,[†] and Georgi N. Vayssilov*[,‡]

[†]*Laboratory of BioCatalysis, Institute of Organic Chemistry, Bulgarian Academy of Sciences, Str. Acad. G. Bontchev, Bl. 9, 1113 Sofia, Bulgaria, and* [‡]*Faculty of Chemistry, University of Sofia, Boulevard James Bouchier 1, 1164 Sofia, Bulgaria*

mran@orgchm.bas.bg; gnv@chem.uni-sofia.bg.

Received May 18, 2010



This computational study provoked by the process of peptide bond formation in the ribosome investigates the influence of the vicinal OH group in monoacylated diols on the elementary acts of ester aminolysis. Two alternative approaches for this influence on ester ammonolysis were considered: stabilization of the transition states by hydrogen bonds and participation of the vicinal hydroxyl in proton transfer (proton shuttle). The activation due to hydrogen bonds of the vicinal hydroxyl via tetragonal transition states was rather modest; the free energy of activation was reduced by only 5.2 kcal/mol compared to the noncatalyzed reaction. The catalytic activation via the proton shuttle mechanism with participation of the vicinal OH in the proton transfer via hexagonal transition states resulted in considerable reduction of the free energy of activation to 33.5 kcal/mol, i.e., 16.0 kcal/mol lower than in the referent process. Accounting for the influence of the environment on the reaction center by a continuum model (for ε from 5 to 80) resulted in further stabilization of the rate-determining transition state by 4−5 kcal/mol. The overall reduction of the reaction barrier by about 16 kcal/mol as compared to the noncatalyzed process corresponds to about 10^9-fold acceleration of the reaction, in agreement with the experimental estimate for acceleration of this process in the ribosome.

Introduction

The elementary chemical reaction leading to peptide bond synthesis in the ribosome is an aminolysis reaction. During the elementary act of peptide bond formation the growing polypeptide chain, esterified to the *cis*-1,2-diol of tRNA 3′-terminal adenosine, reacts with the next amino acid in the ribosome peptidyl transfer center. For this reason, the aminolysis of esters was extensively studied both experimentally[1] and theoretically[2] as a model reaction for the formation of peptide bonds in living cells. Various computational studies on the mechanism of this reaction were based on small model systems. In order to simulate the ribosome interior at the peptidyl transferase center,[3] these model studies are performed under vacuum or in aprotic solvents with low polarity. Thus, the reaction occurs without

(1) (a) Rodnina, M. V.; Beringer, M.; Wintermeyer, W. *Q. Rev. Biophys.* **2006**, *39*, 203–225. (b) Zhong, M. H.; Strobel, S. A. *J. Org. Chem.* **2008**, *73*, 603–611. (c) Simonovic, M.; Steitz, T. A. *Proc. Natl. Acad. Sci. U. S. A.* **2008**, *105*, 500–505. (d) Schroeder, G. K.; Wolfenden, R. *Biochemistry* **2007**, *46*, 4037–4044. (e) Weinger, J. S.; Parnell, K. M.; Dorner, S.; Green, R.; Strobel, S. A. *Nat. Struct. Mol. Biol.* **2004**, *11*, 1101–1106. (f) Dorner, S.; Panuschka, C.; Schmid, W.; Barta, A. *Nucleic Acids Res.* **2003**, *31*, 6536–6542.

(2) (a) Strajbl, M.; Florian, J.; Warshel, A. *J. Am. Chem. Soc.* **2000**, *122*, 5354–5366. (b) Trobro, S.; Åqvist, J. *Proc. Natl. Acad. Sci. U. S. A.* **2005**, *102*, 12395–12400. (c) Trobro, S.; Aqvist, J. *Biochemistry* **2006**, *45*, 7049–7056. (d) Gindulyte, A.; Bashan, A.; Agmon, I.; Massa, L.; Yonath, A.; Karel, J. *Proc. Natl. Acad. Sci. U. S. A.* **2006**, *103*, 13327–13332.

(3) Ban, N.; Nissen, P.; Hansen, J.; Moore, P. B.; Steitz, T. A. *Science* **2000**, *289*, 905–920.

Published on Web 09/15/2010 DOI: 10.1021/jo100886p

© 2010 American Chemical Society

formation of zwitterionic intermediates, typical for reactions taking place in water[4] or in strongly polar enzyme environments.[5] Several groups[6,7] investigated peptide bond formation in formamide from ammonia and formic acid and proposed two reaction pathways, concerted and stepwise, that have comparable reaction barriers or with small preference of one of the reaction mechanisms. Galabov et al.[7] found that accounting for the solvent effect (acetonitrile) via the polarizable continuum model (PCM) reduced the activation barrier of the concerted mechanism as compared to the stepwise one. On the other hand, for larger model reactants such as methylformate, methylacetate, methylamine, etc.,[6d,7a,c] the preference for a concerted or stepwise mechanism depends on the reactants. All these model studies, however, suggested that the activation barrier of the (uncatalyzed) process is typically above 40 kcal/mol, which corresponds to a rather low reaction rate incomparable with the actual reaction rates of peptide bond formation in living cells.

In order to clarify the reasons for the relatively high reaction rate, the catalytic effect of external molecules (e.g., water, ammonia, or larger molecules having both proton-donating and proton-accepting centers) has been modeled.[8−10] Indeed, these external molecules were found to reduce the activation barrier by facilitation of the proton transfer in the reaction center. Although, the XRD studies[3] have hypothesized that water may be present in the ribosome interior, the participation of an occasionally appearing water molecule at the reaction center in the formation of each individual peptide bond cannot be considered as a reliable option. Such water molecules may also cause hydrolysis of the growing peptide chain from the tRNA instead of catalyzing each aminolysis step. An alternative catalytic effect on the reaction could come from the 2′-OH of the 3′ terminal adenosine of tRNA, which is always close to the reaction center. The crucial role of the vicinal 2′-OH on the catalytic activity of ribozymes was experimentally confirmed by the loss of peptidyl transferase activity of the ribosome with mutant 2′-deoxy-peptidyl-tRNA.[1e,11] Thus, despite the remarkable progress in ribosome structure investigations, the mechanism of peptide bond formation in the ribosome remains obscure. In our earlier work we modeled the intramolecular catalytic effect of the vicinal OH group by the ammonolysis of monoacylated catechol.[12] In that case the vicinal OH stabilizes the transition states of the reaction via formation of hydrogen bonds (HB) with reaction centers, but the estimated reduction of the activation energy with respect to a substrate without a vicinal OH group was found to be rather small, 2.2 kcal/mol. Thus, in order to elucidate the influence of the vicinal hydroxyl group, here we investigate its influence within a more flexible diol model, 1-*O*-formyl-1,2-ethanediol. This substrate is suitable as a model since the vicinal hydroxyls are bound to two neighboring sp^3-hybridized carbon atoms, similarly to the 3′- and 2′-OH of tRNA in the 3′ terminal adenosine. In a preliminary communication,[13] we reported considerable reduction of the activation barrier of the whole process due to participation of the vicinal hydroxyl in the proton transfer cycle. Here, we report the detailed results of the investigation including an exhaustive search for various possible conformations of the transition states in which the vicinal hydroxyl group forms intramolecular hydrogen bonds resulting in stabilization of the observed structures or actively participates in the proton transfer, the so-called proton shuttle mechanism. In addition, we determined the optimal positions of an adjacent OH group for lowering the energy of different transition states via formation of hydrogen bonds.

A recent paper by Wallin and Åqvist[14] extended the idea of participation of the vicinal OH in the proton transfer to inclusion of one or two additional water molecules in the transition state, thus forming at least three fused rings (seven- and eight-membered) in which bond formation and breaking occur. The reduction of the activation enthalpy of the reaction to 18 kcal/mol, although fitting well the experimental estimate,[15] should be taken with caution due to neglect of the entropic contribution caused by the frustrated mobility of the water molecules.

Results and Discussion

Various theoretical studies[2,6−10] have established that the noncatalyzed ammonolysis of esters in aprotic media occurs via either a concerted or a stepwise mechanism, shown in the left-hand side of Scheme 1a (for the notation applied see Scheme 1b). The structure of the transition states of both mechanisms is similar: tetragonal formed by C, O, N/O, and H atoms located almost in one plane. The concerted mechanism proceeds in a single step via the transition state TSc[4] and involves nucleophilic attack of the N atom to the carbonyl carbon atom, simultaneous proton transfer from ammonia to the substrate molecule, and a cleavage of the ester C−Oe bond, leading to formation of the products. On the other hand, the stepwise mechanism goes through formation of an intermediate, I, in which the NH_3 molecule is attached to the C=O bond of the ester and the former carbonyl carbon atom is in a tetrahedral configuration. The transition states for formation and decomposition of this intermediate, TS1 and TS2, include active participation of the carbonyl Oc atom in the process via subsequent addition of ammonia and elimination of alcohol.

(4) (a) Chalmet, S.; Harb, W.; Ruiz-Lopez, M. F. *J. Phys. Chem. A* **2001**, *105*, 11574–11581. (b) Sung, D. D.; Koo, I. S.; Yang, K.; Lee, I. *Chem. Phys. Lett.* **2006**, *426*, 280–284.

(5) Perdih, A.; Hodoscek, M.; Solmajer, T. *Proteins* **2009**, *74*, 744–759.

(6) (a) Oie, T.; Loew, G. H.; Burt, S. K.; Binkley, J. S.; MacElroy, R. D. *J. Am. Chem. Soc.* **1982**, *104*, 6169–6174. (b) Jensen, J. H.; Baldridge, K. K.; Gordon, M. S. *J. Phys. Chem.* **1992**, *96*, 8340–8351. (c) Wang, L.; Zipse, H. *Liebigs Ann.* **1996**, 1501–2509. (d) Zipse, H.; Wang, L.; Houk, K. N. *Liebigs Ann.* **1996**, 1511–1522.

(7) (a) Ilieva, S.; Galabov, B.; Musaev, D. G.; Morokuma, K.; Schaefer, H. F., III. *J. Org. Chem.* **2003**, *68*, 1496–1502. (b) Galabov, B.; Atanasov, Y.; Ilieva, S.; Schaefer, H. F., III. *J. Phys. Chem. A* **2005**, *109*, 11470–11474. (c) Galabov, B.; Ilieva, S.; Hadjieva, B.; Atanasov, Y.; Schaefer, H. F., III. *J. Phys. Chem. A* **2008**, *112*, 6700–6707.

(8) (a) Oie, T.; Loew, G. H.; Burt, S. K.; MacElroy, R. D. *J. Am. Chem. Soc.* **1983**, *105*, 2221–2227. (b) Williams, I. H. *J. Am. Chem. Soc.* **1987**, *109*, 6299–6307. (c) Strajbl, M.; Florian, J.; Warshel, A. *J. Phys. Chem. B* **2001**, *105*, 4471–4484. (d) Sharma, P. K.; Xiang, Y.; Kato, M.; Warshel, A. *Biochemistry* **2005**, *44*, 11307–11314.

(9) Yang, W.; Drueckhammer, D. G. *Org. Lett.* **2000**, *2*, 4133–4136.

(10) Jin, L.; Wu, Y.; Kim, C. K.; Xue, Y. *J. Mol. Struct.* (*THEOCHEM*) **2010**, *942*, 137–144.

(11) Changalov, M. M.; Ivanova, G. D.; Rangelov, M. A.; Acharya, P.; Acharya, S.; Minakawa, N.; Földesi, A.; Stoineva, I. B.; Yomtova, V. M.; Roussev, C. D.; Matsuda, A.; Chattopadhyaya, J.; Petkov, D. D. *ChemBioChem* **2005**, *6*, 992–996.

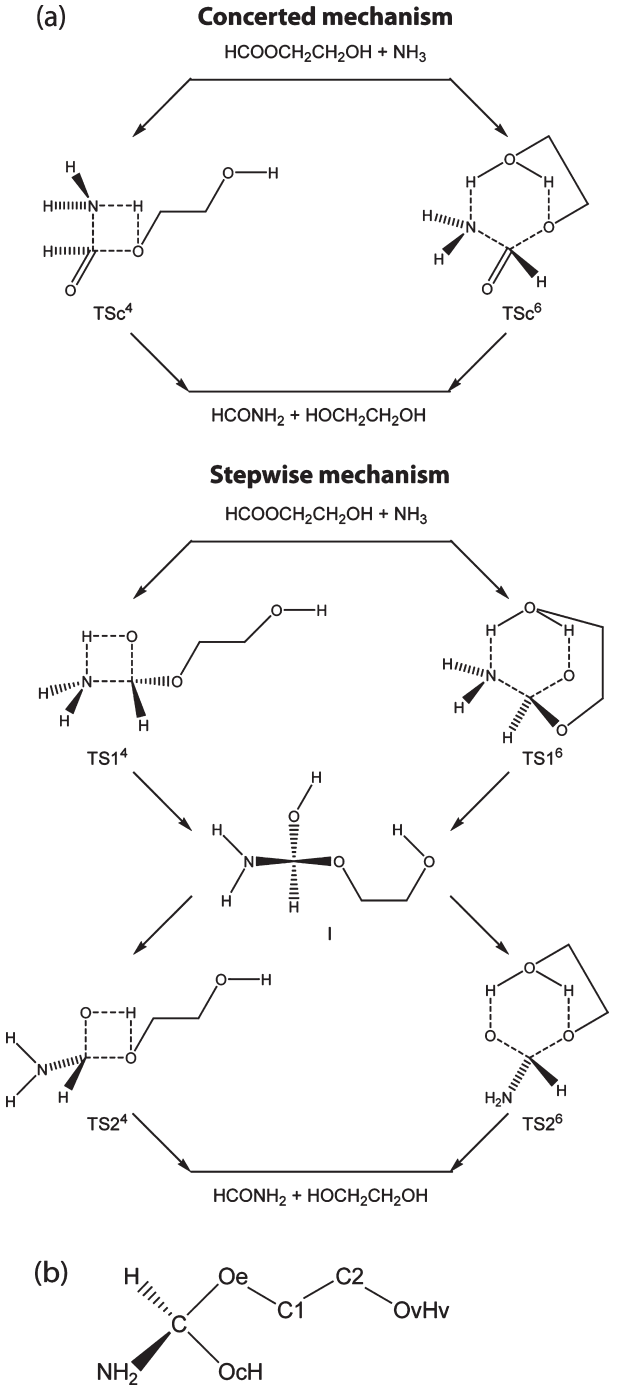
(12) Rangelov, M. A.; Vayssilov, G. N.; Yomtova, V. M.; Petkov, D. D. *Org. Biomol. Chem.* **2005**, *3*, 737–744.

(13) Rangelov, M. A.; Vayssilov, G. N.; Yomtova, V. M.; Petkov, D. D. *J. Am. Chem. Soc.* **2006**, *128*, 4964–4965.

(14) Wallin, G.; Åqvist, J. *Proc. Natl. Acad. Sci. U. S. A.* **2010**, *107*, 1888–1893.

(15) Sievers, A.; Beringer, M.; Rodnina, M. V.; Wolfenden, R. *Proc. Natl. Acad. Sci. U. S. A.* **2004**, *101*, 7897–7901.

SCHEME 1. Proposed Mechanisms for the Ammonolysis of Formyl-1,2-ethanediol via Tetragonal and Hexagonal Transition States (a) and Notation of the Atoms in the Modeled System on the Example of the Tetrahedral Intermediate I (b)



Our search for possible transition states and intermediates during the ammonolysis of monoacylated ethanediol suggested that the vicinal hydroxyl group could influence the reaction mechanism of the studied processes in two different ways: (i) by formation of intramolecular hydrogen bonds with the transition states and intermediates during the reaction resulting in the stabilization of the observed structures; (ii) by participation in the proton transfer (proton shuttle) both as proton donor and acceptor. In the first case the overall reaction path and topology of the transition states are not changed as compared to the noncatalyzed reaction, and the transition states remain tetragonal.

The active participation of the vicinal hydroxyl group in the proton transfer results in formation of a hexagonal TS cycle in which the bond breaking and forming occur due to participation of both Ov and Hv atoms of the vicinal hydroxyl in the elementary act. In both types of catalytic activation via vicinal OH group the intermediate I formed during the stepwise reaction path is the same (Scheme 1); that is, each of the transition states TS1 and TS2 could be either tetragonal or hexagonal (the type of reaction cycle is denoted as superscript). Obviously, the formation of hexagonal transition states is not possible for substrates lacking a vicinal OH group. However, such a role could be played by additional proton-donating and proton-accepting molecules (e.g., water, ammonia, alcohols, etc.) also acting as proton shuttle catalysts.[8a,9] For this reason, we also considered the catalytic influence of an external water molecule as a referent reaction.

The discussion of the different structures below uses the calculated electronic energies relative to the prereaction complex of 1-*O*-formyl-1,2-ethanediol and ammonia, while the analysis of the energetics of the reaction paths for different mechanisms is based on the corresponding Gibbs free energy values.

Catalytic Activation by a Hydrogen Bond from the Vicinal Hydroxyl (Tetragonal Transition States). Concerted Mechanism. The search for transition-state structures with intramolecular hydrogen bonds resulted in six distinguishable structures of TSc^4 with energy lower than that of the referent transition-state structure without a hydrogen bond shown in Figure 1 as filled black symbols and a black bar at the ordinate, respectively. In the different structures we found three types of hydrogen bonds: (i) HB(Oc−Hv) between the carbonyl Oc and the Hv atom from vicinal hydroxyl group (squares); (ii) HB(Ov−Ha) between Ov of the vicinal hydroxyl and one Ha atom from ammonia (diamonds); and (iii) HB(Oe−Hv) between the ester Oe atom and the proton from the vicinal hydroxyl Hv (triangles). In the figure we plotted the relative energy of the modeled transition states against the hydrogen bond length calculated as the distance between either the proton and the proton-acceptor center (a and c) or the proton-donor and proton-acceptor atoms (b and d).

The three couples of conformations differ mainly in the position of the C2 atom relative to the plane defined by the Oe, C1, and Ov atoms. For the structures with intramolecular hydrogen bonds the energy of the structure was found to depend on the proton transfer angle. The average proton transfer angle was estimated to be $125.6 \pm 1.9°$, much smaller than the optimal one of 180°. The first type of hydrogen bonds, HB(Oc−Hv), slightly shorter than the other types, was found in the most stable structure of TSc^4. This structure has also an additional HB between an ammonia hydrogen and Ov and is 7.7 kcal/mol more stable than the referent structure of TSc^4 without hydrogen bonds.

Stepwise Mechanism. For the first transition state of the stepwise mechanism, $TS1^4$, we found the same three types of hydrogen bonds already observed in the TSc^4 states: (i) Oc−Hv, (ii) Ov−Ha, and (iii) Oe−Hv. As could be expected, all obtained geometries with a hydrogen bond are more stable than the corresponding referent structures without a

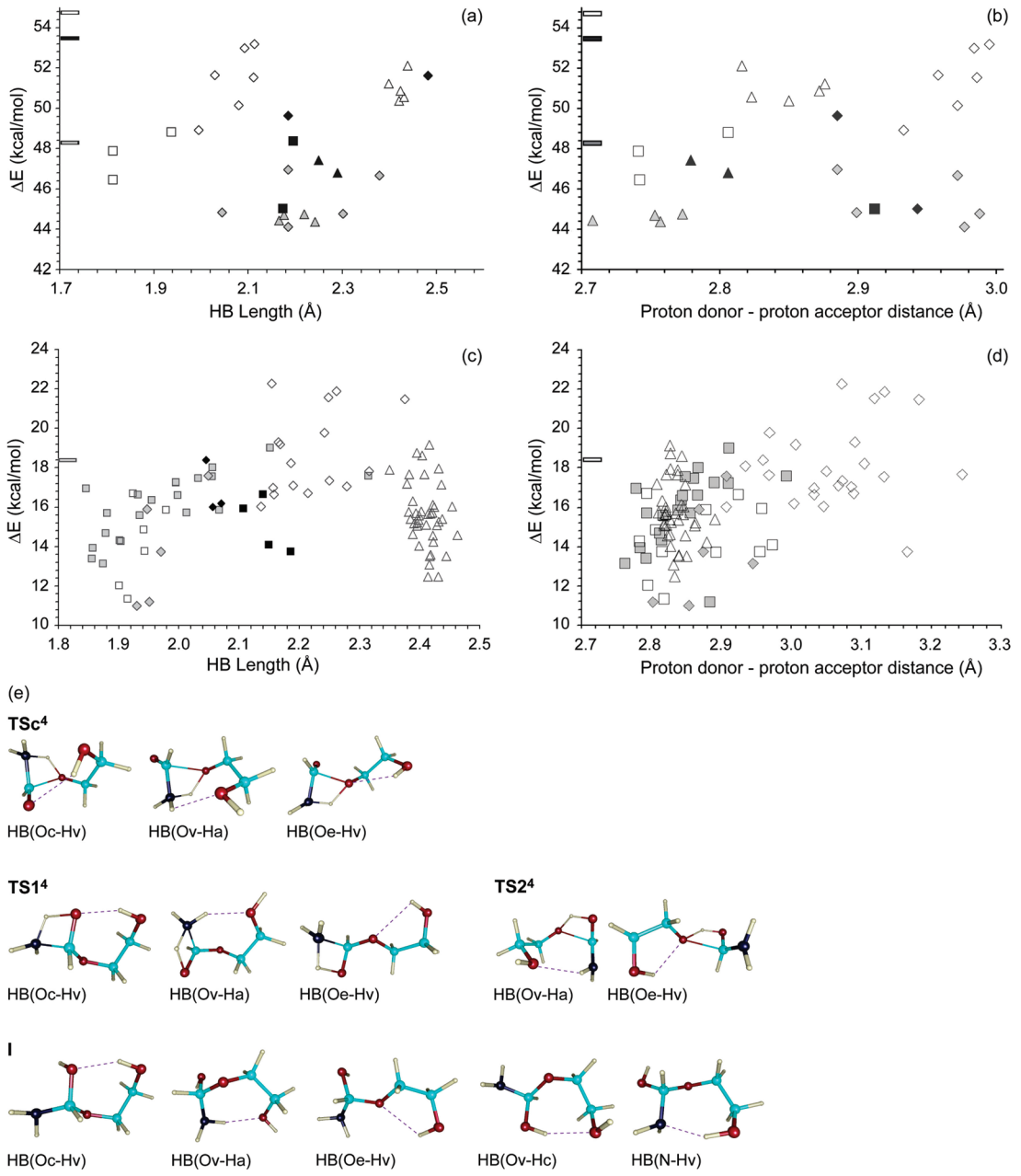


FIGURE 1. Relative energy of the various structures of the modeled tetragonal transition states (panels a and b) and intermediate (panels c and d) versus the length of the formed intramolecular hydrogen bond measured as the distance between the proton and the proton-acceptor center (panels a and c) or the distance between proton-donor and proton-acceptor atoms (panels b and d). Black, white, and gray colors of the symbols in panels (a) and (b) correspond to TSc^4, $TS1^4$, and $TS2^4$ transition state structures, respectively. The type of hydrogen bond is denoted as follows: Oc−Hv, squares; Ov−Ha, diamonds; Oe−Hv, triangles. The energy of the corresponding referent structures without a hydrogen bond is represented by bold bars on the ordinate axis. The type of hydrogen bond in the intermediate in panels (c) and (d) is denoted as follows: Oc−Hv, white squares; Ov−Ha, white diamonds; Oe−Hv, white triangles; Ov−Hc, gray squares; N−Hv, gray diamonds; the black symbols are applied for structures with more than one hydrogen bond. The energy of the referent structures without a hydrogen bond is represented by a bold bar on the ordinate axis. The reported energies are obtained at the B3LYP/6-31+G* level. (e) Examples of different types of hydrogen bonds in the transition states and the intermediate (color coding H, white; C, light blue; O, red; N, dark blue).

hydrogen bond (see Figure 1a,b; white symbols and white bar on the ordinate, respectively).

Similarly, the shortest hydrogen bonds are observed in the first type of structures with HB(Oc−Hv) as the average energy is estimated as 47.7 kcal/mol, and the structures are 7.0 kcal/mol more stable than the referent structure.

More than 70 stable conformations of intermediate I formed after $TS1^4$ along the stepwise reaction path were found. The large number of conformers is determined by the presence of three groups, NH_2, OvHv, and OcHc, that can form hydrogen bonds both as proton donors and proton acceptors. In addition, the Oe atom can act as a proton acceptor; that is, in total nine types of HB could be formed. However, four of these hydrogen bonds (N−Hc, Oc−Ha, Oe−Ha, and Oe−Hc) could be realized only via a four-membered cycle, which is disfavored as compared to five-membered cycles. On the other hand,

the vicinal OH group due to its distant location from the reaction centers forms large hydrogen-bonded cycles and takes part in the five remaining types of HB, observed in the stable structures of the intermediate. The influence of the hydrogen bond length on the stability of the modeled structures is presented in Figure 1c,d.

The structures with hydrogen bonds including the two hydroxyl groups, OcHc and OvHv, display the shortest hydrogen bonds in the intermediate with bond lengths of ca. 1.9 Å (Figure 1c) or 2.8 Å (Figure 1d), estimated as the distance between the proton acceptor and the proton or the proton donor. While the structures with OcHc as proton donor have a shorter HB, the structures with the reverse type of HB, i.e., with Oc as proton acceptor, have lower energy. The conformations with a HB between the N atom of the amino group as proton acceptor and the vicinal OH group as proton donor also have low energy, while the structures with reversed proton donor/acceptor are the least stable among all modeled intermediate structures. This is not surprising considering the relatively high basicity of the NH_2 group and the relatively high acidity of the OH group.

Similarly to TSc[4] and TS1[4], the formation of intramolecular hydrogen bonds results in stabilization of the second transition state, TS2, of the stepwise mechanism compared to the referent structure without a hydrogen bond (Figure 1a; gray symbols). Most of the observed structures with a HB have very similar energies, around 44 ± 2 kcal/mol. Unlike TSc and TS1 transition states, in this case only the last two types of hydrogen bonds are found: HB(Ov−Ha) (ii, diamonds) and HB(Oe−Hv) (iii, triangles). The HB(Oe−Hv) bonds have average energy of ca. 45.5 kcal/mol. The most stable structure among these conformers features the largest proton transfer angle, 130°.

Influence of the Orientation of the Hydrogen Bond. Since the structures containing an Oc−Hv hydrogen bond with vicinal OH as proton donor were found to be the most stable among the different modeled forms of the two rate-determining transition states TSc[4] and TS1[4], it could be instructive to estimate the influence of the hydrogen bond orientation on the stability of the two transition structures. For this reason, we studied the strength of the hydrogen bond formed between a water molecule and the Oc center of the TSc[4] and TS1[4] transition states for formic acid ammonolysis. The analysis is performed via stepwise variation of the valence angle C−Oc−Hw (Hw from the water molecule, participating in the hydrogen bond), denoted as A, and the dihedral angle D between the planes formed by C, Oc, and Hw, on one hand, and C, Oc, and N atoms, on the other (see left-hand part of Figure 2). The variation of the chosen angles is schematically presented in Figure S1 of the Supporting Information. In the applied procedure only the direction of the O−Hw bond in the water molecule is kept fixed, while the normal coordinates of the water molecule as well as the positions of the other atoms in the H_2O molecule relative to the transition-state structure are optimized. The obtained results are summarized in Figure 2 (a and b panels correspond to TSc[4] and TS1[4], respectively), representing the potential energy surface (PES) slice versus the two angles A and D.

According to the results obtained, the stabilization of TSc[4] resulting from the formation of a hydrogen bond with the Oc atom is ca. 5 kcal/mol for a large range of angles A and D. On the other hand, the hydrogen bond is most effective at angles

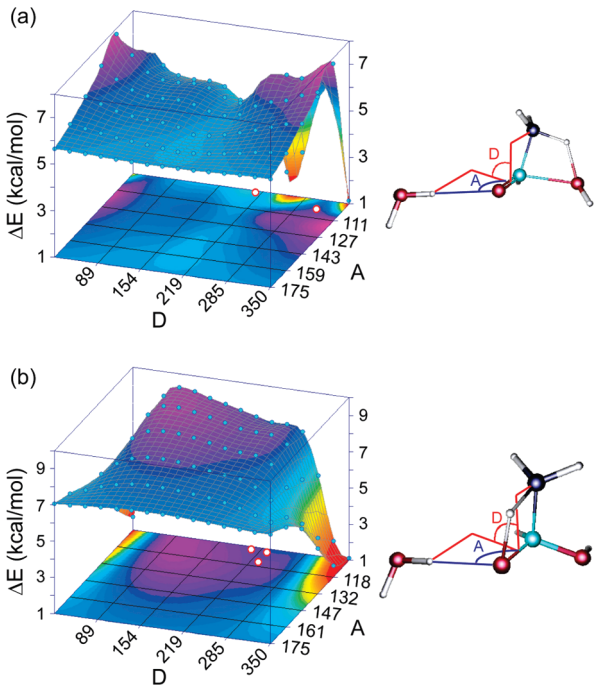


FIGURE 2. PES slice representing the influence of a water molecule on the stability of transition states TSc[4] (a) and TS1[4] (b) in the ammonolysis of formic acid. The blue points depict calculated values for the stabilization energy, while the white points represent the structures with minimal energy for formylethanediol as substrate. Definitions of angles A and D are shown on the right.

A = 120 ± 10° and D = 0 ± 10°, resulting in a decrease of the energy of the structure by 8 kcal/mol. The stabilization could be explained by the formation of an additional hydrogen bond between the Ha atom from the ammonia molecule and the oxygen atom Ow in the water molecule, and the contribution of such an additional hydrogen bond is roughly estimated to be 2−3 kcal/mol (Figure 2).

As discussed above, a similar effect was indeed observed in the case of the most stable structure of TSc[4] during ammonolysis of formylethanediol in which the formation of the two hydrogen bonds Oc−Hc and Ov−Ha results in stabilization of the transition state by 7.7 kcal/mol compared to the referent structure. The angles A and D (notation in Figure 2) for the most stable structure of the transition state TSc[4] in the ammonolysis process of formylethanediol are estimated to be A = 104.3° and D = −47.1°, i.e., close to the optimal values since the mobility of the vicinal OH group as related to the reaction center is limited by the covalent bonds.

The stabilization of the TS1[4] (Figure 2b) is estimated to be about 7 kcal/mol for a wide range of values of the angles A and D, while the maximal stabilization that can be achieved via the hydrogen bond is 9.5 kcal/mol for the optimal values of the angles A and D of 106° and 100°, respectively. The corresponding TS1[4] structures for formylethanediol with lowest energy (see the white circles on the projected PES plot) are characterized by almost optimal values of the valence angle A, around 110°, but the dihedral angle D, around 220°, differs considerably from the optimal one. The optimal value of the latter angle cannot be achieved since the position of the vicinal OH group in the ethanediol system is at the reverse side of the plane, defined by the atoms participating in the proton transfer process. The stabilization

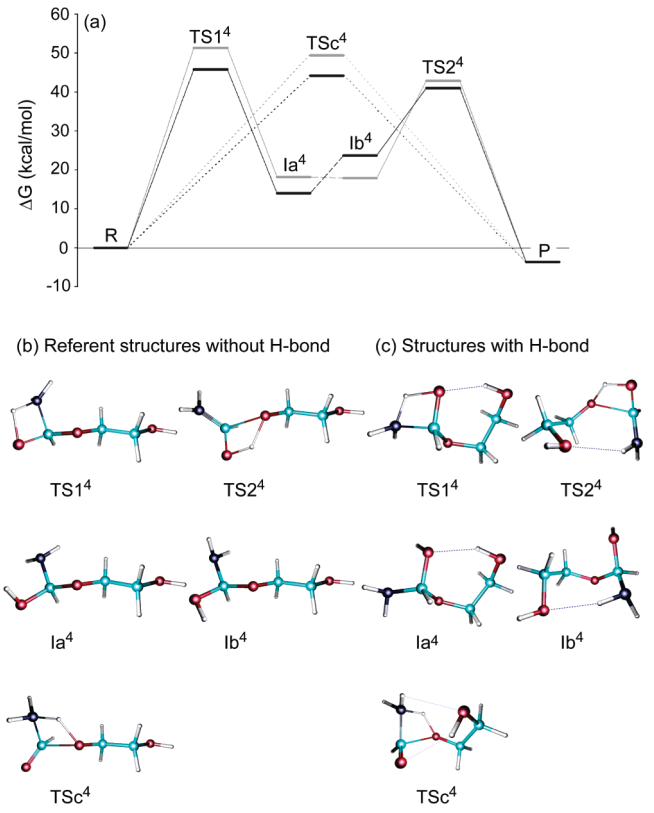


FIGURE 3. Gibbs free energy profile (at 298 K) of the ammonolysis reaction with tetragonal transition states. The energies of the referent structures without hydrogen bonds (with vicinal hydroxyl in *trans* position relative to the ether oxygen atom) are represented in dark gray. The energies of the lowest energy transition states with hydrogen bonds are represented in black. The stepwise mechanism is depicted with a solid line and the concerted one is depicted with a dotted line. The dashed lines in the stepwise reaction path represent sections where rotational barriers are located. The structures of the lowest energy transition states and corresponding intermediates are shown in panels (b) and (c).

of the most stable $TS1^4$ structure for the ethanediol model due to the hydrogen bond amounts to 7.8 kcal/mol.

Gibbs Free Energy Profile. The free energy profiles of the concerted and stepwise mechanisms for the ammonolysis of monoacylated ethanediol are presented in Figure 3, only the most stable structures of the tetragonal transition states with hydrogen bonds being included. For comparison, the optimized referent structures without hydrogen bonds (with the vicinal hydroxyl group in the *anti* position to the ether oxygen atom) are also shown. For the intermediate I we included two structures: the structure that is produced from the most stable structure of the TS1, and the structure from which the most stable conformation of TS2 is obtained.

If we consider the referent reaction path of ammonolysis of the conformer with the *anti*-oriented 2-OH group, i.e., without intramolecular hydrogen bonds, the reaction is found to be slightly exogonic, by 3.7 kcal/mol (Table 1). The concerted and the stepwise mechanisms have very similar free energies of activation, $\Delta G^{\#}$ (49.4 and 51.3 kcal/mol, respectively), as previously calculated for the aminolysis of 2-deoxyesters. This suggests that the *anti*-oriented 2-OH does not affect the mechanism of alkyl ester aminolysis

TABLE 1. Energy Values, Electronic Energy ΔE, and Gibbs Free Energy ΔG (both in kcal/mol) of the Transition States, Intermediate, and Product Calculated with Respect to the Initial State[a]

energy[b]	TSc	TS1	I1	I2	TS2	product[c]
ΔE(ref)	51.5	52.7	16.6	16.1	45.2	−4.5
ΔE(TG)	43.8	44.9	9.9	20.5	41.2	−4.5
ΔE(HG)	49.3	31.2	10.0	15.1	40.3	−4.5
ΔE(wat)	38.6	27.9	8.0	11.2	11.6	−2.9
ΔG(ref)	49.4	51.3	18.2	18.0	42.9	−3.7
ΔG(TG)	44.3	45.9	14.0	23.7	41.0	−3.7
ΔG(HG)	48.9	33.5	15.4	18.7	39.3	−3.7
ΔG(wat)[d]	38.9	30.0	13.0	14.9	29.5	−3.6
ΔG_{solv}(ref)	−7.2	−7.9	−1.9	−1.9	−3.4	−0.3
ΔG_{solv}(TG)	−3.9	−6.1	−2.4	−0.5	−2.1	−0.3
ΔG_{solv}(HG)	−0.9	−5.0	−2.4	−0.5	−0.9	−0.3
ΔG_{solv}(wat)	−7.9	−8.0	−2.7	−2.0	−4.3	−3.8
CCSD(T)						
ΔE(ref)	55.0	54.1	13.4	13.2	49.5	−3.1
ΔE(TG)	45.6	45.3	6.9	16.1	44.1	−3.1
ΔE(HG)	52.2	32.2	6.5	11.5	44.0	−3.1

[a]Calculations are performed at the B3LYP/6-31++G** level. In addition the Gibbs free energies of solvation, ΔG_{solv} (relative to the reactants), in acetonitrile and the values of the electronic energies obtained at the CCSD(T)/6-311++G**//MP2/6-311++G** level are reported. [b]The type of transition state is denoted in parentheses: ref: referent reaction; TG: tetragonal transition states; HG: hexagonal transition states; wat: reaction catalyzed by water. Only the energy of the most stable structures of each species is reported. [c]The reported energy values correspond to a complex formed by the species produced during the reaction. [d]The reported Gibbs free energy values are calculated relative to a prereaction complex including reactants and a water molecule as catalyst; taking into consideration the entropy contribution of the free water molecule before formation of the prereaction complex leads to an increase of all reported values by 3.0 kcal/mol.

due to its induction influence. The concerted transition state TSc^4 is found to be 1.1 kcal/mol more stable than the rate-determining TS1 of the stepwise mechanism.

Formation of hydrogen bonds with the vicinal OH group stabilizes the transitions states TSc^4 and $TS1^4$ by 5.2 and 5.5 kcal/mol, respectively; that is, the free energy of activation $\Delta G^{\#}$ of the reaction is reduced to 44.3 kcal/mol and the difference between the energy barriers for the concerted and the stepwise mechanisms remains only 1.6 kcal/mol. Despite some minor variations in the Gibbs free energies of the intermediate and $TS2^4$ due to formation of hydrogen bonds, the first step of the stepwise mechanism remains rate-determining.

In order to check for the influence of the computational level, we reoptimized the structures of the stationary points along the reaction path at the MP2 level and calculated the electronic energies of the species with the CCSD(T) method (Table 1). The higher-level computational method resulted in a small increase of the energies of all transition states by 0.3 to 4.3 kcal/mol, and the conclusions from the density functional calculations reported above are not altered.

Vicinal Hydroxyl As Proton Transfer Mediator (Hexagonal Transition States). In addition to the stabilization of the transition state via hydrogen bonds reported above, we also considered the vicinal OH group as a proton shuttle mediator in the aminolysis process as both proton donor and acceptor. Unlike the tetragonal transition states, a hexagonal cycle for the proton transfer is formed in these transition states (see right-hand side of Scheme 1a). The requirement for formation of a larger cycle in the transition state reduces the steric constraints in the structure and leads to a wider and thus more favorable angle for proton transfer. Since the vicinal hydroxyl group participates in the proton transfer,

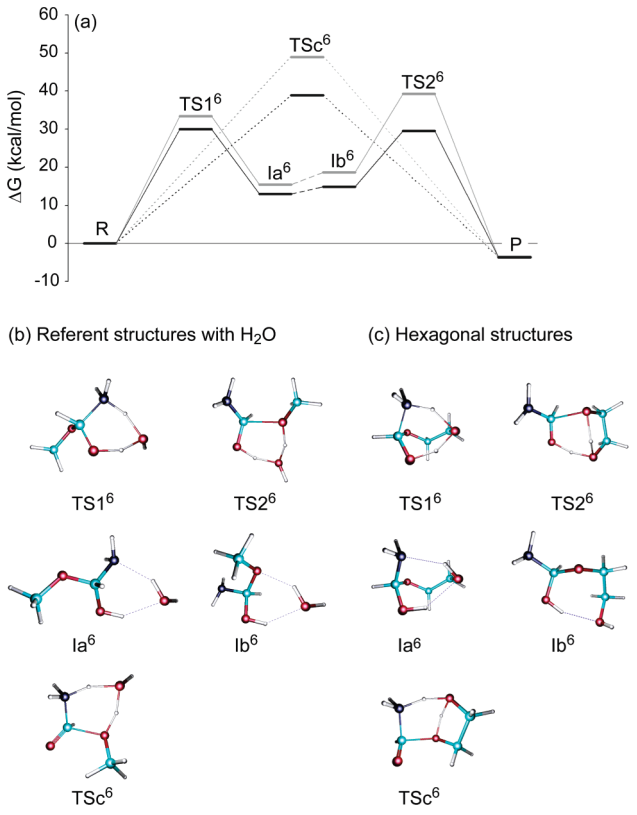


FIGURE 4. Gibbs free energy profile (at 298 K) for the ammonolysis of formyl-1,2-ethanediol via hexagonal transition states (in gray). Stepwise mechanism: solid line. Concerted mechanism: dotted line. The referent reaction of methyl formate ammonolysis, assisted by a water molecule, is shown with a black solid line. Dashed lines represent sections where rotational barriers are located. The structures of the lowest energy transition states and corresponding intermediates are shown in panels (b) and (c).

additional hydrogen bonds cannot be formed in the transition states and the conformational freedom is rather restricted.

A hexagonal structure of the transition states was already modeled in the case of ester ammonolysis catalyzed by different additional molecules that facilitate proton transfer.[7a,8,10] In this connection, as a referent system for the hexagonal transition states we modeled the ammonolysis of methyl formate catalyzed by a free water molecule instead of the vicinal OH group as a proton-mediating moiety (see Figure 4 and Gibbs Free Energy Profile section). Such a model allows us to evaluate the influence of the conformational constraints of the ethanediol moiety and the geometry restrictions of the vicinal OH group (in particular its position relative to the reaction center) on the energy of the transition states.

Both the concerted and stepwise mechanisms for ammonolysis of monoacylated ethanediol could occur via hexagonal transition states. The transition state TSc^6 of the concerted mechanism includes nucleophilic attack of the N atom to the carbonyl carbon atom and simultaneous proton transfers from the ammonia moiety to the vicinal hydroxyl and from the vicinal hydroxyl to the ester oxygen atom, Oe. The transfer of two protons is accomplished via hexagonal cycle. However, one of them, Hv, is transferred from Ov to the Oe center and participates in a pentagonal cycle as well. In addition to the restrictions from the smaller ring, the proton transfer between the vicinal oxygen atoms requires an unfavorable eclipsed conformation of ethanediol. For the transition state TSc^6 we found two conformations of the ethanediol moiety with similar energy. In both structures the cleavage and formation of the bonds between the heavy atoms is in a more advanced stage than the proton transfers.

The stepwise mechanism (Scheme 1a) includes formation of the same intermediate I as in the case of the tetragonal transition states. However, the transition state $TS1^6$, leading to this intermediate, differs from $TS1^4$. In $TS1^6$ the Ha proton from the ammonia moiety is not transferred directly to the Oc atom, as in $TS1^4$, but to the vicinal OvHv group, resulting in simultaneous migration of the proton Hv to the Oc atom. The second hexagonal transition state, $TS2^6$, besides cleavage of the C−Oe bond includes simultaneous proton transfer from the OcH group of the intermediate I to the Ov atom of the vicinal hydroxyl and from the vicinal hydroxyl to the ester oxygen atom, Oe. So, in both transition states the vicinal hydroxyl mediates the proton transfer.

Similarly to TSc^6, depending on the conformation of the ethanediol fragment, two conformations have been found for both hexagonal transition states of the stepwise mechanism $TS1^6$ and $TS2^6$. The structure of $TS2^6$ requires formation of an additional pentagonal cycle for the proton transfer of Hv, again similar to TSc^6. On the other hand, the second cycle for $TS1^6$ is larger, heptagonal, and has lower steric restrictions, which allow formation of the more favorable *gauche* conformation of the ethanediol moiety.

Gibbs Free Energy Profile. The reaction paths via hexagonal transition states for the studied and the referent systems are presented in Figure 4. The participation of the vicinal hydroxyl (or water molecule in the referent reaction) in the proton transfer cycle during the ammonolysis considerably changes the reaction energy profile compared to the noncatalyzed reaction. As can be seen, the stepwise mechanism becomes the lower energy path for the monoacylated ethanediol ammonolysis with a free energy barrier 15.5 kcal/mol lower than that of the concerted mechanism. While the Gibbs free energy of transition state $TS1^6$ in the stepwise mechanism is 5.8 kcal/mol lower than the second one ($TS2^6$), the first energy barrier is 12.9 kcal/mol higher than the second one due to the rather high energy of the intermediate. Thus, the free energy barrier of the reaction path via hexagonal transition states is 33.5 kcal/mol, 10.8 kcal/mol lower than that for the tetragonal TS structures.

Comparing the free energy barriers of the individual hexagonal transition states of the concerted mechanism with those calculated for the tetragonal transition states, one finds that the tetragonal transition state TSc^4 with a hydrogen bond is 4.7 kcal/mol more stable than the hexagonal one, TSc^6. The high energy of the latter structure is probably due to constraints caused by formation of the pentagonal ring and the unfavorable conformation of the ethanediol moiety discussed above. For the same reason the hexagonal form of the second transition state of the stepwise mechanism, $TS2^6$, is stabilized by 1.7 kcal/mol only as compared to the tetragonal one, $TS2^4$. The main advantage of the hexagonal transition state concerns the first transition state of the stepwise mechanism, which is stabilized by 17.9 kcal/mol relative to the corresponding most stable conformer of $TS1^4$.

In the referent reaction paths, where the proton transfer is carried out with the help of a water molecule, all structures

have lower energy as compared to the structures with proton transfer helped by the vicinal hydroxyl group. This energy difference of the corresponding transition states could be used for evaluation of the influence of steric constraints on TSc[6], TS1[6], and TS2[6]. The decrease of the TS1[6] barrier in the case of water-catalyzed ammonolysis is rather small, 3.5 kcal/mol, which implies a weak effect of the steric constraints in this transition state. Indeed, TS1[6] requires the formation of two unconstrained hexagonal and heptagonal cycles. The stabilization of the other two transition states, TSc[6] and TS2[6], is much stronger, by 10.0 and 9.8 kcal/mol, respectively. The comparable stabilization of these two transition states reflects their similar structure in the case of reaction with a monoacylated diol, which requires formation of a sterically constrained pentagonal cycle where the transfer of a proton between the two vicinal oxygen atoms of the diol (Ov and Oe) takes place. In addition, the covalent bonds in the ethanediol moiety fix the distance between Ov and Oe atoms participating in the proton transfer.

Similarly to the tetragonal transition states, the calculations with the CCSD(T)//MP2 approach (Table 1) lead to slight destabilization of the transition states by 1.2−4.1 kcal/mol. Thus, the reaction path with the hexagonal transition states occurs preferably via a stepwise mechanism, as we already concluded from the DFT results.

If we extend the interpretation of the computational results for catalysis by an additional water molecule to the process inside the ribosome, we have to take into account the difference in the entropy contributions of all components participating in the reaction step. In the real process the reaction occurs between two amino acid residues (represented in our model by ammonia and acylated ethanediol), each of them bound via covalent bonds to tRNA and with no separate translational and rotational entropy components. If catalysis is accomplished by the vicinal OH group, it is also part of the tRNA; that is, the translational and rotational entropy of the catalyst have no separate contributions. On the other hand, if one considers the additional water molecule as a catalytic species, then the entropy loss from its free state into a fixed position in the transition states should be taken into account. The evaluation of the translational and rotational entropy contribution of a free water molecule results in 14 kcal/mol at 310 K (corresponding to the ΔG value of a free water molecule). When the molecule is coordinated to the reaction center, this entropy loss is partially compensated by the enthalpy gain due to formation of hydrogen bonds. Our estimation for the change in ΔG from free to coordinated water is 3.0 kcal/mol; that is, the process is slightly endergonic and the prereaction complex is less stable than the system with free water. As described in the Computational Details the coordinated state of water is used as the initial state for calculation of the free energy profile of the reaction, shown in Figure 4 and reported in Table 1. Thus, in order to compare adequately the two alternative catalytic species, vicinal OH and additional water, we have to add 3.0 kcal/mol to the calculated $\Delta G^{\#}$ values of the transition states in the case of water. In this way the calculated free energy of the rate-determining transition state, TS1[6], for catalysis by an additional water molecule will be essentially equal to that of the corresponding transition state for the catalysis by the vicinal OH. The same approach could be followed in the analysis of the results of other model studies considering the catalytic effect from additional water (or another small molecule).

Reaction Path with Acetylated Vicinal Hydroxyl. In order to estimate the influence of a substituent at the carbonyl carbon atom, we calculated the reaction path via the tetragonal and hexagonal transition states for monoacetylated ethanediol as well. The structures corresponding to the various stationary points along the reaction paths were optimized starting from the structures of the formylated reactant with the methyl group at the position of the H atom bound to the carbonyl C atom. In all cases the calculated Gibbs free energies of the transition states are higher than the corresponding structures for ammonolysis of formylethanediol (see Figure S2 in the Supporting Information). The increase is similar for the tetragonal and the hexagonal transition states: 2.7, 4.9, and 2.7 kcal/mol for TSc[4], TS1[4], and TS2[4] and 3.0, 3.5, and 4.6 kcal/mol for TSc[6], TS1[6], and TS2[6]. Since the changes are synchronous, the presence of the additional methyl group does not affect the preferred reaction mechanism, but the Gibbs free energy of activation of the process increases to 37.0 kcal/mol.

Evaluation of the Influence of the Environment on the Gibbs Free Energies. Since the environment of the reaction center both in aprotic solvents and inside the ribosome is different from vacuum, we evaluated the influence of the surroundings of the reaction center on the reaction energetics by calculation of the free Gibbs energies of solvation for all stationary points along the modeled reaction paths. This approach accounts for the nonspecific interactions of the dielectric medium with the reactants, transition states, and intermediates. For the calculations we selected three solvents with different dielectric constants: chloroform with $\varepsilon = 4.71$, acetonitrile with $\varepsilon = 35.69$, and "water" with $\varepsilon = 78.35$ (note that only electrostatic and dispersion interactions are taken into account, while the specific interactions such as formation of hydrogen bonds or proton transfer are not considered in this approach).

Solvation was found to stabilize all transition states, as the stabilization of certain species increases with the dielectric constant of the solvent (see Figures S5−7 of the Supporting Information). Accounting for the polarization of the surroundings, however, does not result in qualitative alteration of the preferred reaction mechanism, and the energetically most favorable route is via hexagonal transition states. The reduction of the Gibbs free energy barriers of the referent reaction path without formation of a hydrogen bond and via tetragonal transition states due to solvation is 7.2 and 3.9 kcal/mol, respectively, as can be seen from Table 1, where the calculated ΔG_{solv} values for acetonitrile as solvent are shown. The influence of the medium was most pronounced for transition state TS1 in all modeled reaction paths. In particular, for the most preferable reaction path via the hexagonal transition states the Gibbs free energy barrier is reduced due to the effect of the surroundings by 3.8, 5.0, and 5.3 kcal/mol for chloroform, acetonitrile, and water; that is, for a medium with ε around 35 the reaction barrier is reduced from 33.5 kcal/mol under vacuum to 28.5 kcal/mol.

Conclusions

The present computational model study evaluates the influence of the vicinal OH group in acylated diols on the reaction paths for ester ammonolysis. Two alternative

approaches for this influence were considered: stabilization of the (tetragonal) transition states along the reaction path via hydrogen bonds and participation of the vicinal hydroxyl in proton transfer (proton shuttle mechanism).

The catalytic activation of the ester ammonolysis by a hydrogen bond from the vicinal hydroxyl via tetragonal transition states (occurring preferably via a concerted mechanism) was found to be rather modest, the free energy of activation being reduced by 5.2 kcal/mol only. The resulting free energy of activation, $\Delta G^{\#} = 44.3$ kcal/mol, is still rather high, and for this reason the pathway via tetragonal transition states is unlikely to occur. The reason for this weak catalytic effect is the rather small proton transfer angles in the transition states, about 125−130°, much smaller than the optimal angle of 180°. The comparison with stabilization of the transition states via a hydrogen bond from an external water molecule suggests that the stabilization in the case of monoacylated ethanediol is close to the maximally possible stabilization of this type.

The other mechanism of catalytic activation of the ester ammonolysis—by participation of the vicinal hydroxyl in the proton transfer via hexagonal transition states—does not affect considerably the stability of the transition states in the concerted mechanism and the second step of the stepwise mechanism. However, it stabilizes considerably the first transition state of the stepwise mechanism; the Gibbs free energy of activation is reduced by 16.0 and 10.8 kcal/mol with respect to the referent value and the barrier for stabilization of the transition states via a hydrogen bond. The resulting free energy of activation, 33.5 kcal/mol, is significantly lower than the barriers calculated for the noncatalyzed reaction or the reaction occurring via the tetragonal transition states. The main reason for this effect[13] is the replacement of a single unfavorable proton transfer in TS1[4] by two favorable proton transfers in TS1[6] that decreases the angular distortions for the proton transfers, as can be concluded from the larger angles, 149° and 155°.

A similar catalytic effect has been proposed for water-assisted aminolysis of 2-deoxy esters,[9] where the OH group of water acts as a proton shuttle in the same way as the vicinal OH in monoacylated 1,2-ethanediol aminolysis modeled here. As we have shown, however, the proper accounting of the (translational and rotational) entropy of the free water molecule resulted in an increase of the free Gibbs energy of activation for the water-assisted process. Such entropy loss does not influence the free energy of the transition states in the case of catalysis by vicinal OH since the catalytic group is bound by a covalent bond to the reaction center. In addition, the vicinal 2′-OH of ribose, modeled here as ethanediol, is readily available, being next to the reaction center during the synthesis of each peptide bond. Catalysis including an additional water molecule would require the approach of an external water molecule to the reaction center to accomplish each reaction step. Thus, we consider the vicinal 2′-OH of the ribose as a realistic and relevant proton transfer mediator for the peptide bond formation in the ribosome. This conclusion is also supported by the lack of reactivity of the modified peptidyl tRNA in which A76 2′-OH was substituted by H, F, or a methoxy group.[2e,11] The 2′-OH keeps its catalytic activity even when embedded into an active site of six neighboring 2′-deoxyribose nucleosides.[16] In addition, the proton shuttle role of the 2′-OH corroborates the crystal structure analysis[17] and computational modeling.[2b]

In summary, the proton shuttle role of the vicinal OH was found to provide stronger activation of the reaction of peptide bond formation than the activation via an additional hydrogen bond from this group. The more favorable structure of the transition states for ester aminolysis due to participation of the vicinal hydroxyl in the proton transfer results in a decrease of the free energy of activation by 16.0 kcal/mol, which corresponds to about 10^9-fold acceleration of the reaction with respect to the noncatalyzed process. This value is in agreement with the lowest experimental estimate for acceleration of this process in the ribosome, 10^6-fold, reported by Weinger and Strobel.[18]

Accounting for the influence of the environment on the reaction center by a continuum model (for ε from 5 to 80) resulted in further stabilization of the rate-determining transition state by 4−5 kcal/mol.

As discussed in the present paper, the transformations in the reaction center during the elementary steps of the ester aminolysis catalyzed by the vicinal hydroxyl have two components: proton transfer and cleavage/formation of a bond between heavier atoms (C−O or C−N). We have shown that the transition-state energies are reduced when the structure of the reaction center allows formation of C−N or cleavage of C−O bonds together with favorable arrangement for simultaneous proton transfer. The proton transfer itself can be influenced also by other factors and processes, which have been extensively studied in connection with the importance of the proton transfer in enzymes, nucleic acids, and various other biochemical systems. Recently, Warshel and co-workers[19−22] have presented a series of studies with critical analysis of the different ideas on the proton transfer processes in enzymes. They have pointed out that the fluctuations of the polar environment, which modify the reaction barrier, are actually responsible for facilitation of the proton transfer and for the enormous catalytic power of enzymes in general. On the basis of the analysis of available experimental results and related computational modeling at the microscopic level, they have shown that the tunneling, as accounted for by the kinetic isotope effect, does not contribute significantly to the catalytic activity of the enzymes since similar effects occur in the referent noncatalyzed reactions in solution.[19,21] Taking into account the analogies in the catalysis by the enzymes and by the ribosome, one may assume that these features would also influence the proton transfer processes in the ribosome, as a component of the elementary reaction step for peptide bond formation.

(16) Erlacher, M. D.; Lang, K.; Wotzel, B.; Rieder, R.; Micura, R.; Polacek, N. *J. Am. Chem. Soc.* **2006**, *128*, 4453–4459.

(17) Schmeiling, T. M.; Huang, K. S.; Kitchen, D. E.; Strobel, S. A.; Steitz, T. A. *Mol. Cell* **2005**, *20*, 437–448.

(18) Weinger, J. S.; Strobel, S. A. *Blood Cells Mol., Dis.* **2007**, *38*, 110–116.

(19) Braun-Sand, S.; Olsson, M. H. M.; Mavri, J.; Warshel, A. In *Hydrogen Transfer Reactions*; Hynes, J. T.; Klinman, J. P.; Limbach, H.-H.; Schowen, R. L., Eds.; Wiley-VCH: Weinhein, 2007; pp 1171−1205.

(20) Warshel, A.; Sharma, P. K.; Kato, M.; Xiang, Y.; Liu, H.; Olsson, M. H. M. *Chem. Rev.* **2006**, *106*, 3210–3235.

(21) Kamerlin, S. C. L.; Mavri, J.; Warshel, A. *FEBS Lett.* **2010**, *584*, 2759–2766.

(22) Kamerlin, S. C. L.; Sharma, P. K.; Chu, Z. T.; Warshel, A. *Proc. Natl. Acad. Sci.* **2010**, *107*, 4075–4080.

Computational Details

All *ab initio* molecular orbital calculations were performed with the Gaussian03[23] program suite. Analytical gradient optimization methods were used to locate the minima, corresponding to reactants, intermediates, and products, and saddle points corresponding to transition states. Transition states were identified by finding only one negative eigenvalue of the analytic force constant matrix and by geometric analysis of its eigenvector components. All lowest points of reaction paths were optimized at the B3LYP/6-31++G** level,[24,25] and the electronic energies of the obtained structures were refined by single-point calculations with the high-level post-Hartree−Fock method CCSD(T) with the 6-311++G** basis set. The latter method allows avoiding the well-known "delocalization error" of modern density functional methods, which could result in an overstabilization of fractional charges and thus could affect the relative stability of the transition states.[26] In addition, we reoptimized the structures of the stationary points along the reaction path at the MP2/6-311++G** level starting from the structures optimized with the B3LYP/6-31++G** approach. Subsequently, the electronic energies of the structures were recalculated with the CCSD(T) method and the obtained CCSD(T)//MP2 energies are reported in Table 1. The energy difference between the CCSD(T)//B3LYP and CCSD(T)//MP2 methods for different stationary points was found to be at most 1.3 kcal/mol (0.5 kcal/mol on average).

The influence of the surroundings on the relative Gibbs free energies of the transition states was estimated as the solvent effect of solvents with different dielectric constants (from $\varepsilon = 4.71$ to $\varepsilon = 78.35$). The calculations were performed in single-point fashion (B3LYP/6-31++G** level) with the polarized continuum model.[27]

The energies of all structures within each reaction path are calculated with respect to the energy of the initial complex formed by the reactant molecules formyl-1,2-ethanediol and ammonia with two intramolecular hydrogen bonds (Ha−Oc and Hv−N). Thus, the energy of the complex formed by the product molecules is considered as the reaction energy. Since all species along each reaction path have the same composition, the correction for basis set superposition error is not calculated. The activation barriers of the transition states TS1 and TSc are considered with respect to the reactants, while the activation barriers of the second transition states TS2 are estimated with respect to the intermediate I, which is geometrically closest to TS2. The changes of the Gibbs free energy values ΔG of all stationary points along the reaction paths were also calculated with respect to the corresponding value of the reactants. For the reaction path with an additional water molecule as a catalyst participating in the proton transfer we also considered the translational and rotational entropy contribution of a free water molecule (corresponding to the ΔG value of the free water molecule). This is necessary for correct comparison of different reaction paths since all other components of the reaction are parts of large tRNA molecules, while only the water molecule is free.

A complete model study of the reaction mechanism and energetics requires a search not only of all possible intermediates and transition states along the different reaction paths but also of the different conformations of all stationary points along each reaction path in order to find those with lowest energy. For this reason, our investigation included a complete conformational search aiming at finding all lowest energy structures. The applied computational procedure, described in detail in ref 28, is based on the generation of a set of initial structures via stepwise variation of different dihedral angles (N−C−Oe−C1, C−Oe−C1−C2, Oe−C1−C2−Ov, and C1−C2−Ov−Hv) by 10°. Thus, about 46 000 to 160 000 initial structures were generated for each transition state and intermediate, which were further sifted out by elimination of equivalent structures.

The carbonyl carbon atom is prochiral, and after nucleophilic attack of ammonia a chiral intermediate is formed; that is, two reaction paths with *R* or *S* intermediates are possible. However, both reaction paths are energetically equivalent, and we consider only the pro *R* attack and *R* configuration of the intermediates.

Rotational barriers between the intermediates along the reaction paths were not calculated since these barriers are significantly lower than the transition states, and therefore they cannot influence the reaction kinetics (for more details see Figure S3 of the Supporting Information.

The dependence of the Gibbs free energy of activation for the different transition states on temperature was also studied (see Figure S4 of the Supporting Information. The analysis shows that the changes in the barriers of the studied reaction paths are synchronous for each group of transition structures, and variation of the temperature does not result in interchange of the rate-determining stages in the temperature range 293−333 K. One should note, however, that the variation of the temperature may strongly affect the fluctuations of the environment and thus influence the dynamics of the proton transfer reactions via modification of the energy barrier for the process, as concluded for proton transfer processes in enzymes.[19]

The following notation is applied for the stationary points along concerted and stepwise reaction pathways: TSc, transition state of concerted mechanism; TS1 and TS2, first and second transition states of the stepwise path; I, intermediate of the stepwise path. The superscript (4 or 6) denotes the number of atoms participating in the cycle of the corresponding transition states. The notation of atoms is represented in Scheme 1b with the example of the tetrahedral transition state, I, observed in the stepwise mechanisms of the reaction.

Acknowledgment. The authors are grateful to the National Research Fund of Bulgaria for financial support via Grant Nos. DO 02-133/2008, DO 02-210/2008, and the Center of Excellence for Supercomputer Applications DO

(23) Frisch, M. J.; Trucks, G. W.; Schlegel, H. B.; Scuseria, G. E.; Robb, M. A.; Cheeseman, J. R.; Montgomery, J. A., Jr.; Vreven, T.; Kudin, K. N.; Burant, J. C.; Millam, J. M.; Iyengar, S. S.; Tomasi, J.; Barone, V.; Mennucci, B.; Cossi, M.; Scalmani, G.; Rega, N.; Petersson, G. A.; Nakatsuji, H.; Hada, M.; Ehara, M.; Toyota, K.; Fukuda, R.; Hasegawa, J.; Ishida, M.; Nakajima, T. ; Honda, Y.; Kitao, O.; Nakai, H.; Klene, M.; Li, X.; Knox, J. E.; Hratchian, H. P.; Cross, J. B.; Bakken, V.; Adamo, C.; Jaramillo, J.; Gomperts, R.; Stratmann, R. E.; Yazyev, O.; Austin, A. J.; Cammi, R.; Pomelli, C.; Ochterski, J. W.; Ayala, P. Y.; Morokuma, K.; Voth, G. A.; Salvador, P.; Dannenberg, J. J.; Zakrzewski, V. G.; Dapprich, S.; Daniels, A. D.; Strain, M. C.; Farkas, O.; Malick, D. K.; Rabuck, A. D.; Raghavachari, K.; Foresman, J. B.; Ortiz, J. V.; Cui, Q.; Baboul, A. G.; Clifford, S.; Cioslowski, J.; Stefanov, B. B.; Liu, G.; Liashenko, A.; Piskorz, P.; Komaromi, I.; Martin, R. L.; Fox, D. J.; Keith, T.; Al-Laham, M. A.; Peng, C. Y.; Nanayakkara, A.; Challacombe, M.; Gill, P. M. W.; Johnson, B.; Chen, W.; Wong, M. W.; Gonzalez, C.; Pople, J. A. *Gaussian 03*, Revision E.01; Gaussian, Inc.: Wallingford, CT, 2004.

(24) (a) Ditchfield, R.; Hehre, W. J.; Pople, J. A. *J. Chem. Phys.* **1971**, *54*, 720–723. (b) Hehre, W. J.; Ditchfield, R.; Pople, J. A. *J. Chem. Phys.* **1972**, *56*, 2257–2261. (c) Hariharan, P. C.; Pople, J. A. *Mol. Phys.* **1974**, *27*, 209–214. (d) Gordon, M. S. *Chem. Phys. Lett.* **1980**, *76*, 163–168. (e) Hariharan, P. C.; Pople, J. A. *Theor. Chim. Acta* **1973**, *28*, 213–222.

(25) McLean, A. D.; Chandler, G. S. *J. Chem. Phys.* **1980**, *72*, 5639–5648.

(26) (a) Gritsenko, O. V.; Ensing, B.; Schipper, P. R. T.; Baerends, E. J. *J. Phys. Chem. A* **2000**, *104*, 8558–8565. (b) Mori-Sanchez, P.; Cohen, A. J.; Yang, W. T. *Phys. Rev. Lett.* **2008**, *100*, 146401.

(27) (a) Miertuš, S.; Scrocco, E.; Tomasi, J. *Chem. Phys.* **1981**, *55*, 117–129. (b) Miertuš, S.; Tomasi, J. *Chem. Phys.* **1982**, *65*, 239–245. (c) Tomasi, J.; Mennucci, B.; Cammi, R. *Chem. Rev.* **2005**, *105*, 2999–3094.

(28) Rangelov, M. A.; Petrova, G. P.; Yomtova, V. M.; Vayssilov, G. N. *J. Mol. Graphics Modell.* **2010**, *29*, 246−255.

02-115/08. This work is dedicated to the memory of Prof. D.Sc. Dimiter D. Petkov, who inspired and started it.

Supporting Information Available: Scheme of variation of the angles A and D used in evaluation of the influence of the orientation of the hydrogen bond; Gibbs free energy profile for the reaction path with acetylated vicinal hydroxyl; energy profile for rotation of different torsion angles in the intermediate I; temperature dependence of Gibbs free energy barriers; figures with Gibbs free energy profile of the reaction paths including solvation energy for different solvents; tables of atom coordinates and absolute energies of the stationary points along the modeled reaction paths. This material is available free of charge via the Internet at http://pubs.acs.org.

Journal of Molecular Graphics and Modelling 30 (2011) 10–14

Contents lists available at ScienceDirect

Journal of Molecular Graphics and Modelling

journal homepage: www.elsevier.com/locate/JMGM

Determination of the optimal position of adjacent proton-donor centers for the activation or inhibition of peptide bond formation – A computational model study

Miroslav A. Rangelov[a], Galina P. Petrova[b], Vihra M. Yomtova[a], Georgi N. Vayssilov[b,*]

[a] Laboratory of BioCatalysis, Institute of Organic Chemistry, Bulgarian Academy of Sciences, Sofia 1113, Bulgaria
[b] Faculty of Chemistry, University of Sofia "St. Kliment Ohridski", 1, James Bourchier Ave., Sofia 1126, Bulgaria

ARTICLE INFO

Article history:
Accepted 24 May 2011
Available online 22 June 2011

Keywords:
Ester ammonolysis
Catalytic map
Hydrogen bond
Activation
Inhibition

ABSTRACT

The study reports a computational analysis of the influence of proton donor group adjacent to the reaction center during ester ammonolysis of an acylated diol as a model reaction for peptide bond formation. This analysis was performed using catalytic maps constructed after a detailed scanning of the available space around the reaction centers in different transition states, a water molecule acting as a typical proton donor. The calculations suggest that an adjacent proton donor center can reduce the activation barrier of the rate determining transition states by up to 7.2 kcal/mol, while no inhibition of the reaction can be achieved by such a group.

© 2011 Elsevier Inc. All rights reserved.

1. Introduction

Protein biosynthesis is an aminolysis reaction in which the amino group of an amino acid in the ribosome attacks the carbonyl of an amino acid esterified to the 3′-ribose of tRNA [1]. In a series of papers based on various experimental and computational approaches [2–11] it was shown that the elementary act of peptide bond formation includes a crucial catalytic influence of the vicinal OH group in ribose. This catalytic activation is accomplished via the so-called "proton shuttle" mechanism in which the vicinal OH directly participates in the proton transfer via hexagonal transition states [2,6,7]. Herein, we present a model study exploring the additional catalytic effect of an external group adjacent to the reaction center on the aminolysis reaction barriers. We modeled the effect of a water molecule (as proton donor) forming a hydrogen bond with the O center of the vicinal OH group. The influence of water molecules on peptide bond synthesis via formation of hydrogen bonds both with the nucleobase of the 3′ adenosine and with the 2′ vicinal hydroxyl has already been explored computationally [12] by inclusion of one or two additional water molecules in the rate determining transition state of the proton transfer that reduced the activation enthalpy of the reaction.

Our present modeling extends the analysis of the influence of an additional water or another adjacent proton donor group on the reaction to a detailed scanning of the available space around the vicinal OH in different transition states as obtained in our previous simplified model study of peptide bond formation based on the ammonolysis of monoacylated ethanediol [7]. We propose an alternative approach that allows us to evaluate the effect of such groups not only from a specific position but to map the whole available space around the reaction center using water as a typical proton donor model. To achieve this we calculated the difference between the interaction energies of the adjacent water and the Ov atom from the vicinal hydroxyl in the initial reaction complex and in the corresponding transition state of a concerted or a stepwise mechanism. Graphical representation of such a difference can be regarded as a *catalytic map* and can be used in determining the influence of adjacent groups in enzymes [13] and especially in the construction of theozymes or compuzymes [14,15]. In addition, such maps provide a convenient tool to design drug molecules with functional groups oriented appropriately for the activation or inhibition of the modeled processes.

2. Computational details and model

All quantum chemical calculations were performed with the Gaussian03 program suite [16]. The structures of the reaction complex (1-O-formyl-1,2-ethanediol + NH_3) and the transition states were initially optimized at the B3LYP/6-31+G* level [17–22] which has previously proved to provide adequate description of the geometry of the model system including formation of hydrogen bonds [23]. For each transition state about 100 structures with different orientation of the water molecule were studied.

* Corresponding author.
E-mail addresses: mran@orgchm.bas.bg (M.A. Rangelov), gnv@chem.uni-sofia.bg (G.N. Vayssilov).

1093-3263/$ – see front matter © 2011 Elsevier Inc. All rights reserved.
doi:10.1016/j.jmgm.2011.05.004

Catalytic maps for the ammonolysis reaction of formylethanediol as a mimic of the ribosomal peptide synthesis reaction were constructed. Various possible structures of different modeled transition states are described in detail in Ref. [7]. The current investigation was carried out for the most stable transition state structures only (according to Ref. [7]) of the rate determining steps of the different reaction pathways – concerted and stepwise mechanisms via tetragonal and hexagonal transition states, TSc^4, TS1^4 and TSc^6, TS1^6 [24] (for the reaction scheme see Refs. [7,23]).

Since the effect of a catalyst is to change the energy barrier of the rate determining reaction step, in order to estimate the catalytic effect of any factor on a studied process, it is necessary to calculate the difference in the energy change due to this factor for the reactants, on the one hand, and for the transition states, on the other. Thus, the catalytic effect of hydrogen bond formation could be quantified by computing the difference in the energy of interaction between the proton acceptor and the adjacent proton donor (here a water molecule) according to the following equation:

$$E_{cat} = -\{[E_{TS+wat} - (E_{TS} + E_{wat})] - [E_{initail+wat} - (E_{initial} + E_{wat})]\} \quad (1)$$

In this equation $E_{initial}$, E_{TS}, and E_{wat} are the total electron energies of the reactant, the transition state, and the isolated water molecule, respectively. The terms E_{TS+wat} and $E_{initial+wat}$ correspond to the energy of the complexes formed via a hydrogen bond between the water molecule and the Ov atom from the vicinal hydroxyl (as proton acceptor) in the transition state structure or the reactant molecule. The position of the water molecule in both complexes was optimized at the same values of the angles A and D while the geometry of the transition state and the reactant was kept fixed. The definition of the angles A and D around the vicinal OH group is shown in Fig. 1 on the example of TS1^4. The first angle, A, is defined between the second carbon atom from the ethanediol fragment (C2), the vicinal oxygen atom (Ov) and the proton from the water molecule Hw participating in the new hydrogen bond with Ov. The dihedral angle D is between C1, C2, Ov, and Hw atoms. In order to map the catalytic effect of the hydrogen bond between the adjacent proton-donating group and Ov, we optimized 100 geometries of each species corresponding to 10 points for both angles the angles A and D being varied in the range 68–140° and 132–240°, respectively. Thus, we covered the whole available space around the vicinal OH. From the 200 points obtained for the reactant-transition state couple, the energy difference, E_{cat}, was calculated according to Eq. (1). By applying the method of Akima [25], the net of points obtained was further extrapolated to 3D NURBS (non-uniform rational basis spline) surface representing the catalytic effect. All figures are produced by MolRan program [23].

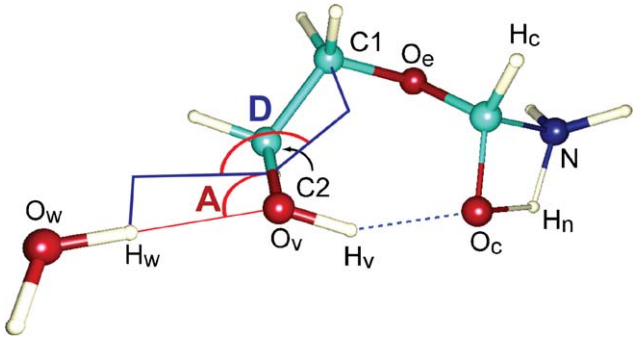


Fig. 1. Definition of the angles A and D, kept fixed during mapping the difference in the hydrogen bond strength in the reactant and transition – state structures. Designation of atoms is analogous to that in Ref. [7]: Oe, Oc, and Ov – oxygen atoms in the ester, carbonyl and vicinal OH groups, respectively; Hc, Hv, Hn – hydrogen atoms connected to the carbonyl C atom, the oxygen atom Ov from the vicinal OH group, and the N atom from the ammonia molecule, respectively; Hw and Ow – hydrogen and oxygen atoms from the coordinated water molecule.

A positive value of E_{cat} corresponds to activation of the reaction resulting from the stronger stabilization of the transition state due to the additional hydrogen bond, i.e. to a reduction of the activation barrier. On the other hand, a negative value of E_{cat} corresponds to inhibition of the reaction by the hydrogen bond with the proton donor.

3. Results and discussion

3.1. Tetragonal transition states

The modeled reaction of ester ammonolysis without external catalytic centers occurs in one or two steps by a concerted or stepwise mechanism (reaction scheme, shown in Refs. [6,7,23]). The concerted mechanism proceeds via the transition state TSc^4 which includes bonding of the N atom to the carbonyl carbon atom and simultaneous transfer of the proton Hn from ammonia to the Oe atom leading to a cleavage of the ester C–Oe bond. In the stepwise mechanism the Hn proton is initially transferred (transition state TS1^4) to the carbonyl Oc atom leading to the formation of an intermediate, I, and in the second step TS2^4, the intermediate is decomposed by proton transfer to the Oe atom and cleavage of the ester bond. The rate determining step in the stepwise mechanism is the formation of TS1^4 with an energy barrier of 52.7 kcal/mol, which is slightly higher than the barrier for the concerted mechanism, 51.5 kcal/mol [7]. When the reaction occurs via the same tetragonal transition states but with formylated ethanediol (as a simplified model of ribose) the vicinal OH group of the substrate can affect the process by formation of hydrogen bonds with Oe, Oc or N centers thus stabilizing the rate determining transition states TSc^4 and TS1^4 and reducing the corresponding barriers to 43.8 and 44.9 kcal/mol [7] (E_{act} in Table 1).

As mentioned above, we investigate here the effect of an additional proton-donor center (modeled as a water molecule) on the activation barriers by formation of a hydrogen bond with the oxygen center Ov of the vicinal hydroxyl of the substrate (Fig. 2). In this way the adjacent water molecule has only a secondary order influence on the reaction since it does not interact directly with any of the reaction centers, only increasing the acidity of the vicinal OH. Indeed, the catalytic map for the first tetragonal transition state TS1^4 of the stepwise mechanism (Fig. 2a) shows that the catalytic effect of the hydrogen bond formed with participation of an adjacent proton donor center is modest and does not exceed 1.7 kcal/mol. The observed result could be rationalized by the weak change of the charge at the carbonyl oxygen center Oc, which increases during the transition from reactants to the intermediate.

In the case of the tetragonal transition state of the concerted path of the ammonolysis reaction TSc^4 (Fig. 2b), the new HB(Ov-Hw) hydrogen bond strengthens the other two hydrogen bonds with participation of the vicinal OH, HB(Oc-Hv) and HB(Hn-Ov), formed with the atoms from the reaction ring (see Refs. [6,7]). The increase of the catalytic effect, observed when the water molecule approaches the N atom from the ammonia molecule, can be related to the formation of an additional hydrogen bond between a proton from the ammonia and the oxygen atom Ow from the water molecule. The formation of a second hydrogen bond with the water molecule results in a somewhat more pronounced catalytic effect of the water molecule on TSc^4 transition state, up to 5.7 kcal/mol, higher than in TS1^4. Here, however, we found some positions of the adjacent proton-donor that result in negative values of E_{cat} which corresponds to inhibition of the reaction, when it occurs via a concerted mechanism with a tetragonal transition state. Such effect appears when the water is at the A and D angles of 132° and 132°,

Table 1
Optimal position of the adjacent proton-donor center (angles in°, energies in kcal/mol, distances in Å) for different transition states.

TS	E_{act}[c]	Activation[a]				Inhibition[b]			
		A	D	E_{cat}	Ov-Hw[d]	A	D	E_{cat}	Ov-Hw[d]
TS1[4]	44.9	100	132	1.7	1.87	116	228	(0.3)	2.21
TSc[4]	43.8	140	228	5.7	1.80	132	132	−3.0	2.08
TS1[6]	31.2	140	228	7.2	1.82	68	240	(1.6)	3.10
TSc[6]	49.3	140	240	4.6	1.89	180	132	−2.8	2.18

[a] Position from the catalytic map with the highest value of E_{cat}.
[b] Position from the catalytic map with the highest (in absolute value) negative value of E_{cat}.
[c] Activation energy of the reaction with no adjacent proton-donor center [7].
[d] Hydrogen bond length in the corresponding optimal position.

respectively (Table 1). For this reason, the additional hydrogen bond increases the energy barrier of the reaction by up to 3.0 kcal/mol.

3.2. Hexagonal transition states

The vicinal hydroxyl group can also influence the mechanism of ester ammonolysis by the so-called proton shuttle mechanism when it is involved directly in the proton transfer via formation of hexagonal transition state cycles. In this way the vicinal OH stabilizes considerably the rate determining step of the stepwise mechanism TS1[6], by 21.5 kcal/mol to 30.0 kcal/mol, due to the more favorable angle for proton transfer. Unlike the tetragonal transition state, where the vicinal OH does not participate in the reaction cycle, in this case it participates in the proton transfer. Thus, the additional hydrogen bond of the adjacent proton-donor group to the Ov atom is expected to exert a stronger catalytic effect. As described below, this is indeed true in the case of TS1[6] but not in the case of TSc[6] transition state. Even after this reduction of the energy barrier to 30.0 kcal/mol the calculated value for our model is still rather high compared to the experimental barrier, 17.0 kcal/mol, reported by Johansson et al. [26]. This difference is due to the small model employed in the calculations and the lack of the surrounding effects. Indeed, the corresponding energy barriers obtained from calculations accounting for the environment of the peptidyl transferase center in the ribosome [12,27] are much closer to the experimental estimate.

The formation of a hydrogen bond between a water molecule and the vicinal hydroxyl results in a considerable catalytic effect, up to 7.2 kcal/mol, in the case of the first hexagonal transition state TS1[6] of the stepwise mechanism (Fig. 3a). The observed effect could be explained by a stronger interaction of the water in the transition state with the negatively charged Ov center as a result of the non-synchronous proton transfer of the two protons, Hv and Hn, interacting with the Ov center in this transition state: the Hn proton transfer from NH_3 is in an early stage while the proton Hv from the vicinal hydroxyl is almost transferred to the carbonyl oxygen center Oc. It should be noted that in all orientations of the adjacent proton-donor group the calculated catalytic effect, E_{cat}, is positive, i.e. the additional hydrogen bond only activates (strongly or weakly) but cannot inhibit the process via TS1[6].

The formation of a hydrogen bond between an additional water molecule and the vicinal hydroxyl of the ethanediol fragment results in a lower catalytic effect for the concerted hexagonal TSc[6] transition state, up to 4.6 kcal/mol. The weaker effect compared to the other hexagonal transition state TS1[6] could be explained with the smaller variations in the charge distribution in the TSc[6] transition state as a result of the more synchronous proton transfer. Similarly to the concerted tetragonal transition state, here, as well, the additional hydrogen bond has an inhibiting effect on the reaction for some orientations of the adjacent proton-donor since it increases the energy barrier for this reaction path by up to 2.7 kcal/mol (for the angles A = 68° and D = 240°).

3.3. Relevance to protein biosynthesis in the ribosome

The presence of a water molecule close to the reaction center for peptide bond formation of the ribosome is connected with the possibility for binding of this molecule to some proton donor or acceptor centers in the vicinity of the 3′ end of tRNA. The evolutionary conservatism of this 3′ nucleoside, which is adenosine in all organisms, supports the idea that adenine may be of importance for the aminolysis process. The nucleobase may influence the reaction by binding a water molecule via a hydrogen bond to the N3 atom of the nucleobase. This water molecule forms an addi-

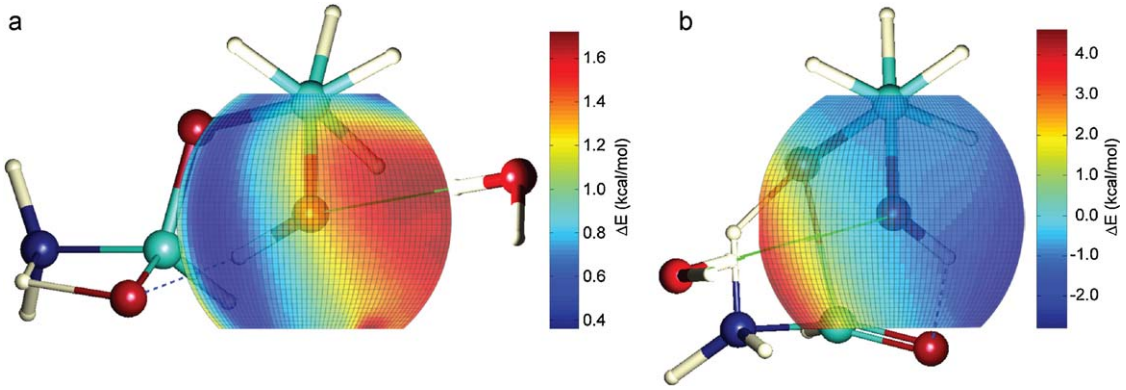


Fig. 2. Catalytic maps of the hydrogen bond with a proton donor for the tetragonal transition states with lowest energy for the stepwise, TS1[4] (a), and the concerted, TSc[4] (b), mechanisms of ammonolysis of 1-O-formyl-1,2-ethanediol.

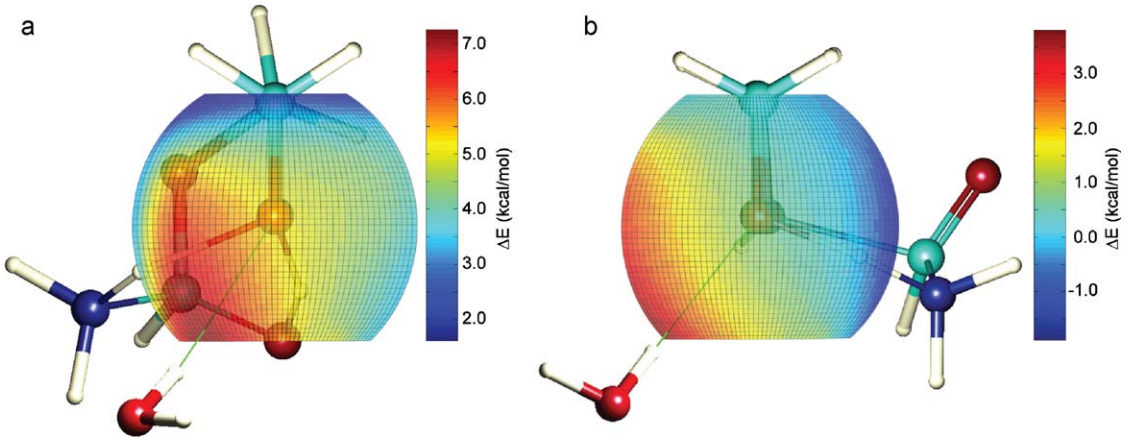


Fig. 3. Catalytic maps of the hydrogen bond with a proton donor for the hexagonal transition states with lowest energy for the stepwise, TS1[6] (a), and the concerted, TSc[6] (b), mechanisms of ammonolysis of 1-O-formyl-1,2-ethanediol.

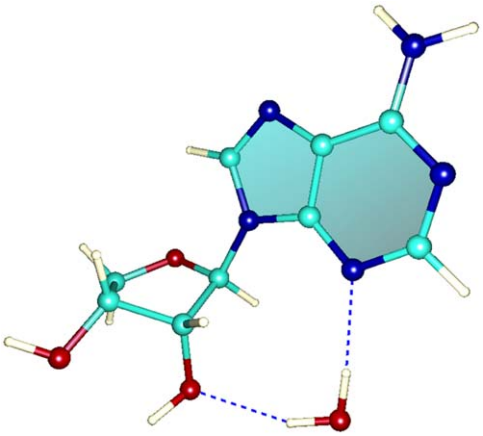


Fig. 4. Optimized structure of the complex of the adenosine analogue and a water molecule stabilized via hydrogen bonds to the N3 atom of the nucleobase and the oxygen atom of the vicinal hydroxyl OvHv.

tional hydrogen bond to the oxygen atom of the vicinal hydroxyl OvHv, thus activating the aminolysis process as described above. In connection with this idea we modeled computationally the interaction of the whole nucleoside, adenosine, with a water molecule (Fig. 4). In the obtained complex the water molecule is coordinated to the N3 atom of the adenine fragment and the vicinal hydroxyl OvHv. The obtained orientation of the water molecule in this complex can be used to analyze the effect of such proton donor center on the preference for attack of the amino group from the *re* or *si* face of the carbonyl group and formation of pro-*R* and pro-*S* transition states. In order to do this we considered the catalytic maps for the hexagonal transition state TS1[6] for the ammonolysis of formylated cis-tetrahydrofurandiol (possessing the same heterocyclic ring as ribose) for the structures with pro-*R* and pro-*S* attack (Fig. 5). Comparing the orientation of the water molecule, hydrogen bonded to 2′OH and the nucleobase in 3′ terminal adenosine of tRNA in Fig. 4, we can conclude that such water molecule is located suitably to facilitate a pro-*S* attack by about 7 kcal/mol. On the other hand, the location of such a water molecule is not particularly favorable in the case of a pro-*R* attack, where the stabilization of the transition state is about 3 kcal/mol. This result is in agreement with experimental data that show preference for pro-*S* attack in the ribosome peptidyltransferase center [4].

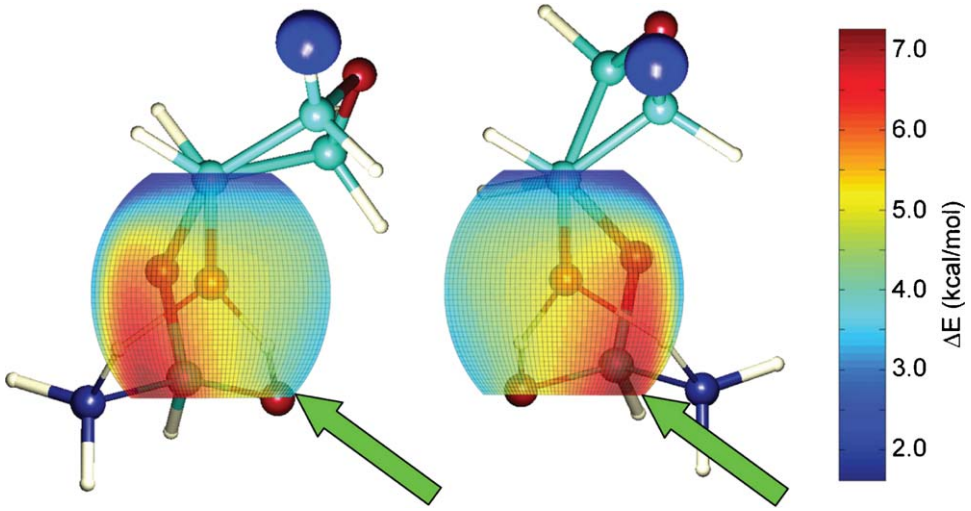


Fig. 5. Catalytic maps of the hydrogen bond with a proton donor for the hexagonal transition state TS1[6] for reactions with attack of the amino group from the *re* (a) and *si* (b) of the carbonyl group plane. The arrows point at the position of the water molecule stabilized in the complex shown in Fig. 4.

4. Conclusions

The catalytic maps for the influence of the adjacent proton donor group on the transition states for ammonolysis of acylated ethanediol, described in this study, suggest that participation of the Ov center of the vicinal hydroxyl in a hydrogen bond with an adjacent proton donor can reduce the activation energy of the reaction steps by up to 7.2 kcal/mol. The catalytic effect is most clearly pronounced for the rate-limiting step of the reaction, i.e. the first hexagonal transition state of the stepwise mechanism TS1[6]. For all orientations of the adjacent group the hydrogen bond has a positive catalytic effect, i.e. the additional proton-donor group is only able to activate but cannot inhibit the process via the rate determining transition state.

The modeling of a water molecule stabilized within an extended model of adenosine by hydrogen bonds to 2′OH of ribose and the N3 atom of the nucleobase allowed us to conclude that such an adjacent proton donor center would facilitate a pro-*S* attack of the amino group by about 7 kcal/mol, while the effect in the case of a pro-*R* attack would be twice smaller. This result is in agreement with available experimental data.

In general, the catalytic maps, constructed in the way reported here, can be used to predict the optimal position of groups in hypothetic ribozyme or enzyme active sites. They can also help in the construction of new or in the modification of known drugs targeting enzyme active sites, as well as, for the prediction of drug activity targeting known receptors.

Acknowledgments

The work was supported by Bulgarian National Fund for Scientific Research (contract DO 02-210) and the Center for supercomputer applications Super CA++.

References

[1] M.V. Rodnina, M. Beringer, W. Wintermeyer, Mechanism of peptide bond formation on the ribosome, Q. Rev. Biophys. 39 (2006) 203–225.
[2] S. Trobro, J. Åqvist, Mechanism of peptide bond synthesis on the ribosome, Proc. Natl. Acad. Sci. U.S.A. 102 (2005) 12395–12400.
[3] M.D. Erlacher, K. Lang, B. Wotzel, R. Rieder, R. Micura, N. Polacek, Efficient ribosomal peptidyl transfer critically relies on the presence of the ribose 2′-OH at A2451 of 23S rRNA, J. Am. Chem. Soc. 128 (2006) 4453–4459.
[4] T.M. Schmeing, K.S. Huang, D.E. Kitchen, S.A. Strobel, T.A. Steitz, Structural insights into the roles of water and the 2′ hydroxyl of the P site tRNA in the peptidyl transferase reaction, Mol. Cell 20 (2005) 437–448.
[5] M.M. Changalov, G.D. Ivanova, M.A. Rangelov, P. Acharya, S. Acharya, N. Minakawa, A. Földesi, I.B. Stoineva, V.M. Yomtova, C.D. Roussev, A. Matsuda, J. Chattopadhyaya, D.D. Petkov, 2′/3′-*O*-Peptidyl adenosine as a general base catalyst of its own external peptidyl transfer: Implications for the ribosome catalytic mechanism, Chembiochem 6 (2005) 992–996.
[6] M.A. Rangelov, G.N. Vayssilov, V.M. Yomtova, D.D. Petkov, The syn-oriented 2-OH provides a favorable proton transfer geometry in 1,2-diol monoester aminolysis: implications for the ribosome mechanism, J. Am. Chem. Soc. 128 (2006) 4964–4965.
[7] M.A. Rangelov, G.P. Petrova, V.M. Yomtova, G.N. Vayssilov, Catalytic role of vicinal OH in ester aminolysis: proton shuttle versus hydrogen bond stabilization, J. Org. Chem. 75 (2010) 6782–6792.
[8] W. Yang, D.G. Drueckhammer, Computational studies of the aminolysis of oxoesters and thioesters in aqueous solution, Org. Lett. 2 (2000) 4133–4136.
[9] S. Chalmet, W. Harb, M.F. Ruiz-Lopez, Computer simulation of amide bond formation in aqueous solution, J. Phys. Chem. A 105 (2001) 11574–11581.
[10] S. Ilieva, B. Galabov, D.G. Musaev, K. Morokuma, H.F. Schaefer III, Computational study of the aminolysis of esters. The reaction of methylformate with ammonia, J. Org. Chem. 68 (2003) 1496–1502.
[11] B. Galabov, S. Ilieva, B. Hadjieva, Y. Atanasov, H.F. Schaefer III, Predicting reactivities of organic molecules. Theoretical and experimental studies on the aminolysis of phenyl acetates, J. Phys. Chem. A 112 (2008) 6700–6707.
[12] G. Wallin, J. Åqvist, The transition state for peptide bond formation reveals the ribosome as a water trap, Proc. Natl. Acad. Sci. U.S.A. 107 (2010) 1888–1893.
[13] T. Dudev, C. Lim, Principles governing Mg, Ca, and Zn binding and selectivity in proteins, Chem. Rev. 103 (2003) 773–788.
[14] D.J. Tantillo, J. Chen, K.N. Houk, Theozymes and compuzymes: theoretical models for biological catalysis, Curr. Opin. Chem. Biol. 2 (1998) 743–750.
[15] Y.M. Lee, C.S. Babu, Y.C. Chen, M. Milcic, Y. Qu, C. Lim, Conserved structural motif for recognizing nicotinamide adenine dinucleotide in poly(ADP-ribose) polymerases and ADP-ribosylating toxins: implications for structure-based drug design, J. Med. Chem. 53 (2010) 4038–4049.
[16] M.J. Frisch, G.W. Trucks, H.B. Schlegel, G.E. Scuseria, M.A. Robb, J.R. Cheeseman, J..A. Montgomery Jr., T. Vreven, K.N. Kudin, J.C. Burant, J.M. Millam, S.S. Iyengar, J. Tomasi, V. Barone, B. Mennucci, M. Cossi, G. Scalmani, N. Rega, G.A. Petersson, H. Nakatsuji, M. Hada, M. Ehara, K. Toyota, R. Fukuda, J. Hasegawa, M. Ishida, T. Nakajima, Y. Honda, O. Kitao, H. Nakai, M. Klene, X. Li, J.E. Knox, H.P. Hratchian, J.B. Cross, V. Bakken, C. Adamo, J. Jaramillo, R. Gomperts, R.E. Stratmann, O. Yazyev, A.J. Austin, R. Cammi, C. Pomelli, J.W. Ochterski, P.Y. Ayala, K. Morokuma, G.A. Voth, P. Salvador, J.J. Dannenberg, V.G. Zakrzewski, S. Dapprich, A.D. Daniels, M.C. Strain, O. Farkas, D.K. Malick, A.D. Rabuck, K. Raghavachari, J.B. Foresman, J.V. Ortiz, Q. Cui, A.G. Baboul, S. Clifford, J. Cioslowski, B.B. Stefanov, G. Liu, A. Liashenko, P. Piskorz, I. Komaromi, R.L. Martin, D.J. Fox, T. Keith, M.A. Al-Laham, C.Y. Peng, A. Nanayakkara, M. Challacombe, P.M.W. Gill, B. Johnson, W. Chen, M.W. Wong, C. Gonzalez, J.A. Pople, Gaussian 03, Revision E.01, Gaussian, Inc., Wallingford, CT, 2004.
[17] R. Ditchfield, W.J. Hehre, J.A. Pople, Self-consistent molecular-orbital methods. IX. An extended Gaussian-type basis for molecular-orbital studies of organic molecules, J. Chem. Phys. 54 (1971) 724–728.
[18] W.J. Hehre, R. Ditchfield, J.A. Pople, Self-consistent molecular orbital methods. XII. Further extensions of Gaussian-type basis sets for use in molecular orbital studies of organic molecules, J. Chem. Phys. 56 (1972) 2257–2261.
[19] P.C. Hariharan, J.A. Pople, Accuracy of AH_n equilibrium geometries by single determinant molecular orbital theory, Mol. Phys. 27 (1974) 209–214.
[20] M.S. Gordon, The isomers of silacyclopropane, Chem. Phys. Lett. 76 (1980) 163–168.
[21] P.C. Hariharan, J.A. Pople, The influence of polarization functions on molecular orbital hydrogenation energies, Theor. Chim. Acta 28 (1973) 213–222.
[22] A.D. McLean, G.S. Chandler, Contracted Gaussian basis sets for molecular calculations. I. Second row atoms, $Z = 11–18$, J. Chem. Phys. 72 (1980) 5639–5648.
[23] M.A. Rangelov, G.P. Petrova, V.M. Yomtova, G.N. Vayssilov, Hierarchical approach to conformational search and selection of computational method in modeling the mechanism of ester ammonolysis, J. Mol. Graphics Modell. 29 (2010) 246–255.
[24] The applied notation for the stationary points along concerted and stepwise reaction pathways is analogous to that in Ref. [7]: TSc – transition state of concerted; TS1 and TS2 – first and second transition states of the stepwise path; I – intermediate of the stepwise path. The superscript (4 or 6) denotes the number of atoms participating in the cycle of the corresponding transition states.
[25] H. Akima, A method of bivariate. Interpolation and smooth surface fitting for irregularly distributed data points, ACM Trans. Math. Softw. 4 (1978) 148–159.
[26] M. Johansson, E. Bouakaz, M. Lovmar, M. Ehrenberg, The kinetics of ribosomal peptidyl transfer revisited, Mol. Cell 30 (2008) 589–598.
[27] J. Kästner, P. Sherwood, The ribosome catalyzes peptide bond formation by providing high ionic strength, Mol. Phys. 108 (2010) 293–306.

Received: 4 December 2018 | Revised: 6 January 2019 | Accepted: 8 January 2019

DOI: 10.1002/ddr.21514

Check for updates

WILEY DDR

RESEARCH ARTICLE

Anticonvulsant evaluation and docking analysis of VV-Hemorphin-5 analogues

Petar Todorov[1] | Miroslav Rangelov[2] | Petia Peneva[1] | Nadezhda Todorova[3] | Jana Tchekalarova[4]

Enabling Technologies		Strategy, Management & Health Policy	
Hit, Lead & Candidate Discovery	Preclinical Research & Development	Clinical Research	Post-Market Research

[1]Department of Organic Chemistry, University of Chemical Technology and Metallurgy, Sofia, Bulgaria

[2]Laboratory Chemistry and Biophysics of Proteins and Enzymes, Institute of Organic Chemistry with Centre of Phytochemistry, Bulgarian Academy of Sciences, Sofia, Bulgaria

[3]Department of Ecosystem Research, Institute of Biodiversity and Ecosystem Research, Bulgarian Academy of Sciences, Sofia, Bulgaria

[4]Department of Behavioral Neurobiology, Institute of Neurobiology, Bulgarian Academy of Sciences, Sofia, Bulgaria

Correspondence
Jana Tchekalarova, Institute of Neurobiology, Bulgarian Academy of Sciences, 1113 Sofia, Bulgaria.
Emails: janetchekalarova@gmail.com; jane@bio.bas.bg

Funding information
The Scientific Research Centre at UCTM, Grant/Award Number: 11813/2018

Abstract

VV-Hemorphin-5 is an endogenous opioid peptide of the Hemorphin family with affinity at opioid receptors. A series of C-amide analogues have been synthesized, based on the structure of VV-Hemorphin-5, modified at position 1 and 7 by the un/natural amino acids (***Aa8***-Val-Val-Tyr-Pro-Trp-Thr-Gln-NH_2 and Val-Val-Tyr-Pro-Trp-Thr-***Aa1***-NH_2) using SPPS, Fmoc-chemistry. The peptide derivatives were evaluated for their anticonvulsant activity in three acute seizure tests in male ICR mice, the maximal electroshock (MES), the 6 Hz psychomotor seizure test, and the timed intravenous pentylenetetrazole (ivPTZ) infusion test. Their neurotoxicity was assessed in the rotarod test. Among the tested peptide analogues, V4 showed anticonvulsant activity in the three seizure tests that was comparable to the VV-Hemorphin-5 (V1) used as a positive control. While V5, V6, and V7 peptide derivatives exhibited anticonvulsant activity in the MES and 6 Hz test, they were inactive (V7) or showed pro-convulsant effect (V5 and V6) in the i.v. PTZ test. At a dose of 10 μg/mouse the peptide V2 was effective against clonic seizures induced by PTZ. Motor coordination was not affected by newly developed analogues of VV-Hemorphin-5. Docking study results suggest that kappa opioid receptor binding could be the mechanism of action of peptide derivatives with anticonvulsant activity. The results suggest that incorporation of nonproteinogenic and/or natural amino acids at position 1 and 7 of the VV-Hemorphin-5 scaffold deserve further evaluation in models of epilepsy and derivatization.

KEYWORDS

anticonvulsant activity, docking, Hemorphin analogues, mice, SPPS

1 | INTRODUCTION

Epilepsy, considered a chronic neurological disease, is characterized by seizures that are caused by a loss of balance between classical excitatory glutamatergic and inhibitory gama amino acid (GABA) neurotransmitter system (Meldrum, 2002). Epileptic seizures might be limited to a part of the brain or to propagate to other areas or to generalize the entire brain as a result of synchronous and excessive electrical discharges in a particular group of neurons (Fisher et al., 2014). The therapy of epilepsy is mostly symptomatic to control seizure activity through antiepileptic drugs (AEDs). However, about 30% of the patients remain refractory to pharmacological treatments (Laxer et al., 2014). Alternative approaches involve vagus stimulation or surgical hippocampal resection (Morris & Mueller, 1999; Ryvlin & Rheims, 2008). In addition, most of the current AEDs have serious side effects including exacerbation of the comorbid depression, ataxia, headache, etc. (Perucca & Gilliam, 2012). The endogenous neuropeptide signaling, including dynorphin, neuropeptide Y, galanin, active

 © 2019 Wiley Periodicals, Inc.

peptides of renin-angiotensin system, ghrelin and somatostatin, have an important role in the modulation of neuronal excitability and represent a potential target for treatment (Dobolyi et al., 2014).

Hemorphins are naturally occurring, endogenous peptides belonging to the family of "atypical" opioid peptides released from sequentially hydrolyzed hemoglobin with affinity at opioid receptors and morphinomimetic properties (Blishchenko et al., 2002; Cohen, Fruitier-Arnaudin, & Piot, 2004; Jinsmaa & Yoshikawa, 2002). The mRNA of the only prodynorphin (pDyn) gene distributed in mammals is highly expressed in the limbic system of humans (Nikoshkov et al., 2005) and rodents (Lin et al., 2006). Several Hemorphins have been identified (Erchegyi, Kastin, Zadina, & Qiu, 1992; Glämsta et al., 1991; Glämsta, Meyerson, Silberring, Terenius, & Nyberg, 1992; Glämsta, Morkrid, Lantz, & Nyberg, 1993). All of them are short-chain peptides containing from 4 to 10 amino acids initially obtained from a particular region of the β chain of hemoglobin (human 32–41 fragment and bovine hemoglobin fragment 31–40). Hemorphins are also isolated from brain, plasma, cerebroventricular fluid, spinal cord, and erythrocytes. Under physiological conditions, they are found in tissues as families of structurally related peptides differing in their N- and C-terminal degradation (Duethman, Dewan, & Conlon, 2000; Mäkinen, Sewon, & Mäkinen, 1996). A series of structural overlapped bioactive peptides and their amino acid sequences (Tyr-Pro-Trp), which are essential for binding to opioid receptors, are shown in Table 1 (Blishchenko et al., 2002; Cohen et al., 2004; Jinsmaa & Yoshikawa, 2002).

The heptapeptide VV-Hemorphin-5 (VV-5) (Val-Val-Tyr-Pro-Trp-Thr-Gln), also known as valorphin, is an endogenous opioid peptide that binds both δ- (DORs) and k-opiate (KORs) opioid receptors, respectively (Song, Wang, & Song, 2012). Hemorphins demonstrated numerous physiological effects such as antitumor (Blishchenko et al., 2002), anti-inflammatory (Sanderson, Nyberg, & Khalil, 1998), and activity on cardio-vascular system (Moisan et al., 1998). The LVV-Hemorphin 7 (LVV-H7) is a functional agonist of the biologically active angiotensin peptide, angiotensin IV (Ang IV) which acts via an inhibition of the aminopeptidase-N (Garreau et al., 1998). The hexapeptide Ang IV possesses an anticonvulsant activity by alleviating the development of the pentylenetetrazole (PTZ) kindling in mice (Tchekalarova, Sotiriou, Georgiev, Kostopoulos, & Angelatou, 2005) and pilocarpine-induced status epilepticus in rats (Stragier et al., 2006). The hexapeptide Ang IV effects are blocked by a somatostatin receptor antagonist and similar to LVV-H7 its anticonvulsant effect in the hippocampus depends on the activity of the IRAP (insulin-regulated aminopeptidase) enzyme (Stragier et al., 2006). The LVV-5 and VV-5 Hemorphins regulate the blood pressure by inhibiting angiotensin-converting enzyme (ACE) (Zhao & Piot, 1997), which blocks the conversion of Ang I into Ang II (Yoshikawa, 2015).

TABLE 1 Hemorphin peptides sequence

Peptide	Sequence	
Hemorphin-4	***Tyr-Pro-Trp-Thr***	*YPWT*
Hemorphin-5	***Tyr-Pro-Trp-Thr***-*Gln*	*YPWTQ*
Hemorphin-6	***Tyr-Pro-Trp-Thr***-*Gln-Arg*	*YPWTQR*
Hemorphin-7	***Tyr-Pro-Trp-Thr***-*Gln-Arg-Phe*	*YPWTQRF*
Hemorphin-8	***Tyr-Pro-Trp-Thr***-*Gln-Arg-Phe-Phe*	*YPWTQRFF*
VV-Hemorphin-5	*Val-Val-**Tyr-Pro-Trp-Thr**-Gln*	*VVYPWTQ*
LVV-Hemorphin-5	*Leu-Val-Val-**Tyr-Pro-Trp-Thr**-Gln*	*LVVYPWTQ*
LVV-Hemorphin-6	*Leu-Val-Val-**Tyr-Pro-Trp-Thr**-Gln-Arg*	*LVVYPWTQR*
VV-Hemorphin-7	*Val-Val-**Tyr-Pro-Trp-Thr**-Gln-Arg-Phe*	*VVYPWTQRF*
LVV-Hemorphin-7	*Leu-Val-Val-**Tyr-Pro-Trp-Thr**-Gln-Arg-Phe*	*LVVYPWTQRF*

In continuation of our efforts to find new bioactive peptides, in the present study we report the synthesis, pharmacological evaluation, and docking study of a series of peptide analogues of VV-5, modified at position 1 and 7 by the un/natural amino acids followed the structures ***Aa8***-Val-Val-Tyr-Pro-Trp-Thr-Gln-NH_2 and Val-Val-Tyr-Pro-Trp-Thr-***Aa1***-NH_2, where ***Aa8*** is Ile or Aib (α-aminoisobutyric acid) and ***Aa1*** is Lys/Orn/Dap (2,3-diaminopropanoic acid)/Dab (2,4-diaminobutanoic acid).

2 | MATERIALS AND METHODS

2.1 | Chemicals and instrumentation

The protected amino acids and Fmoc (9-fluorenylmethoxycarbonyl)-Rink amide MBHA (4-methylbenzhydrylamine) resin were purchased from Iris Biotech (Germany). All other reagents and solvents were analytical or HPLC grade and were bought from Merck (Germany). Mass analysis was carried out on a Q Exactive hybrid quadrupole Orbitrap mass spectrometer (ThermoScientific) equipped with a heated electrospray ionization module IonMax (ThermoScientific). The optical rotation was measured on automatic standard polarimeter Polamat A, Carl Zeis, Jena.

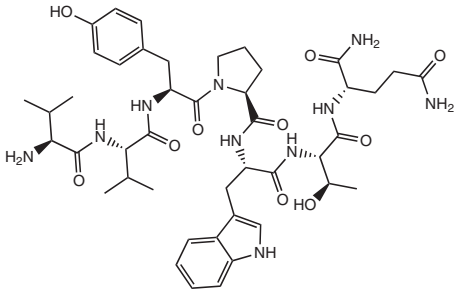
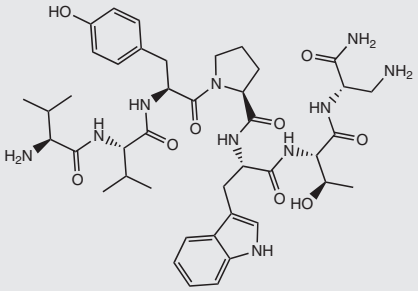
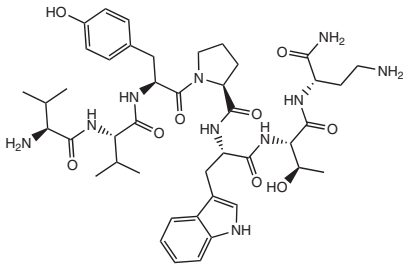
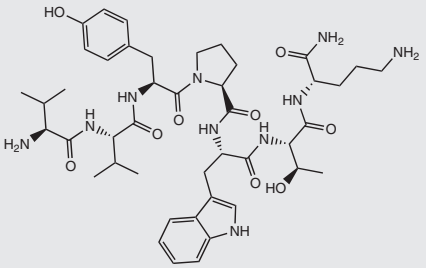
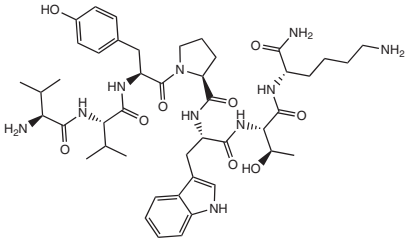
2.2 | General procedure for the peptide synthesis of compounds V1–V7

All of the VV-Hemorphin-5 analogues have been prepared by our recently described procedure (Todorov, Peneva, Pechlivanova, Georgieva, & Dzhambazova, 2018). RP-HPLC and ESI-MS data of all the compounds were identical to those previously described (Todorov et al., 2018). The synthesized peptides were checked by optical rotation and the analytical data are shown in Table 2.

2.3 | Animals

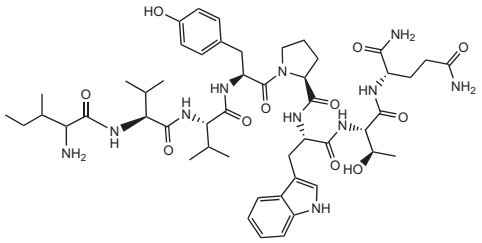
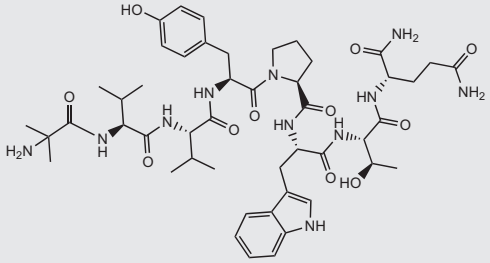
Male albino ICR mice, weighing 25–30 g, were used. Experimental animals were maintained at an ambient temperature 22 ± 1 °C, in groups of eight per cage, under standard laboratory conditions and free access to food and water. All procedures were performed in agreement with the European Communities Council Directive 2010/63/EU. The experimental design was approved by the Institutional Ethics Committee at the Institute of Neurobiology.

TABLE 2 Analytical data of synthetic peptides

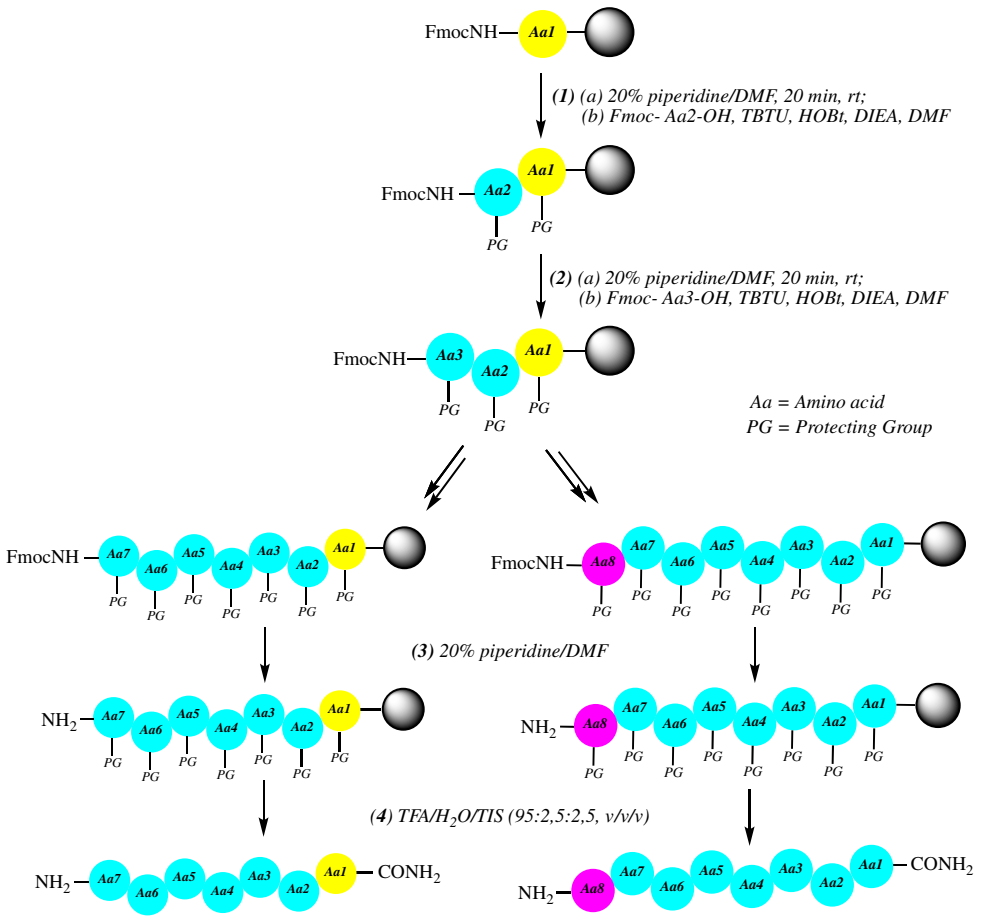
Nº	Peptides	[a] $[\alpha]_{546}^{20}$ (°)	Molecular formula	[b] $t_{R,\ min}$	[c] $[MH]^+$ calculated	[c] $[MH]^+$ observed
V1		−22.8	$C_{44}H_{62}N_{10}O_{10}$	16.72	891.0	891.4
V2		−10.6	$C_{42}H_{60}N_{10}O_9$	15.48	848.9	849.4
V3		−11.4	$C_{43}H_{62}N_{10}O_9$	15.22	863.0	863.4
V4		−11.1	$C_{44}H_{64}N_{10}O_9$	15.07	877.0	877.4
V5		−10.4	$C_{45}H_{66}N_{10}O_9$	15.28	890.9	891.5

(Continues)

TABLE 2 (Continued)

Nº	Peptides	[a] $[\alpha]_{546}^{20}$ (°)	Molecular formula	[b] $t_{R,\ min}$	[c] $[MH]^+$ calculated	[c] $[MH]^+$ observed
V6		−10.2	$C_{50}H_{73}N_{11}O_{11}$	18.90	1,004.1	1,004.5
V7		−9.5	$C_{48}H_{69}N_{11}O_{11}$	17.87	976.1	976.5

[a] Optical rotation in methanol (c = 0.01) at 20 °C.
[b] t_R is the retention time determined by HPLC.
[c] The mass ion (MH^+) was obtained by electrospray ionization mass spectrometry (ESI-MS).



SCHEME 1 Synthesis of peptide derivatives of VV-Hemorphin-5 by solid-phase peptide synthesis (SPPS)

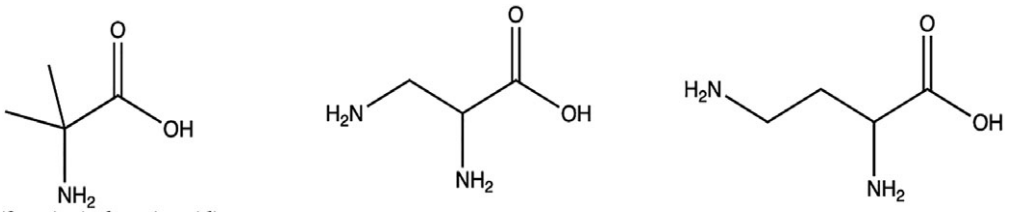


FIGURE 1 Structures of unnatural amino acids

2.4 | Drugs and dosage

Control group (treated with vehicle) and experimental groups (treated with Hemorphin peptide analogues) were infused intracerebroventricularly (i.c.v.) (5 μL/ventricle) at doses of 5, 10 and 20 μg, respectively by means of 28-gauge stainless steel needle attached to a 10-μL Hamilton® syringe. The injection needle was left in place for 2 min to avoid back diffusion of the solution. The anticonvulsant activity was assessed 10 min following drug treatment.

2.5 | Anticonvulsant activity

2.5.1 | Maximal electroshock test (MES test)

A drop of a local anesthetic was applied to the eyes of each animal before delivery of electric stimulus (50 mA, 60 Hz, 0.2 s) through corneal electrodes (Constant Current Shock Generator). The tonic component was considered abolished, if the hind limb extension did not exceed a 90° with the plane of the body. Abolition of hind limb tonic extensor component of the seizure in half or more of the animals was defined as a criterion of protection.

TABLE 3 Anticonvulsant activities of VV-Hemorphin-5 analogues in MES test

Peptide	Dose μg/5 μL	No. of mice protected/ No. of mice tested	% protection
	5	1/6	16
V1	10	3/6	50 +
	20	5/8	63 +
	5	1/5	20
V2	10	1/5	20
	20	2/6	33
	5	2/5	40
V3	10	1/5	20
	20	2/5	40
	5	3/5	60 +
V4	10	1/5	20
	20	1/5	20
	5	5/7	71 +
V5	10	3/5	60 +
	20	1/5	20
	5	3/6	50 +
V6	10	2/6	33
	20	3/6	50 +
V7	5	2/5	40
	10	1/5	20
	20	3/5	60 +

Note. The symbol "+" in the third column of the table indicate the minimum dose, whereby bioactivity or neurotoxicity was demonstrated in at least 50% of treated animals.

2.5.2 | 6-Hz psychomotor seizure test

The 6-Hz psychomotor seizure test was used to assess the efficacy of the compounds against electrically induced seizures through corneal electrodes (32 mA, 6 Hz, 3 s) (Barton, Klein, Wolf, & White, 2001). The seizure in the controls is characterized by a minimal clonic phase or stereotyped, automaticity behavior, including twitching of the vibrissae or Straub-tail. The criterion of protection against psychomotor seizures was accepted if a mouse resumed its normal position within 10 s after stimulation.

2.5.3 | Intravenous pentylenetetrazole (ivPTZ) seizure test

PTZ (10 mg/mL) was infused into the tail vein at a constant rate of 0.005 mL/s. The seizure threshold was determined as was described in our previous studies and elsewhere (Nutt, Taylor, & Little, 1986; Tchekalarova & Georgiev, 1999; Tchekalarova, Kambourova, & Georgiev, 2001). The end point of the infusion was taken as the onset of each consecutive phase (general excitation with myoclonic jerks, clonic, and tonic seizures). The seizure threshold in mg/kg was calculated from the quantity of infused PTZ in milliliters, body weight and PTZ concentration. Because of the well-recognized day-to-day variability in the seizure threshold (Löscher & Fiedler, 1996), the appropriate control group injected with saline, was always tested at the same time as the experimental ones.

2.6 | Docking of Hemorphin-5 analogues on Delta- and Kappa-opioid receptors

In this study, we elucidate models of delta opioid receptor (DOR) and kappa opioid receptor (KOR) on which we perform docking study in order to shed light about possible molecular mechanism of action of the novel peptide derivatives. Delta- (DORs) and KORs receptors were crystallized for our modeling study structures and used data from Protein Data Bank. For DOR structure a recombinant protein 4EJ4 from mouse was used (Granier et al., 2012). For KOR structure 6B73 was used, which contained a stabilized active conformation of human KOR (Che et al., 2018). In the KOR structure all amino acids that differed between mice and human protein were mutated in silico in order to obtain mouse protein as it is used in our in vivo experiments.

Both protein data bank structures were checked and several structural improperties were corrected. Other nonprotein species as well as all protons were removed. The missing amino acids from DOR, 36–40 and 329–342 and from KOR 1-to 110 and 400–418, were not added as they were situated at the beginning and the end

TABLE 4 Anticonvulsant activities of VV-Hemorphin-5 analogues in 6-Hz test

Peptide	Dose μg/10 μL	No. of mice protected/ No. of mice tested	% protection
	5	5/6	83 +
V1	10	6/8	75 +
	20	3/6	50 +
	5	4/6	67 +
V2	10	3/6	50 +
	20	0/6	0
	5	2/6	33
V3	10	2/6	33
	20	3/7	43
	5	3/6	50 +
V4	10	5/6	83 +
	20	4/6	67 +
	5	4/6	67 +
V5	10	3/6	50 +
	20	2/6	33
	5	5/6	83 +
V6	10	4/6	67 +
	20	5/6	83 +
V7	5	5/6	83 +
	10	6/7	86 +
		5/7	71 +

Note. The symbol "+" in the third column of the table indicate the minimum dose, whereby bioactivity or neurotoxicity was demonstrated in at least 50% of treated animals.

of the polypeptide chains so that their absence would not modify the polypeptide integrity or would affect the active center of the DOR and KOR.

From KOR protein data bank (PDB) the A chain was used, as it contained more resolved amino acids. Ser301 was also added, as well as amino acids 203, 204, and 205, in order to better complete the loops and to yield a whole protein molecule. The reason for these additions was that these amino acids were situated closer to the active site. The above described procedures were conducted with COOT 0.8.8 software where missing amino acids were placed according to the electron density map of the structures, despite the low electron densities there.

New protons were added in order to achieve right protonation state at 7.0 pH as the experimental study was carried out at physiological conditions. Further all bond lengths were blocked and steepest descent algorithm was used with AMBER10 force field in order to minimize maximal interactions (as they were relatively high in newly added residues) and relaxed the systems.

As the XRD (X-ray diffraction) structures of the DOR and KOR were in complexes with ligands, cavity of the receptors active site was used without modifications. The VV-Hemorphin-5 analogues (V1–V7) were built at ionization states corresponding to pH 7 and stochastic and LowModeMD conformation search was done. The lowest 100 obtained conformations of every species were subject to the further docking.

To find optimal positions for placement of the ligands inside the active site of both receptors a finder procedure was accomplished as it was implemented in MOE2016 package. For further calculations we used only positions inside the active site region.

Constructed ligand conformation database was further used in docking, where "Triangle Matcher" method was applied for the placement of conformations in every site point with London dG scoring. "Induced fit" method followed as refinement step with GBVI/WSA dG scoring function as it was implemented in MOE2016 software.

The used GBVI/WSA ΔG was a force-field-based scoring function which estimated the free energy of binding of the ligand from a given pose. It was trained using the MMFF94x and AMBER99 force-field on the 99 protein-ligand complexes of the SIE training set (Naim et al., 2007). The functional form was a sum of terms [MOE]:

$$\Delta G \approx c + \alpha\left[\frac{2}{3}\left(\Delta E_{\text{Coul}} + \Delta E_{\text{sol}}\right) + \Delta E_{\text{vdW}} + \beta \Delta SA_{\text{Weighted}}\right]$$

where:

c—represents the average gain/loss of rotational and translational entropy.

α, β—are force-field-dependent constants determined during training.

E_{coul}—is the coulombic electrostatic term which is calculated using currently loaded charges, using a constant dielectric of $\varepsilon_i = 1$.

TABLE 5 Quantitative anticonvulsant assessment of VV-Hemorphin-5 analogues

Peptide	Test	ED_{50} (μg/10 μL)	95% confidence interval	Hill slope	Standard errors of the slope
V1	MES	11.48	(7.41–17.78)	1.81	0.44
	6-Hz	2.28	(2.14–2.42)	2.02	0.04
V2	6-Hz	9.97	(9.07–10.90)	2.49	0.17
V4	MES	3.63	(2.45–5.38)	1.42	0.18
	6-Hz	5.09	(4.31–6.02)	2.51	0.28
V5	MES	3.19	(2.62–3.87)	2.00	0.14
	6-Hz	9.89	(8.64–11.34)	2.59	0.27
V6	MES	16.77	(11.08–25.36)	1.77	0.41
	6-Hz	2.55	(2.51–2.58)	2.35	0.01
V7	MES	16.55	(12.78–21.41)	2.90	0.62
	6-Hz	6.61	(6.59–6.62)	4.38	0.01

Note. The values represented are in the 95% confidence interval. Median effective doses (ED_{50}).

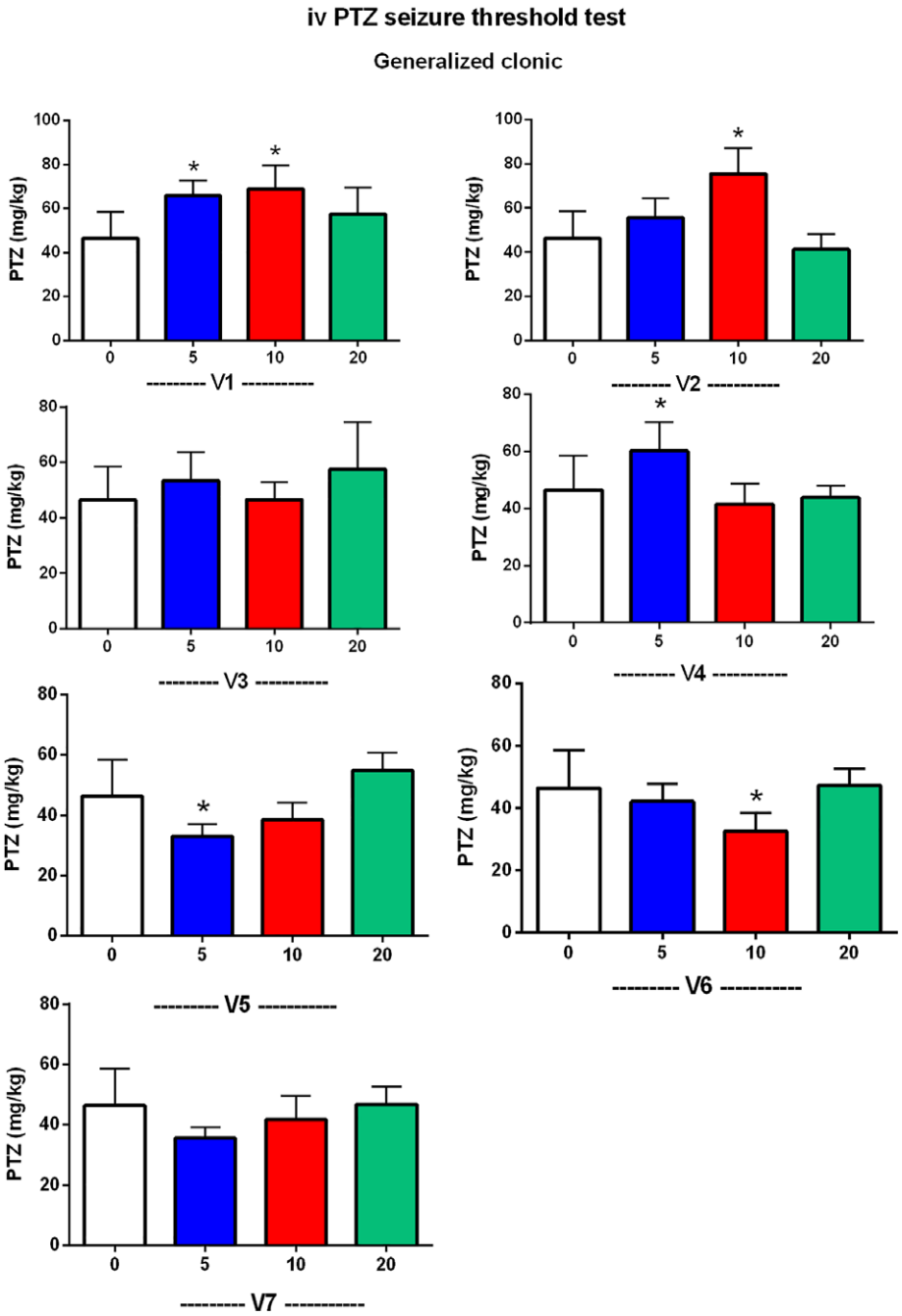


FIGURE 2 Effect of Hemorphins V1–V7 on the threshold for the onset of first generalized clonus in the i.v. PTZ seizure threshold test in mice. VV-Hemorphin-5 peptide analogues were administered i.c.v. 10 min prior to the test. The doses are shown on the abscissa. Control animals received vehicle. Each experimental group consisted of 8–10 animals. Each bar represents the mean (mg/kg PTZ) + *SEM*. **p* < 0.05 vs. the control group

E_{sol}—is the solvation electrostatic term which is calculated using the GB/VI solvation model. [MOE].

E_{vdW}—is the van der Waals contribution to binding.

$SA_{weighted}$ is the surface area, weighted by exposure. This weighting scheme penalizes exposed surface area.

2.7 | Statistical analysis

The ED_{50} (the dose effective in 50% of tested animals) was calculated by means of probit analysis with 95% confidence interval in the quantitative analysis of in vivo data from MES and 6-Hz test. In-vitro data were expressed as mean ± *SEM* for six experiments. The one-way analysis of variance (ANOVA) followed by Dunnett's post hoc test was employed for i.v. PTZ test. Statistical significance was accepted at $p = 0.05$. All calculations were carried out with Sigmastat (version SigmaStat® 11.0) for Windows.

3 | RESULTS AND DISCUSSION

3.1 | Chemistry

This work is a continuation of our previous study on the synthesis and nociceptive effects of some new VV-Hemorphin-5 analogues (Todorov

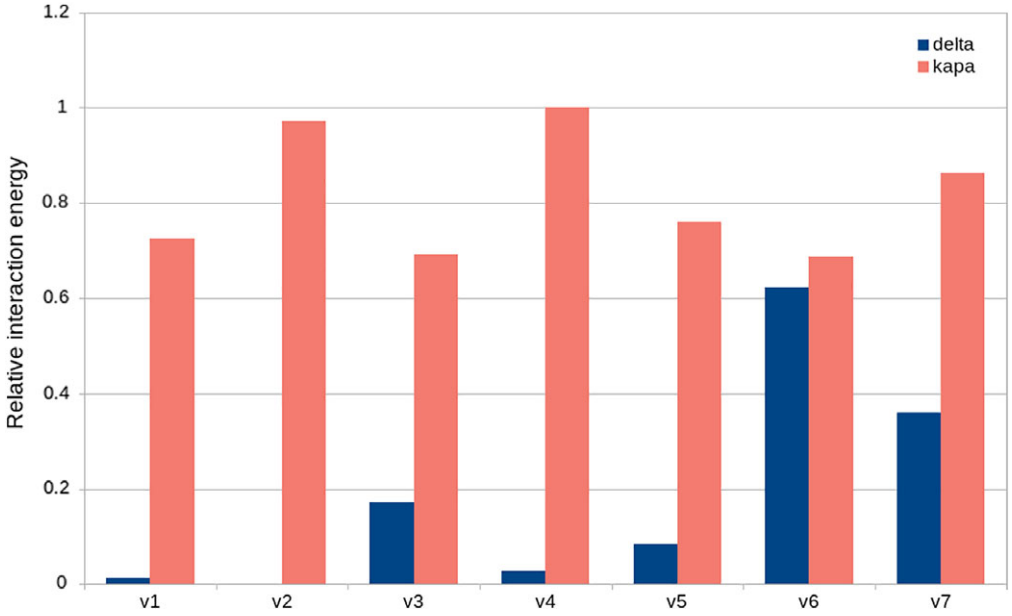


FIGURE 3 GBVI/WSA ΔG of interaction between ligands and DOR and KOR receptors are represented. Both interaction energies are normalized together

et al., 2018). The peptides V1–V7, presented in Table 2, have been prepared by SPPS-Fmoc (9-fluorenylmethoxycarbonyl) strategy (see Scheme 1) according to the procedure described by us (Todorov et al., 2018). Based on Val-Val-Tyr-Pro-Trp-Thr-Gln-NH_2 as a chemical template, we synthesized new C-amide peptide derivatives of VV-Hemorphin-5 by replacement of Gln at position 7 with nonproteinogenic and/or natural amino acids (Val-Val-Tyr-Pro-Trp-Thr-***Aa1***-NH_2), where ***Aa1*** is Lys/Orn/Dap/Dab. For exploring the influence of amino acid residues have been incorporated of Ile/Aib (***Aa8***) at position 1 (***Aa8***-Val-Val-Tyr-Pro-Trp-Thr-Gln-NH_2) (see Figure 1 and Table 2). The analytical data of the synthetic peptides are shown in Table 2.

The replacement of the C-terminal carboxyl group with amide group led to molecules with high biological activity. All of the synthesized peptide were C-terminal amides. It has been determined that the peptides with C-terminal amide group are more resistant to enzyme degradation and that their conformation suits better the interaction with the corresponding receptors (Mortensen, Raaschou-Nielsen, & Breddam, 1994; Pogozheva, Przydzial, & Mosberg, 2005).

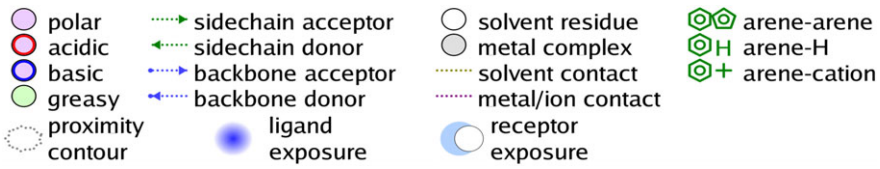
The handling of the amino acidic scaffold can be regarded as a potentially powerful tool in both bioorganic and biomedical investigations and the development of new drugs. Among accumulated number of publications in this area, a few general reviews addressing unnatural amino acids, including their synthesis and their use in diverse fields, are currently available in the literature (Stevenazzi, Marchini, Sandrone, Vergani, & Lattanzio, 2014).

In order to estimate the relationship, we prepared the compounds V2–V5 by replacement of the glutamine (Gln) with un/natural aliphatic amino acids. In general, unnatural amino acids are more resistant than proteinogenic α-amino acids to enzymatic degradation (Gademann, Hintermann, & Scheiber, 1999) and they have often relevant roles in medicinal chemistry (Fülöp, 2001; Ojima, Lin, & Wang, 1999). It is known that the α,α-dialkylated amino acids induce conformational constraints in the peptide backbone, thereby stabilizing a desired conformation. The prototypic member of these amino acids namely α-aminoisobutyric acid (Aib) has been shown to induce β-turn in small peptides and helical conformation in larger ones (Karle & Balaram, 1990; Prasad et al., 1995).

3.2 | Anticonvulsant activity

3.2.1 | MES test

Except of V2 and V3 Hemorphin analogues, which were ineffective in the MES test, the rest of peptide analogues exhibited potency to suppress tonic–clonic seizures in at least 50% of treated mice (Table 3). The peptide analogues V4, V5 and V6 exhibited activity against tonic seizures at the lowest dose of 5 μg used while the positive control V1 exerted anticonvulsant effect at doses of 10 and 20 μg, respectively.



SCHEME 2 Symbols used to describe interactions between DOR or KOR and ligand molecules

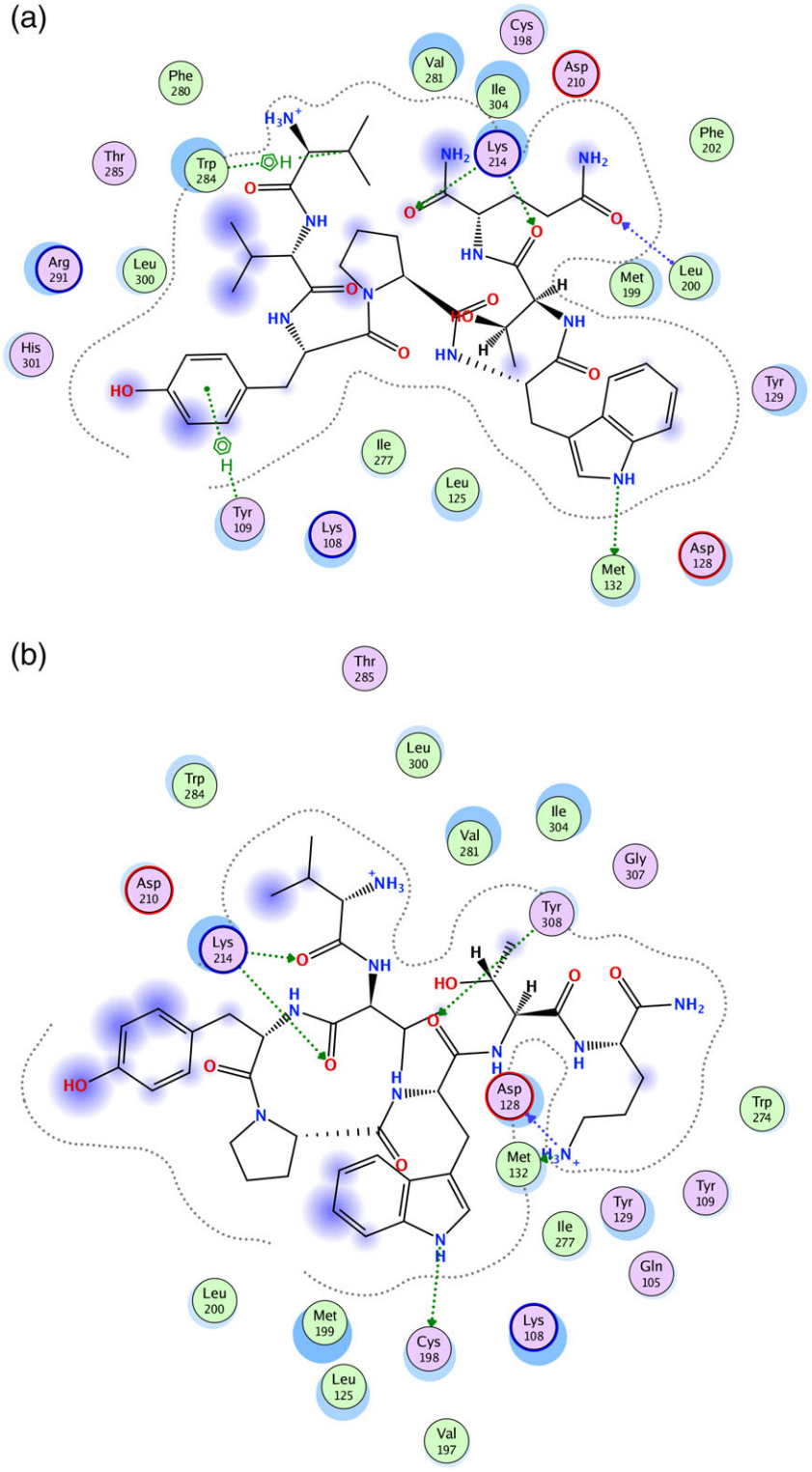


FIGURE 4 Representation of the best interacting conformation of V1 with DOR (a) and V4 with DOR (b)

3.2.2 | 6-Hz psychomotor seizure test

All tested peptide analogues were characterized with more than 50% protection against psychomotor seizures induced by 6-Hz stimulation. The peptide analogues V4, V6, and V7 exhibited comparable to V1 peptide activity at the three tested doses (Table 4).

Further, peptides V1, V2, V4, V5, and V6 were subjected to phase II trial to quantify their anticonvulsant activity (indicated by ED_{50}) in MES and 6-Hz test, respectively (Table 5). In the MES test, the peptides V4 and V5 displayed the lowest ED_{50} values of 3.63 and 3.19 μg, respectively, which were with more than three times higher potency compared to the positive control V1 (ED_{50} of 11.48 μg). The quantitative data for the 6-Hz test demonstrated that the peptide V6 exhibited ED_{50} value of 2.55 μg, which was comparable to that of peptide V1 with ED_{50} value of 2.28 μg (Table 5).

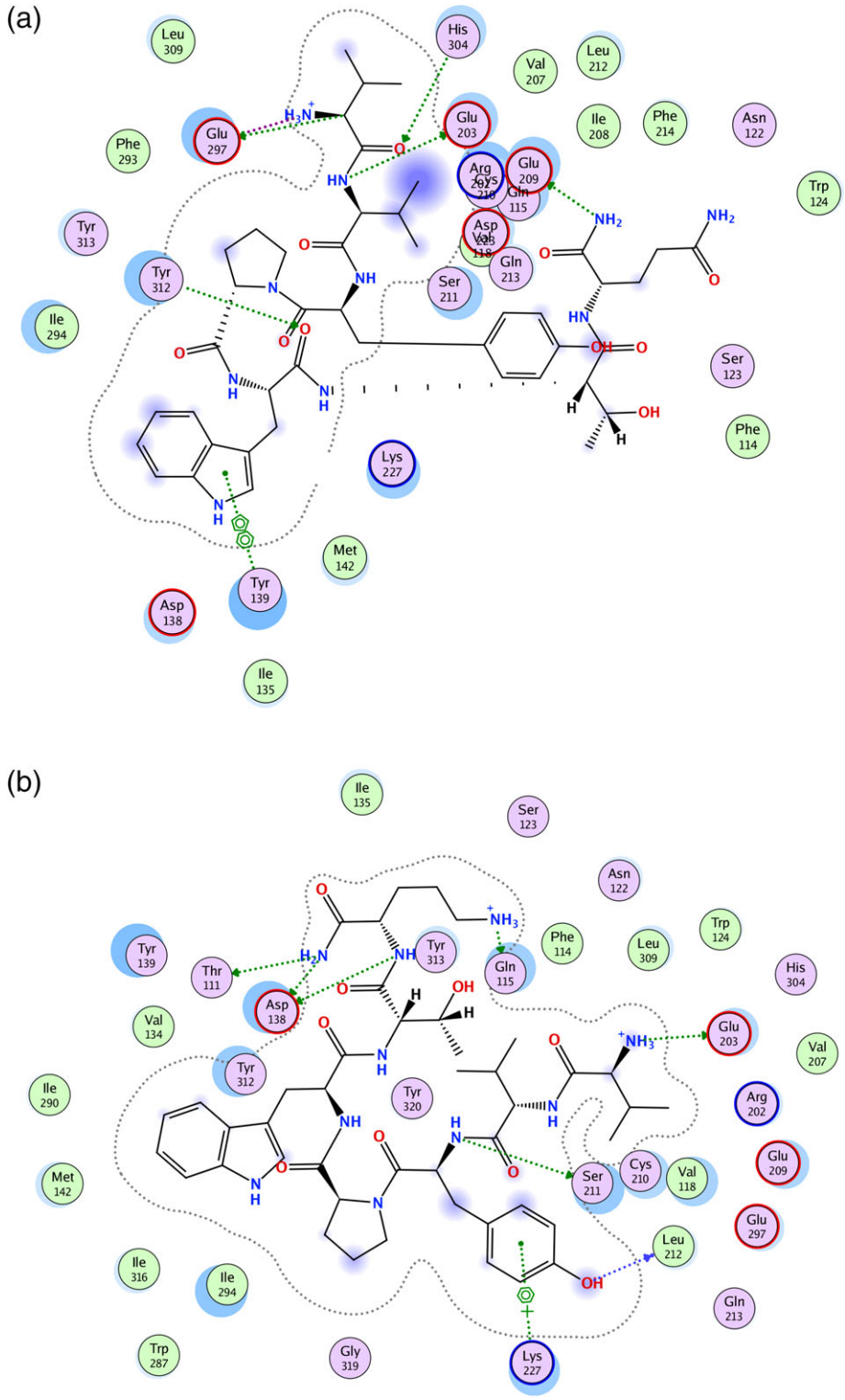


FIGURE 5 Representation of the best interacting conformation of V1 with KOR (a) and V4 with KOR (b)

3.2.3 | Intravenous scPTZ seizure test

In the i.v. PTZ test, only the results on the clonic seizure threshold have been shown because they best characterized the convulsive excitability induced by the convulsant (Swinyard, Boson, & Goodman, 1964). The V1 peptide at doses of 5 μg and 10 μg increased seizure threshold in comparison to control group treated by a vehicle ($p < 0.01$). From the tested peptide analogues only V2 and V4 compounds demonstrated statistically significant increase in the clonic seizure threshold at a dose of 10 μg ($p < 0.01$) and 5 μg ($p = 0.023$), respectively. On contrary, V5 and V6 exhibited pro-convulsant effects by decreasing the threshold for clonic seizures induced by i.v. PTZ infusion at a dose of 5 μg ($p = 0.027$) and 10 μg ($p = 0.026$), respectively. The V3 and V7 peptide analogues were ineffective at the three tested doses in this test.

All novel Hemorphin analogues did not induce impairment of the motor coordination in mice ($p > 0.05$) at the maximum dose of 20 μg administered in the rotarod test (Figure 2).

It should be mentioned, that the interactions between all the ligands and KOR were energetically favorable with more than 20%, compared to their interactions with DOR. In all cases, the ligands were positioned in the close vicinity of conserved amino acid motifs, crucial for the functioning of opioid receptors and known from the literature (Che et al., 2018; Granier et al., 2012).

To describe interactions between DOR or KOR and ligand molecules, the symbols at the following legend are used (Figure 3; Scheme 2):

As seen from Figures 4 and 5, V1 and KOR showed better interaction energy compared to V1 and DOR mainly due to stronger interactions between the first. While the better interaction energy of V4 and KOR than V4 and DOR, was mainly due to more interactions of similar strength.

In the present study, we aimed to explore the activity of newly developed VV-Hemorphin-5 peptide analogues in three acute seizure models, MES, 6-Hz psychomotor seizures and i.v. PTZ tests, respectively, in mice established as a "gold standard" in screening of new compounds according to the Epilepsy Therapy Screening Program at the University of Utah. All synthetic heptapeptide analogues (V2–V5) contained different amino alkyl residue and differed by the increased number of methylene group (from one to four) suggesting the important role of this group for their anticonvulsant activity. It has to be noted that adding the amino acid residue at Position 1 in VV-5 (V6 and V7) led to a pro-convulsant effect in the i.v. PTZ test.

The mechanism of action of V1 heptapeptide, also known as valorphin, involves activation of both DORs and KORs receptors. The DORs are mostly distributed on neurons, which inhibit glutamatergic neurons, thereby, exerting disinhibition of these excitatory neurons (Burtscher & Schwarzer, 2017). In opposite, KORs are expressed on glutamatergic neurons suggesting that their activation would suppress directly the activity of excitatory neurons. Different expression of DORs and KORs is crucial for their impact on neuronal excitability and can explain controversial effects of agonist on these receptors. Thus, the endogenous dynorphin and agonists of KORs behave mostly as anticonvulsants (Tortella, 1988; Zangrandi & Schwarzer, 2011). However, reports suggest ambiguous and complex effects of agonist on DORs, on seizure susceptibility (Bausch, Garland, & Yamada, 2005; Loacker, Sayyah, Wittmann, Herzog, & Schwarzer, 2007).

The MES test is accepted as a model of tonic–clonic seizures in patients and identifies compounds potent to alleviate seizure spread unlike compounds able to affect seizure focus directly (Barker-Haliski et al., 2018). The 6 Hz test is accepted as a model against focal seizures (Brown, Schiffman, Swinyard, & Goodman, 1953). Although the 6-Hz psychomotor seizure test has been mostly described as a model of drug-resistant epilepsy, GABAergic substances also showed effectiveness suggesting that this definition is appropriate mainly for sodium channels (Löscher, 2017). Unlike the MES test where a tonic phase appears first and then a clonic phase, the i.v. PTZ test results in clonic–tonic seizures (Goodman, Grewal, Brown, & Swinyard, 1953). The i.v. PTZ test identifies compounds able to raise seizure threshold.

In the present study, V1 peptide analogue demonstrated anticonvulsant effect in three seizure models revealing its potency to block seizures with different mechanism of action, including seizure spread, psychomotor seizures and elevation of seizure threshold. The dose-dependent anticonvulsant effect of V1 peptide in three seizure tests enable us to use it as a positive control and suggest that its mechanism of action may involve mostly activation of KORs. It can be speculated that the anticonvulsant effect of the V2 peptide analogue is mediated through activation of GABAergic system because this compounds revealed potency in the i.v. PTZ seizure test and 6-Hz psychomotor test but not in the MES test. Like the positive control, the V4 peptide analogue showed efficacy against the three seizure models. Results from docking analysis confirms experimental data and suggest possibility for the involvement of multitude neurotransmitter systems, that is, KORs, NMDA channel, and GABAA–BZD-chloride channel in its mechanism of action. Interestingly, the V5 and V6 peptide analogues demonstrated either anticonvulsant effect in the MES and/or 6-Hz psychomotor seizure test or pro-convulsant effect in the i.v. PTZ test. Docking results are in support of the suggestion that their primary target might involve DORs in the i.v. PTZ test. Similarly, the V7 peptide analogue demonstrated anticonvulsant activity in the MES and 6-Hz psychomotor seizure test but was ineffective in the i.v. PTZ test suggesting also multiple and more complex mechanism of action.

4 | CONCLUSION

In summary, we have investigated the pharmacological evaluation and docking study of the recently synthesized VV-Hemorphin-5 analogues containing nonproteinogenic and/or natural amino acids. Based on the divergent effects exerted by the newly developed Hemorphin peptide analogues in three seizure models with different mechanism of action and data from in silico analysis, we can conclude that incorporation of nonproteinogenic amino acid Orn at Position 7 of VV-5 determine multiple target system that might provoke anticonvulsant effect of V4 peptide analogue while replacement Gln with Lys in Position 7 of VV-5 of heptapeptide V5 probably involve activation DORs. On the other hand, this activation may be included when the branched-chain aliphatic amino acid Ile (V6), and α-aminoisobutyric acid Aib (V7) is added at position one of octapeptides V6 and V7, respectively. These data give us ground to suggest that in this case not only the position of modification, but also the nature of the incorporated group, lead to significant changes in the peptide activity and affinity. Future studies with selective antagonist on KORs, DORs, NMDA channels, and GABAA–BZD-chloride channel are required to specify the receptor targets of these peptide analogues.

ACKNOWLEDGMENTS

Our work was supported financially by the University of Chemical Technology and Metallurgy (UCTM), Sofia, Bulgaria, and the Scientific Research Centre at UCTM contract 11813/2018. The authors would like to thank Ludmila Yankova for her technical assistance. We confirm that we have read the Journal's position on issues involved in ethical publication and affirm that this report is consistent with those guidelines.

CONFLICTS OF INTEREST

The authors declare that they have no competing interests.

ORCID

Jana Tchekalarova https://orcid.org/0000-0003-1640-5099

REFERENCES

Barker-Haliski, B., Harte-Hargrove, L. C., Ravizza, T., Smolders, I., Xiao, B., Brandt, C., & Löscher, W. (2018). A companion to the preclinical common data elements for pharmacologic studies in animal models of seizures and epilepsy. A Report of the TASK3 Pharmacology Working Group of the ILAE/AES Joint Translational TASK Force. *Epilepsia Open. Special Issue: Preclinical Epilepsy Common Data Elements of the ILAE/AES Joint Translational Task Force*, *3*, 53–68.

Barton, M. E., Klein, B. D., Wolf, H. H., & White, H. S. (2001). Pharmacological characterization of the 6 Hz psychomotor seizure model of partial epilepsy. *Epilepsy Research*, *47*, 217–227.

Bausch, S. B., Garland, J. P., & Yamada, J. (2005). DOR agonist, has complex, dose-dependent effects on pilocarpine-induced seizures in Sprague–Dawley rats. *Brain Research*, *1045*, 38–44.

Blishchenko, E., Sazonova, O., Surovoy, A., Khaidukov, S., Sheikine, Y., Sokolov, D., … Ivanov, V. (2002). Antiproliferative action of valorphin in cell cultures. *Journal of Peptide Science*, *8*, 438–452.

Blishchenko, E. Y., Sazonova, O. V., Kalinina, O. A., Yatskin, O. N., Philippova, M. M., Surovoy, A. Y., … Ivanov, V. T. (2002). Family of hemorphins: Co-relations between amino acid sequences and effects in cell cultures. *Peptides*, *23*, 903–910.

Brown, W. C., Schiffman, D. O., Swinyard, E. A., & Goodman, L. S. (1953). Comparative assay of an antiepileptic drugs by psychomotor seizure test and minimal electroshock threshold test. *The Journal of Pharmacology and Experimental Therapeutics*, *107*, 273–283.

Burtscher, J., & Schwarzer, C. (2017). The opioid system in temporal lobe epilepsy: Functional role and therapeutic potential. *Frontiers in Molecular Neuroscience*, *10*, 245.

Che, T., Majumdar, S., Zaidi, S. A., Ondachi, P., McCorvy, J. D., Wang, S., … Roth, B. L. (2018). Structure of the nanobody-stabilized active state of the kappa opioid receptor. *Cell*, *172*, 55–67.e15. https://doi.org/10.1016/j.cell.2017.12.011

Cohen, M., Fruitier-Arnaudin, I., & Piot, J. M. (2004). Hemorphins: Substrates and/or inhibitors of dipeptidyl peptidase IV Hemorphins N-terminus sequence influence on the interaction between hemorphins and DPPIV. *Biochimie*, *86*, 31–37.

Dobolyi, A., Kékesi, K. A., Juhász, G., Székely, A. D., Lovas, G., & Kovács, Z. (2014). Neuropeptides in epilepsy tic targets in epilepsy research. *Current Medicinal Chemistry*, *21*, 764–787.

Duethman, D., Dewan, N., & Conlon, J. M. (2000). Isolation of the opioid peptide Leu-Val-Val-hemorphin-7 from bronchoalveolar lavage fluid of a patient with non-small cell lung cancer. *Peptides*, *21*, 137–142.

Erchegyi, J., Kastin, A. J., Zadina, J. E., & Qiu, X. D. (1992). Isolation of a heptapeptide Val-Val-Tyr-pro-Trp-Thr-Gln (valorphin) with some opiate activity. *International Journal of Peptide and Protein Research*, *39*, 477–484.

Fisher, R. S., Acevedo, C., Arzimanoglou, A., Bogacz, A., Cross, J. H., Elger, C. E., … Wiebe, S. (2014). ILAE official report: A practical clinical definition of epilepsy. *Epilepsia*, *55*, 475–482.

Fülöp, F. (2001). The chemistry of 2-aminocycloalkanecarboxylic acids. *Chemical Reviews*, *101*, 2181–2204.

Gademann, K., Hintermann, T., & Scheiber, J. V. (1999). Beta-peptides: Twisting and turning. *Current Medicinal Chemistry*, *6*, 905–925.

Garreau, I., Chansel, D., Vandermeersch, S., Fruitier, I., Piot, J. M., & Ardaillou, R. (1998). Hemorphins inhibit angiotensin IV binding and interact with aminopeptidase N. *Peptides*, *19*, 1339–1348.

Glämsta, E. L., Marklund, A., Hellman, U., Wernstedt, C., Terenius, L., & Nyberg, F. (1991). Isolation and characterization of a haemoglobin-derived opioid peptide from the human pituitary gland. *Regulatory Peptides*, *34*, 169–179.

Glämsta, E. L., Meyerson, B., Silberring, J., Terenius, L., & Nyberg, F. (1992). Isolation of a hemoglobin-derived opioid peptide from cerebrospinal fluid of patients with cerebrovascular bleedings. *Biochemical and Biophysical Research Communications*, *184*, 1060–1066.

Glämsta, E. L., Morkrid, L., Lantz, I., & Nyberg, F. (1993). Concomitant increase in blood plasma levels of immunoreactive hemorphin-7 and beta-endorphin following long distance running. *Regulatory Peptides*, *49*, 9–18.

Goodman, L. S., Grewal, M. S., Brown, W. C., & Swinyard, E. A. (1953). Comparison of maximal seizures evoked by pentylenetetrazol (metrazol) and electroshock in mice, and their modification by anticonvulsants. *Journal of Pharmacology and Experimental Therapeutics*, *108*, 168–176.

Granier, S., Manglik, A., Kruse, A. C., Kobilka, T. S., Thian, F. S., Weis, W. I., & Kobilka, B. K. (2012). Structure of the δ-opioid receptor bound to naltrindole. *Nature*, *485*, 400–4004.

Ivanova, N., Pechlivanova, D., Atanasova, D., Mitreva, R., Lazarov, N., Stoynev, A., & Tchekalarova, J. (2015). Long-term intracerebroventricular infusion of angiotensin II after kainate-induced status epilepticus: Effects on epileptogenesis, brain damage and diurnal behavioral changes. *Epilepsy & Behavior*, *51*, 1–12.

Jinsmaa, Y., & Yoshikawa, M. (2002). Release of Hemorphin-5 from human hemoglobin by pancreatic elastase. *Bioscience Biotechnology and Biochemistry*, *66*(5), 1130–1132.

Karle, I. L., & Balaram, P. (1990). Structural characteristics of alpha-helical peptide molecules containing Aib residues. *Biochemistry*, *29*, 6747–6756.

Laxer, K. D., Trinka, E., Hirsch, L. J., Cendes, F., Langfitt, J., Delanty, N., … Benbadis, S. R. (2014). The consequences of refractory epilepsy and its treatment. *Epilepsy & Behavior*, *37*, 59–70.

Loacker, S., Sayyah, M., Wittmann, W., Herzog, H., & Schwarzer, C. (2007). Endogenous dynorphin in epileptogenesis and epilepsy: Anticonvulsant net effect via kappa opioid receptors. *Brain*, *130*, 1017–1028.

Löscher, W. (2017). The search for new screening models of pharmacoresistant epilepsy: Is induction of acute seizures in epileptic rodents a suitable approach? *Neurochemical Research*, *42*, 1926–1938.

Löscher, W., & Fiedler, M. (1996). The role of technical, biological and pharmacological factors in the laboratory evaluation of anticonvulsant drugs. *Epilepsy Research*, *25*, 3–10.

Mäkinen, K. K., Sewon, L., & Mäkinen, P. (1996). Analysis in gingival crevicular fluid of two oligopeptides derived from human hemoglobin beta-chain. *Journal of Periodontal Research*, *31*, 43–46.

Meldrum, B. S. (2002). Concept of activity-induced cell death in epilepsy: Historical and contemporary perspectives. *Progress in Brain Research*, *135*, 3–11.

Moisan, S., Harvey, N., Beaudry, G., Forzani, P., Burhop, K. E., Drapeau, G., & Rioux, F. (1998). Structural requirements and mechanism of the pressor activity of Leu-Val-Val-hemorphin-7, a fragment of hemoglobin beta-chain in rats. *Peptides*, *19*, 119–131.

Morris, G. L., & Mueller, W. D. (1999). Long-term treatment with vagus nerve stimulation in patients with refractory epilepsy. *Neurology*, *53*, 1731–1735.

Mortensen, U. H., Raaschou-Nielsen, M., & Breddam, K. (1994). Recognition of C-terminal amide groups by (serine) carboxypeptidase Y investigated by site-directed mutagenesis. *The Journal of Biological Chemistry*, *269*, 15528.

Naïm, M., Bhat, S., Rankin, K. N., Dennis, S., Chowdhury, S. F., Siddiqi, I., … Purisima, E. O. (2007). Solvated interaction energy (SIE) for scoring protein-ligand binding affinities. 1. Exploring the parameter space. *Journal of Chemical Information and Modeling*, *47*, 122–133.

Nikoshkov, A., Hurd, Y. L., Yakovleva, T., Bazov, I., Marinova, Z., Cebers, G., … Bakalkin, G. (2005). Prodynorphin transcripts and proteins differentially expressed and regulated in the adult human brain. *The FASEB Journal*, *19*, 1543–1545.

Nutt, D. J., Taylor, S. C., & Little, H. J. (1986). Optimizing the pentetrazol infusion test for seizure threshold measurements. *The Journal of Pharmacy and Pharmacology*, *38*, 697–698.

Ojima, I., Lin, S., & Wang, T. (1999). Recent advances in the medicinal chemistry of taxoids with novel beta-amino acid side chains. *Current Medicinal Chemistry*, *6*, 927–954.

Perucca, P., & Gilliam, F. G. (2012). Adverse effects of antiepileptic drugs. *Lancet Neurology*, *11*, 792–802.

Pogozheva, I. D., Przydzial, M. J., & Mosberg, H. I. (2005). Homology modelling of opioid receptor-ligand complexes using experimental constraints. *The AAPS Journal*, *7*, 434–E448.

Prasad, S., Rao, R. B., & Balaram, P. (1995). Contrasting solution conformations of peptides containing alpha, alpha-dialkylated residues with linear and cyclic side chains. *Biopolymers*, *35*, 11–20.

Ryvlin, P., & Rheims, S. (2008). Epilepsy surgery: Eligibility criteria and presurgical evaluation. *Clinical Neuroscience*, *10*, 91–103.

Sanderson, K., Nyberg, F., & Khalil, Z. (1998). Modulation of peripheral inflammation by locally administered hemorphin-7. *Inflammation Research*, *47*, 49–55.

Song, C. Z., Wang, Q. W., & Song, C. C. (2012). Hemorphin as a prognostic biomarker and potential drug for breast cancer? *International Journal of Cancer*, *131*, 1011–1012.

Stevenazzi, A., Marchini, M., Sandrone, G., Vergani, B., & Lattanzio, M. (2014). Amino acidic scaffolds bearing unnatural side chains: An old idea generates new and versatile tools for the life sciences. *Bioorganic & Medicinal Chemistry Letters*, *24*, 5349–5356.

Stragier, B., Clinckers, R., Meurs, A., De Bundel, D., Sarre, S., Ebinger, G., … Smolders, I. (2006). Involvement of the somatostatin-2 receptor in the anti-convulsant effect of angiotensin IV against pilocarpine-induced limbic seizures in rats. *Journal of Neurochemistry*, *98*, 1100–1113.

Swinyard, E. A., Boson, F., & Goodman, L. (1964). Effects of epinephrine and norepinephrine on excitability of central nervous system of mice. *Journal of Pharmacology and Experimental Therapeutics*, *13*, 52–59.

Tchekalarova, J., Sotiriou, E., Georgiev, V., Kostopoulos, G., & Angelatou, F. (2005). Up-regulation of adenosine A1 receptor binding in pentylenetetrazol kindling in mice: Effects of angiotensin IV. *Brain Research*, *1032*, 94–103.

Tchekalarova, J. D., & Georgiev, V. P. (1999). Adenosine-angiotensin II interactions in pentylenetetrazol seizure threshold in mice. *The Journal of Physiology*, *93*, 191–197.

Tchekalarova, J. D., & Georgiev, V. P. (1999). Angiotensin peptides modulatory system: How is it implicated in the control of seizure susceptibility? *Life Science*, *76*, 955–970.

Tchekalarova, J. D., Kambourova, T., & Georgiev, V. P. (2001). Angiotensin III and IV influence on pentylenetetrazol seizure susceptibility (threshold and kindling). Interaction with adenosine A1 receptors. *Brain Research Bulletin*, *56*, 87–91.

Todorov, P., Peneva, P., Pechlivanova, D., Georgieva, S., & Dzhambazova, E. (2018). Synthesis, characterization and nociceptive screening of new VV-hemorphin-5 analogues. *Bioorganic & Medicinal Chemistry Letters*, *28*, 3073–3079.

Tortella, F. C. (1988). Endogenous opioid peptides and epilepsy: Quieting the seizing brain? *Trends in Pharmacological Sciences*, *9*, 366–372.

Yoshikawa, M. (2015). Bioactive peptides derived from natural proteins with respect to diversity of their receptors and physiological effects. *Peptides*, *72*, 208–225.

Zangrandi, L., & Schwarzer, C. (2011). Activation of kappa opioidreceptors reduces EEG seizure activity in a mouse model of temporallobe epilepsy. *BMC Pharmacology*, *11*, A10.

Zhao, Q., & Piot, J. M. (1997). Investigation of inhibition angiotensin-converting enzyme (ACE) activity and opioid activity of two hemorphins, LVV.hemorphin.5 and VV-hemorphin-5, isolated from a defined peptic hydrolysate of bovine haemoglobin. *Neuropeptides*, *31*, 147–153.

SUPPORTING INFORMATION

Additional supporting information may be found online in the Supporting Information section at the end of the article.

How to cite this article: Todorov P, Rangelov M, Peneva P, Todorova N, Tchekalarova J. Anticonvulsant evaluation and docking analysis of VV-Hemorphin-5 analogues. *Drug Dev Res*. 2019;1–13. https://doi.org/10.1002/ddr.21514